

# Quantum Annealing With Trigger Hamiltonian

Vrinda Mehta



# Chapter 1

## Theoretical Background

### 1.1 Quantum Computing

Analogous to the digital bits used for classical computation, a quantum computer requires quantum bits, more commonly known as qubits, as the fundamental storage unit. However, unlike the classical bits which can acquire the value of either a 0 or a 1, a qubit state can be a linear superposition of the classical bits. A general single qubit state is given as:

$$|\psi\rangle = a_0 |0\rangle + a_1 |1\rangle, \quad (1.1)$$

where  $a_0$  and  $a_1$  are the complex amplitudes such that  $|a_1|^2 + |a_0|^2 = 1$ . According to the principles of quantum mechanics, upon measurement, the qubit state collapses to the states  $|0\rangle$  or  $|1\rangle$ , with probabilities  $|a_0|^2$  and  $|a_1|^2$  respectively.

A qubit state can also be represented in terms of spin of a particle, whose internal angular momentum can take two values :  $\hbar/2$  corresponding to spin-up state ( $|\uparrow\rangle$ ), or  $-\hbar/2$  corresponding to spin-down state ( $|\downarrow\rangle$ ). In this notation, it is conventional to associate state  $|0\rangle$  with  $|\downarrow\rangle$  and state  $|1\rangle$  with  $|\uparrow\rangle$ . Since there are only two values that the internal angular momentum can acquire, the total angular momentum associated with the particle is  $S=1/2$  [Kristel and Hans, and their references]. The three components of the Pauli matrices corresponding to the spin-1/2 operator  $\mathbf{S}$  spanned by these states are:

$$\sigma_x = \begin{pmatrix} 0 & 1 \\ 1 & 0 \end{pmatrix}, \sigma_y = \begin{pmatrix} 0 & -i \\ i & 0 \end{pmatrix}, \sigma_z = \begin{pmatrix} 1 & 0 \\ 0 & -1 \end{pmatrix}.$$

For  $N$  such qubits, the state is a tensor product of the single qubit states. Since each single state is described using two complex amplitudes, a state with  $N$  qubits requires  $2^N = L$  coefficients for its description, i.e.

$$\begin{aligned} |\psi\rangle &= (a_{01} |0\rangle_1 + a_{11} |1\rangle_1) \otimes (a_{02} |0\rangle_2 + a_{12} |1\rangle_2) \otimes \dots \otimes (a_{0N} |0\rangle_N + a_{1N} |1\rangle_N), \\ &= a_{01}a_{02}\dots a_{0N} |00\dots 0\rangle + a_{01}a_{02}\dots a_{1N} |00\dots 1\rangle + a_{11}a_{12}\dots a_{1N} |11\dots 1\rangle, \\ &= a_0 |00\dots 0\rangle + a_1 |00\dots 1\rangle + \dots + a_L |11\dots 1\rangle, \end{aligned} \quad (1.2)$$

where  $a_0 = a_{01}a_{02}\dots a_{0N}$ ,  $a_1 = a_{01}a_{02}\dots a_{1N}$  and similarly,  $a_L = a_{11}a_{12}\dots a_{1N}$ .

The basis in equation (1.2) is known as the computational basis, and is more conveniently notated as  $|00\dots 0\rangle = |0\rangle$ ,  $|00\dots 1\rangle = |1\rangle = \dots$ ,  $|11\dots 1\rangle = |L\rangle$ . In this representation, equation (1.2) thus becomes

$$|\psi\rangle = a_0 |0\rangle + a_1 |1\rangle + \dots + a_L |L\rangle. \quad (1.3)$$

Therefore, the Hilbert space spanned by  $N$  qubits is a  $L=2^N$  dimensional space.

Since Pauli matrices form a complete basis for a vector in  $2 \times 2$  space, any operator acting on a qubit can be expressed as a linear combination of Pauli matrices [Quantum Walks and search algorithms, Renato Portugal]. The action of a Pauli matrix,  $\sigma^\alpha$ , where  $\alpha \in \{x, y, z\}$  on the  $i^{th}$  of the  $N$  qubits is represented as  $\sigma_i^\alpha$ . Since the state in equation (1.2) is a product state, the Pauli operator  $\sigma_j^\alpha$  can act just on the the  $j^{th}$  qubit, while the other qubits are acted upon by identity matrices  $\mathbb{I} = \begin{pmatrix} 1 & 0 \\ 0 & 1 \end{pmatrix}_{i \neq j}$ .

## 1.2 Optimization Problems

Mathematically, an optimization problem comprises of a cost function,  $f_0(x)$  involving N variables  $x_1, x_2, x_3, \dots, x_N$ , such that  $x = (x_1, \dots, x_N)$ . The goal, then, is to find the solution  $x_0$  that optimizes the cost function (generally, interpretable in terms of energy), subjected to a certain number of constraints  $f_i(x_1, \dots, x_k)$ , each imposed to a set of k variables (k-SAT problems) [Convex Optimization, Stephen Boyd (book)]. These multiple constraints, however, can cause frustration in the system, which can give rise to many local minima. This makes the determination of the optimal solution harder [Optimization using quantum mechanics: quantum annealing through adiabatic evolution: Santoro and Tosatti].

For finding the optimal solution, the whole spectrum of the cost function needs to be explored. This requires that the system should be able to escape from a local minimum, if it gets trapped in one, during this course. The method of simulated annealing was therefore devised [Kirkpatrick S, Gelatt C D Jr and Vecchi M P 1983 Science 220 671], where adding thermal fluctuations to the cost function, keeps the system from getting trapped in the local minima. If the barrier potential diverges or becomes very high, this approach can no longer be helpful. However, the quantum tunnelling effect can still allow for the search of global minima of a function of many Boolean variables by escaping from the poor local minima through tunnelling. It was in this spirit that the technique of quantum annealing was originally devised by B.Apolloni, C.Carvalho and D.de Falco in 1988 [Quantum stochastic optimization, Appoloni, Carvalho, de Falco].

## 1.3 Quantum Annealing

Quantum annealing was conceived with the idea of encoding the solution of combinatorial optimization problems in the ground state of a quantum Hamiltonian [Tameem Albash, Lidar: Adiabatic Quantum Computation]. The cost function can then be mapped on to the Ising model of spins, making use of the external magnetic field  $h_i^z$  and the spin couplings  $J_{ij}^z$  of the model. Thus, the optimization problem can be expressed in the terms of the following Hamiltonian:

$$H_P = - \sum_{i=1}^N h_i^z \sigma_i^z - \sum_{\langle i,j \rangle} J_{ij}^z \sigma_i^z \sigma_j^z, \quad (1.4)$$

where  $\sigma_i^z$  denotes the z component of Pauli-spin matrix acting on the  $i^{th}$  spin, and the set  $\langle i, j \rangle$  represents the set of pairwise couplings.

Although the Hamiltonian in equation (1.4) is a 2-local Hamiltonian, the solution for problems with higher order interactions ( $k \geq 3$ ) can still be encoded in the ground state of the Ising Hamiltonian by combining  $\sigma_k^z$  terms into products, such that at each point there are just two terms effectively, but at the expense of imposing more constraints to the cost function. This can lead to a large overhead in the number of variables [Perspectives of quantum annealing :Methods and implementations]. For the present work, we shall confine ourselves to 2-SAT problems.

The recipe for the annealing algorithm consists of starting with an initial Hamiltonian  $H_I$ , whose ground state can be easily determined and realised. Most commonly used is the transverse field Hamiltonian:

$$H_I = - \sum_{i=1}^N h_i^x \sigma_i^x. \quad (1.5)$$

The ground state for  $H_I$  is therefore the uniform superposition state:

$$|\psi\rangle = \frac{1}{(\sqrt{2})^N} (|0\rangle + |1\rangle)_1 * (|0\rangle + |1\rangle)_2 * \dots * (|0\rangle + |1\rangle)_N. \quad (1.6)$$

The Hamiltonian is then slowly swept towards the problem Hamiltonian, with the means of an annealing parameter, say s, defined as  $s = t/T$ , where t is the instantaneous time, and T is the total annealing time. The instantaneous Hamiltonian,  $H(t)$ , corresponding to the most straightforward annealing scheme, is then given by:

$$H(t) = (1 - s(t))H_I + s(t)H_P. \quad (1.7)$$

Figure (1.1) shows the chosen annealing scheme in terms of the annealing parameter.

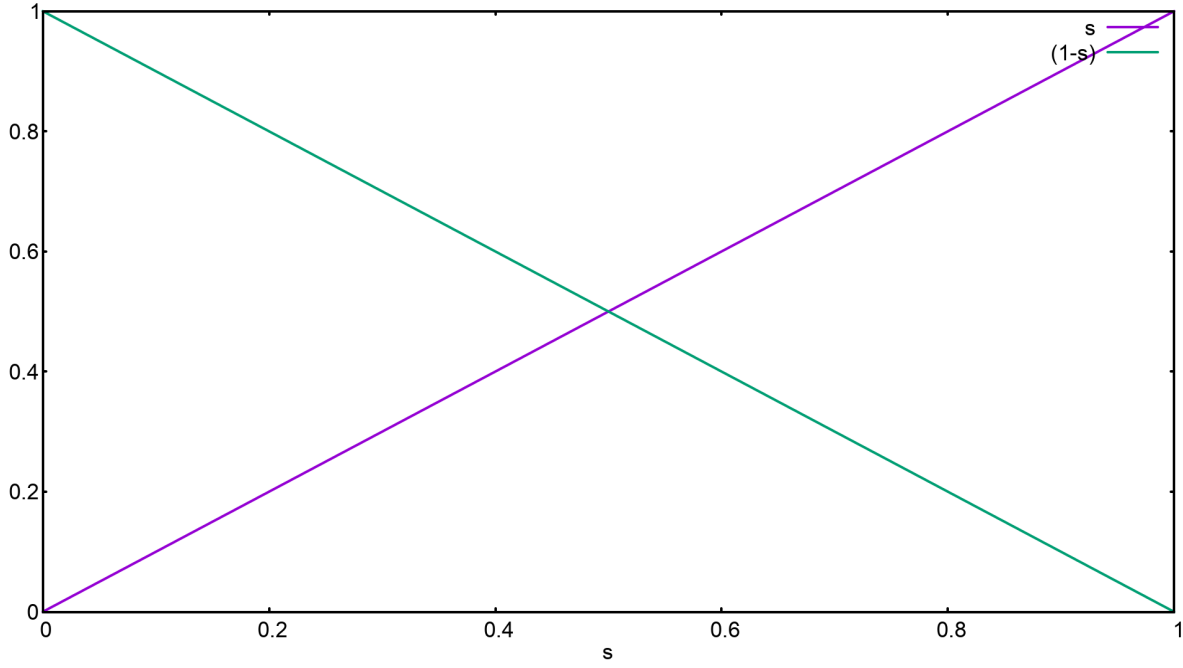


Figure 1.1: The linear annealing scheme chosen, in terms of the annealing parameter  $s$ .

Therefore, the instantaneous Hamiltonian transitions from the initial Hamiltonian,  $H(t = 0) = H_I$  to the problem Hamiltonian,  $H(t = T_A) = H_P$ .

According to the **quantum adiabatic theorem**, the instantaneous state of the system stays close to the ground state of Hamiltonian  $H(t)$ , if one starts with ground state of the initial Hamiltonian and if the driving from the initial Hamiltonian to the problem Hamiltonian is slow enough for the given minimum energy gap,  $\Delta_{min}$ , between the ground state and the first excited state of the Hamiltonian  $H(t)$  for  $t \in [0, T_A]$ . [ADIABATIC QUANTUM COMPUTATION, Enej Ilievsk]. Mathematically, adiabatic theorem of evolution holds when

$$T_A \gg \Delta_{min}^{-2}, \quad (1.8)$$

where  $T_A$  is the total annealing time. [Perspectives of quantum annealing: Methods and implementations]. Thus, the problem of finding the optimal solution reduces to the problem of solving the time dependent Schrödinger equation for the resulting  $H(t)$  (equation 1.7):

$$i \frac{\partial}{\partial t} |\psi\rangle = H(t) |\psi\rangle. \quad (1.9)$$

However, the process of evolution, starting from the trivial ground state of the initial Hamiltonian and going to a non-trivial ground state of the problem Hamiltonian, is accompanied by a quantum phase transition. For such a transition, the minimum gap  $\Delta_{min}$  can be assumed to follow

$$\Delta_{min} \propto e^{-cN}, \quad (1.10)$$

for a positive constant  $c$  and  $N$  number of spins. [Perspectives of quantum annealing: Methods and implementations]. Substituting equation (1.10) in equation (1.8),

$$T \gg e^{2cN}, \quad (1.11)$$

i.e., the total annealing time required for the evolution to be adiabatic grows exponentially with the number of spins. This approach is therefore rendered unsuitable for systems with large number of spins.

However, altering the annealing scheme can help overcome this difficulty of an exponential increase in the computational resources with the number of variables [Perspectives of quantum annealing: Methods and implementations, Adiabatic quantum computation: Tameem Albash, Quantum Adiabatic Evolution Algorithms with Different Paths: Farhi, Different strategies for Optimization Using the Quantum Adiabatic Algorithm: Farhi, Non-stoquastic Hamiltonians and quantum annealing of an Ising spin glass]. In this work we include a third Hamiltonian,

the Trigger Hamiltonian -  $H_T$  in the time dependent Hamiltonian  $H(t)$  (equation 1.7)[Farhi-Goldstein, Farhi (Different), Review, Non-stoquastic]. The trigger Hamiltonian is constituted by the transverse spin couplings  $J_{ij}^x$ . Moreover,  $H_T$  should vanish at both the start and end of the annealing process, so that one can still start with the easily realizable ground state of the initial Hamiltonian, and the resulting state of the problem Hamiltonian remains unaffected. The instantaneous Hamiltonian thus takes the form:

$$H(t) = (1-s)H_I + g * s(1-s)H_T + sH_P, \quad (1.12)$$

where parameter  $g$  controls the strength of the added trigger.

Furthermore, for this thesis we deal with two types of trigger Hamiltonians - The ferromagnetic trigger (F) and the anti-ferromagnetic trigger (A), given as

$$H_T^F = - \sum_{\langle i,j \rangle} \sigma_i^x \sigma_j^x, \quad (1.13)$$

and

$$H_T^A = + \sum_{\langle i,j \rangle} \sigma_i^z \sigma_j^z, \quad (1.14)$$

with the same pairwise coupling set  $\langle i,j \rangle$  as for the problem Hamiltonian. As will be seen in the following chapters, adding these triggers alter the energy spectrum considerably, which in turn affects the overlap of the final state with the ground state in different ways.

There can be yet another approach for increasing the overlap of the final state obtained from the annealing process, with the ground state of the problem Hamiltonian. As seen in (1.8) for problems with small minimum gap  $\Delta_{min}$ , the annealing time required for the evolution to be adiabatic (so that the state of the system always stays close to the instantaneous ground state) can be very large. In such cases, even what otherwise looks like a reasonable time, might actually be short, causing the system to transit to the first excited state at the minimum gap anti-crossing. Since most of the amplitude of the state then lies in the first excited state, the overlap with the ground state might become negligible.

However, if one chooses much smaller annealing times, the state can leak to higher excited states of the spectrum, even before the minimum gap anti-crossing. This gives the system a chance to shift some amplitude of the wave function back to the ground state at the minimum gap. Furthermore, the system can even end in a superposition state consisting of higher energy levels. As a result of this non-adiabatic evolution, the final state can have more chances of having a larger overlap with the ground state of the instantaneous Hamiltonian, than in the case of it closely following the first excited state with vanishing overlap with the ground state. This observation has been confirmed in the work by [Farhi et al: Different Perspectives], where reducing the total annealing time in problems with very small success probabilities, increases the probability of finding the final state close to the ground state of the problem Hamiltonian.

The following sections focus on two approaches that have been used in this work to solve the time-dependent Schrödinger equation. Suzuki-Trotter product formula has been adopted to track the evolution of the state, and to compute the overlap of the final state with the already determined ground state of the problem Hamiltonian. The full diagonalization method, on the other hand, has been used to calculate the errors involved in using the Suzuki-Trotter approximation, and to determine the energy spectra and minimum gaps for  $H(t)$  for  $t \in [0, T_A]$ , where  $T_A$  is the total annealing time.

## 1.4 Exact Diagonalization

This method consists of determining the eigenvalues and eigenvectors of the Hamiltonian matrix, which is a  $L \times L$  ( $2^N \times 2^N$ ) matrix, at each time step.

For constructing the Hamiltonian matrix at time step  $t \in [0, T_A]$ , all the basis vectors in the computational basis are acted upon by the instantaneous Hamiltonian, given by equation (1.12). The action of the Hamiltonian on the  $i^{th}$  basis vector corresponds to the  $i^{th}$  column of the Hamiltonian matrix, e.g. for  $|\psi\rangle = (1, 0, \dots, 0)^T$ ,  $H|\psi\rangle$  gives the first column of the Hamiltonian matrix.

The resulting matrix is then diagonalized to obtain the eigenvalues  $\Lambda$ , and unitary matrix of the eigenvectors,  $V$ . Since  $V^\dagger H V = \Lambda$ , the unitary evolution operator  $U(t) = e^{-itH} = V e^{-it\Lambda} V^\dagger$ .

This approach, however, has some serious limitations. Firstly, the memory requirement to store the Hamiltonian matrix grows exponentially with the number of qubits. Additionally, the full diagonalization takes  $\mathcal{O}(2^{3N})$  floating-point operations [Kristel-Hans paper]. Therefore, this method is rendered impractical for solving the time dependent Schrödinger equation for systems more than 20 qubits.

## 1.5 Suzuki-Trotter Product Formula

Since solving the time dependent Schrödinger equation requires to compute unitary matrix exponentials, Lie-Trotter-Suzuki product formula can be used to construct the following unitary approximations:

$$U(t) = e^{-itH} = e^{-it(H_1 + \dots + H_K)} = \lim_{m \rightarrow \infty} \left( \prod_{k=1}^K e^{-itH_k/m} \right)^m. \quad (1.15)$$

For sufficiently small time step  $t$ , the first order approximation for  $U(t)$  in equation (1.15) is

$$\tilde{U}_1(t) = e^{-itH_1} \dots e^{-itH_K}, \quad (1.16)$$

which holds good for  $t \|H\| << 1$ .

For an improved accuracy, a second order approximation is made to  $U(t)$  in equation (1.15), using  $\tilde{U}_1(t)$  from (1.16):

$$\tilde{U}_2(t) = \tilde{U}_1^\dagger(-t/2)\tilde{U}_1(t/2) = e^{-itH_K/2} \dots e^{-itH_1/2} e^{-itH_1/2} \dots e^{-itH_K/2}. \quad (1.17)$$

If  $\tilde{U}_1(t)$  is unitary, so is  $\tilde{U}_2(t)$ . For unitary  $\tilde{U}_2(t)$ , the measure of error, calculated using the absolute difference between  $U(t)$  and  $\tilde{U}_2(t)$  grows cubically in  $t$  [Kristel-Hans paper, 62 from there], i.e.

$$\|U(t) - \tilde{U}_2(t)\| \leq ct^3 \quad (1.18)$$

for a positive constant  $c$ . If the whole annealing process requires  $n$  such time steps, the involved error becomes

$$\|U(t) - \tilde{U}_2(t)\| \leq nct^3. \quad (1.19)$$

Since  $nt = T_A$ , (1.19) is equivalent to

$$\|U(t) - \tilde{U}_2(t)\| \leq cnT_A t^2 = c't^2 \quad (1.20)$$

Substituting (1.5), (1.13 or 1.14) and (1.4) in (1.12), we obtain:

$$H(t) = (1-s) \left( - \sum_{i=1}^N h_i^x \sigma_i^x \right) + g * s(1-s) \left( \mp \sum_{<i,j>} \sigma_j^x \right) + s \left( - \sum_{i=1}^N h_i^z \sigma_i^z - \sum_{<i,j>} J_{ij}^z \sigma_i^z \sigma_j^z \right). \quad (1.21)$$

The Hamiltonian is then decomposed as follows:

$$H = H_{single} + H_x + H_z, \quad (1.22)$$

where  $H_{single} = -(1-s) \left( \sum_{i=1}^N h_i^x \sigma_i^x \right) - s \left( \sum_{i=1}^N h_i^z \sigma_i^z \right)$ ,  $H_x = \mp(1-s) \left( \sum_{<i,j>} J_{ij}^x \sigma_i^x \sigma_j^x \right)$ , and  $H_z = -s \left( \sum_{<i,j>} J_{ij}^z \sigma_i^z \sigma_j^z \right)$ .

In general,

$$e^{i\mathbf{v} \cdot \boldsymbol{\sigma}} = \cos(v) \mathbb{1} + i \frac{\sin(v)}{v} \mathbf{v} \cdot \boldsymbol{\sigma}, \quad (1.23)$$

where  $\mathbb{1}$  represents the identity matrix, and  $v = \sqrt{v_x^2 + v_y^2 + v_z^2}$ . Then,

$$e^{-itH_{single}} = \prod_{i=1}^N e^{it[(1-s) \sum_i h_i^x \sigma_i^x + s \sum_i h_i^z \sigma_i^z]} = \prod_{i=1}^N \begin{pmatrix} \cos(th_i) + i \frac{sh_i^z}{h_i} \sin(th_i) & i \frac{(1-s)h_i^x}{h_i} \sin(th_i) \\ i \frac{(1-s)h_i^x}{h_i} \sin(th_i) & \cos(th_i) - i \frac{sh_i^z}{h_i} \sin(th_i) \end{pmatrix} \quad (1.24)$$

where  $h_i = \sqrt{(1-s(t))^2 h_i^x{}^2 + s(t)^2 h_i^z{}^2}$ .

The computational basis states are the eigenstates of the Pauli-z operator,  $\sigma_i^z$ . Thus  $e^{-itH^z}$  is a diagonal matrix in the computational basis, and its action on the input state changes the phase of each of the basis vectors. As  $H^z$  is a sum of pair interactions, it is trivial to implement this operation as a sequence of multiplications by  $4 \times 4$  diagonal matrices [Kristel-Hans paper].

The same approach can be adopted for implementing  $H_x$  operations as well, by using the rotation operators  $Y_j$  as follows. Writing  $Y = \prod_{i=1}^N Y_i$ , we obtain

$$e^{-itH^x} = \bar{Y}Y e^{-itH^z} \bar{Y}Y = \bar{Y} e^{it \sum_{\langle i,j \rangle} J_{ij}^x \sigma_i^z \sigma_j^z} Y. \quad (1.25)$$

# Chapter 2

## Landau-Zener Tunnelling

The Landau-Zener model gives the solution for the dynamics of the magnetization of a 2-level spin system, under the action of slowly reversing external magnetic field at zero temperature [Hans Landau-Zener paper]. Consider, the following single spin-  $\frac{1}{2}$  Hamiltonian as an example:

$$H_{LZ}(t) = -\Gamma\sigma_x - ct\sigma_z, \quad (2.1)$$

where  $\Gamma$  sets the scale of the splitting between the two energy levels, and  $c$  is the sweep rate of the applied magnetic field, i.e  $H(t)=ct$ . Thus for a field switching its value from  $-H_0$  to  $H_0$  in time  $T$ ,  $c = \Delta H/T = 2H_0/T$ .

Now, for large negative times  $t$ , and  $|H(t)| \leq |\Gamma|$ ,  $H_{LZ}(t) \approx ct\sigma_z$ . Thus, the spin-down state,  $|\psi\rangle$  is close to the ground state of the Hamiltonian, as  $ct\sigma_z|\downarrow\rangle = -ct|\downarrow\rangle$ . As  $t$  goes to infinity,  $H_{LZ}(t) \approx -ct\sigma_z$ , so that the ground state now lies close to the spin up state, as  $-ct\sigma_z|\uparrow\rangle = -ct|\uparrow\rangle$ . According to quantum adiabatic theorem the state of the system should always lie close to the instantaneous ground state of the Hamiltonian  $H(t)$ , if one starts with the ground state and if the field is changed slowly enough. However, there is a finite probability that the state transits to a higher excited level during the sweep. The probability,  $p'$ , for this nonadiabatic transition (Landau-Zener tunnelling), as given by the Landau-Zener formula, is

$$p' = \exp\left(\frac{-\pi\Gamma^2}{c}\right). \quad (2.2)$$

Therefore, the probability,  $p$ , that the state of the system follows instantaneous ground state of the Hamiltonian adiabatically, by changing the magnetization state of the system, in accordance to the reversing field,  $H(t)$ , is

$$p = 1 - p' = 1 - \exp\left(\frac{-\pi\Gamma^2}{c}\right). \quad (2.3)$$

If the energy splitting between the ground state and the first excited state of the Hamiltonian at the anticrossing is denoted by  $\Delta E$ , then it can be observed that  $\Delta E = 2\Gamma$ . Thus, in terms of  $\Delta E$ , equation(2.4) becomes

$$p = 1 - \exp\left(\frac{-\pi\Delta E^2}{4c}\right). \quad (2.4)$$

The deviation from the ground state occurs at  $H \approx 0$ , with a probability  $p'$ , and is accompanied by a step in the magnetization. This step depends on both the

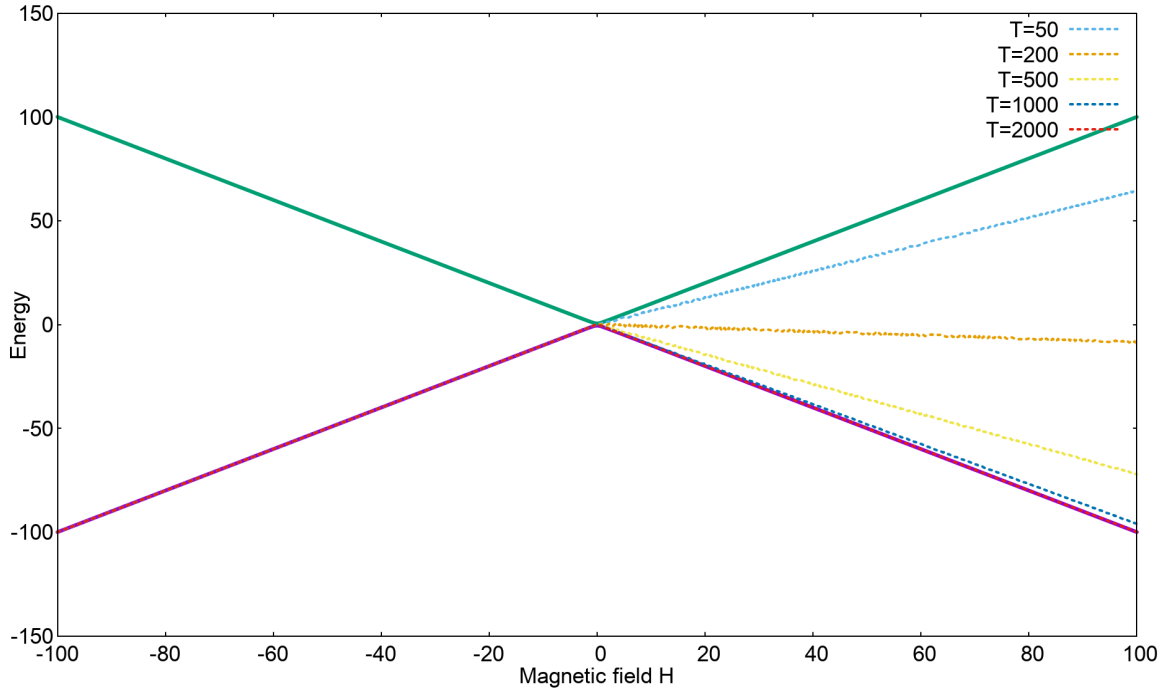


Figure 2.1: Energy spectrum for single qubit Hamiltonian in equation (2.1), with instantaneous energy of the state of the system with different sweeping times.  $\Gamma = 0.5$ ,  $H_0 = 100$ .

energy splitting  $\Gamma$ , and the sweep rate  $c$  [Hans, On Quantum Simulators and Adiabatic Quantum Algorithms: Sarah Mostame?].

For a simple 2-level system where  $\Gamma$  is chosen to be 0.5 and the field is swept from a value from -100 to 100, figure (2.1) gives the energy spectra for the Hamiltonian in equation (2.1). Figure (2.1) also shows the energy evolution of the state of the system corresponding to different times  $T$ , chosen for the sweeping the field. As is evident from the figure, the probability of the state of the system staying close to the ground state increases with decreasing speed (increasing  $T$ ), as expected from (2.3). For a sweeping time of  $T=500$ , figure (2.2) shows the instantaneous magnetization state of the system.

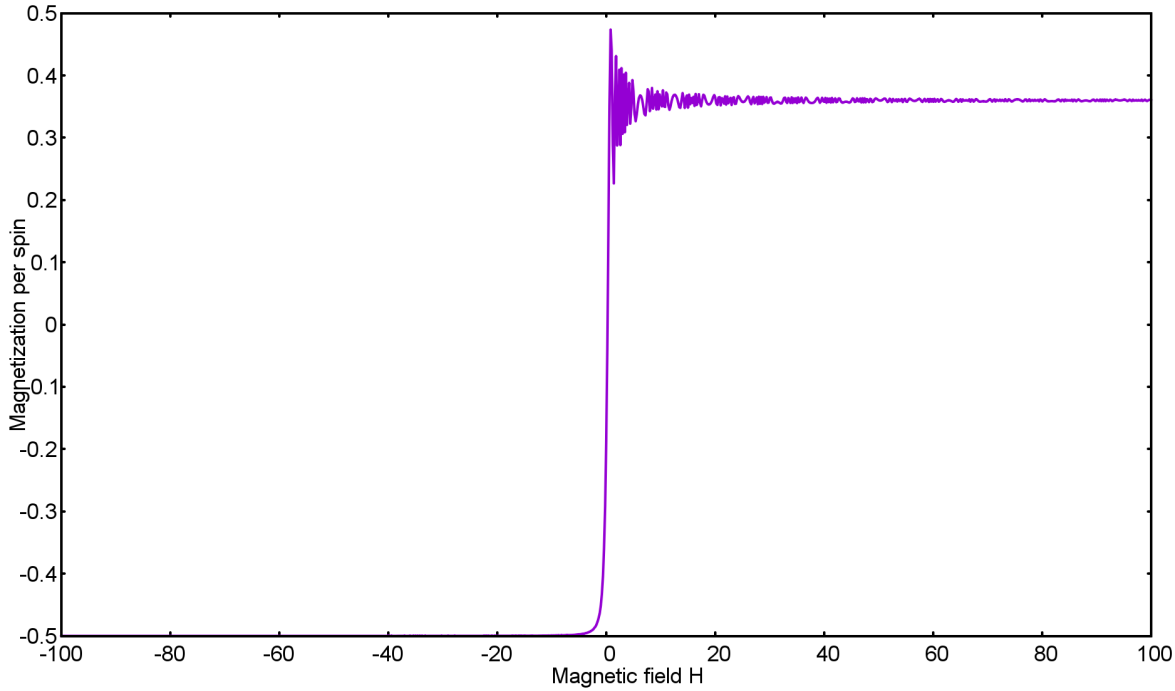


Figure 2.2: Instantaneous magnetization of the system state for  $\Gamma = 0.5$ ,  $H_0 = 100$  and  $c=0.4$ .

Comparing figures (2.1) and (2.2), it can be observed that the step in the magnetization corresponds to the position of the anticrossing between the ground state and the first excited state in the energy spectrum.

For verifying equation (2.3), the overlap of the resulting state was computed with the ground state of the Hamiltonian, for different sweeping times. Figure (2.3) shows the result obtained.

From equation (2.3),  $p = 1 - e^{-\frac{\pi\Gamma^2}{2H_0}T} = 1 - e^{-aT}$ , where  $a = \frac{\pi\Gamma^2}{2H_0}$ . For the chosen parameters,  $a$  was calculated to be  $3.926 \times 10^{-3}$ . This value is found to be in agreement with the value  $3.198 \times 10^{-3}$ , obtained for the fitting parameter in figure (2.3).

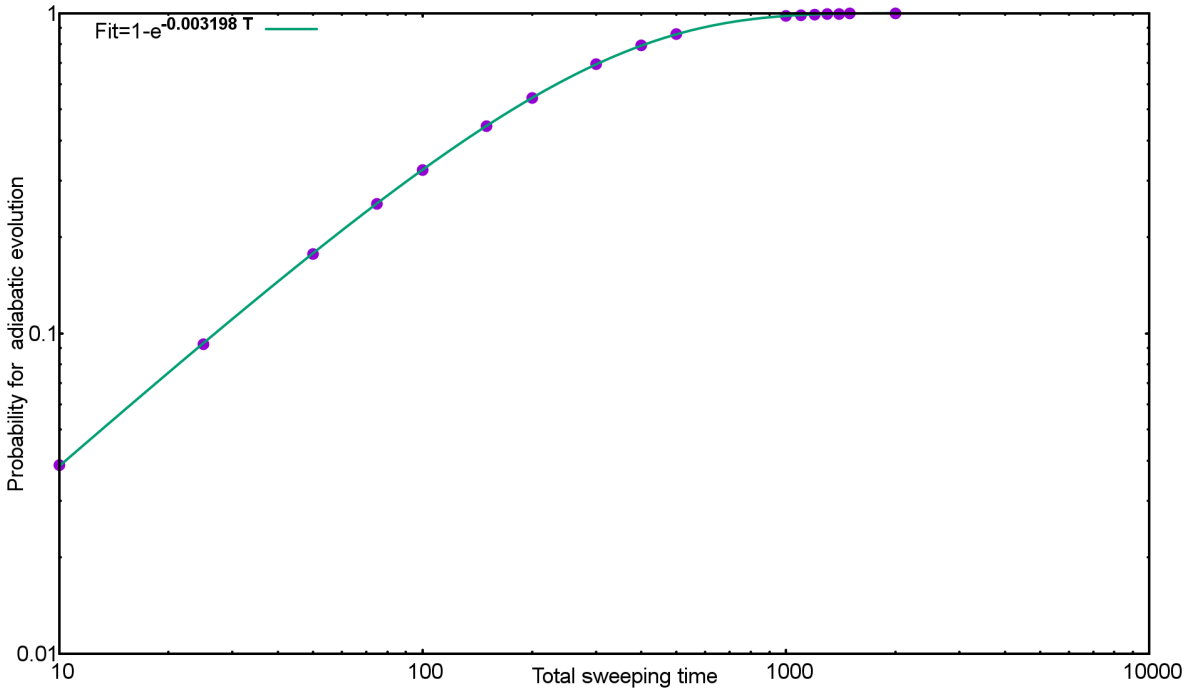


Figure 2.3: Probability for adiabatic evolution as a function of different sweep times for  $\Gamma = 0.5$ .

Although both Quantum annealing and Landau-Zener model deal with time dependent Hamiltonians, and the main task consists of studying the evolution of the state of the system under its action, there are two major points of difference. Landau-Zener formula is applicable to 2-level systems, and the process of reversing the magnetic field is ideally carried over an infinite amount of time. On the other hand, quantum annealing problems generally consist of more than two energy levels, and the evolution is carried out for a limited time, i.e. from  $s=0$  to  $s=1$  in terms of the annealing parameter:  $s=t/T_A$ , where  $T_A$  is the total annealing time.

Despite of these differences, Landau-Zener formula, with minor modifications, can be used as a measure to test if the evolution during the process of quantum annealing is adiabatic. If the dependence of success probability,  $p$ , is found to satisfy (2.4) the evolution can be regarded as adiabatic.

The Ising model in a transverse field, encoding the optimization problem for quantum annealing involving  $N$  variables is one of the simplest microscopic models for uniaxial magnets. Consider, for example, the following Hamiltonian

$$H = -J \sum_{\langle i,j \rangle} \sigma_i^z \sigma_j^z - \Gamma \sum_i \sigma_i^x - H(t) \sum_i \sigma_i^z, \quad (2.5)$$

where set  $\langle i,j \rangle$  defines the interactions between pairs of spins in the cluster. The modified probability for the system state consisting of  $N$  spins to stay close to the ground state is then given by [Hans paper, 5-6 reference there]

$$p_N = 1 - p' = 1 - \exp\left(\frac{-\pi \Delta E^2}{4Nc}\right). \quad (2.6)$$

Choosing a two spin system, with  $\Gamma = 0.5$ ,  $J = 3$ , and  $H_0 = 100$ , figure (2.4) shows the instantaneous energy spectra as a function of the magnetic field.

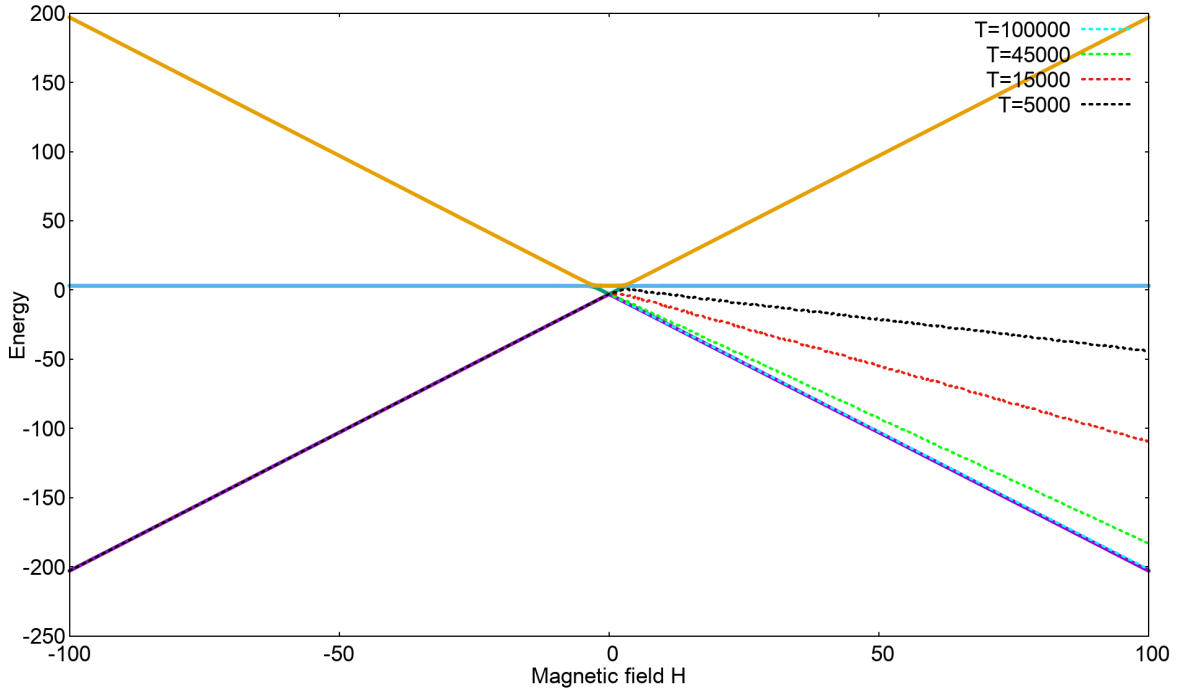


Figure 2.4: Energy spectrum for two spin Hamiltonian in equation (2.5), with instantaneous energy of the state of the system with different sweeping times.  $\Gamma = 0.5$ ,  $J = 3$ ,  $H_0 = 100$ .

Figures (2.5) and (2.6) show the instantaneous magnetization values for two different speeds. Similar to the case of a single spin Hamiltonian, the steps in the magnetization values correspond to the position of anticrossing between the energy levels of the spectrum, in this case as well. Other than the step in the magnetization at  $H \approx 0$ , in this case, the other step corresponds to the value of  $H$  where energy levels become nearly degenerate.

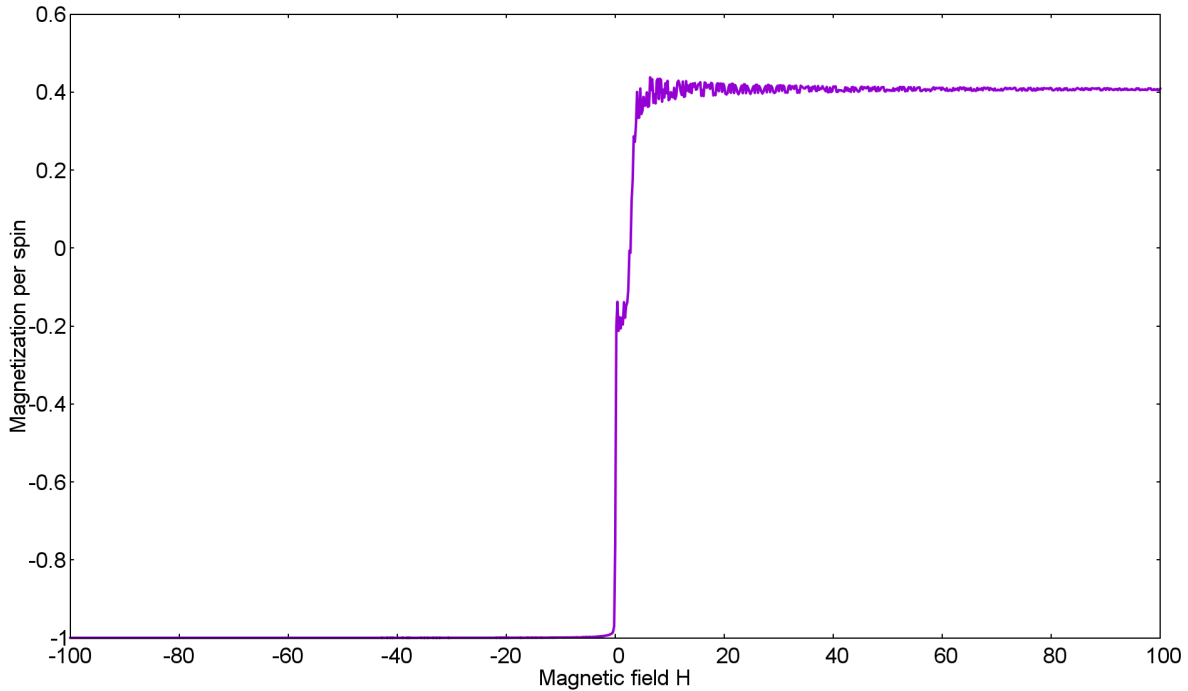


Figure 2.5: Instantaneous magnetization of the system state for  $\Gamma = 0.5$ ,  $H_0 = 100$  and  $c=0.02$ .

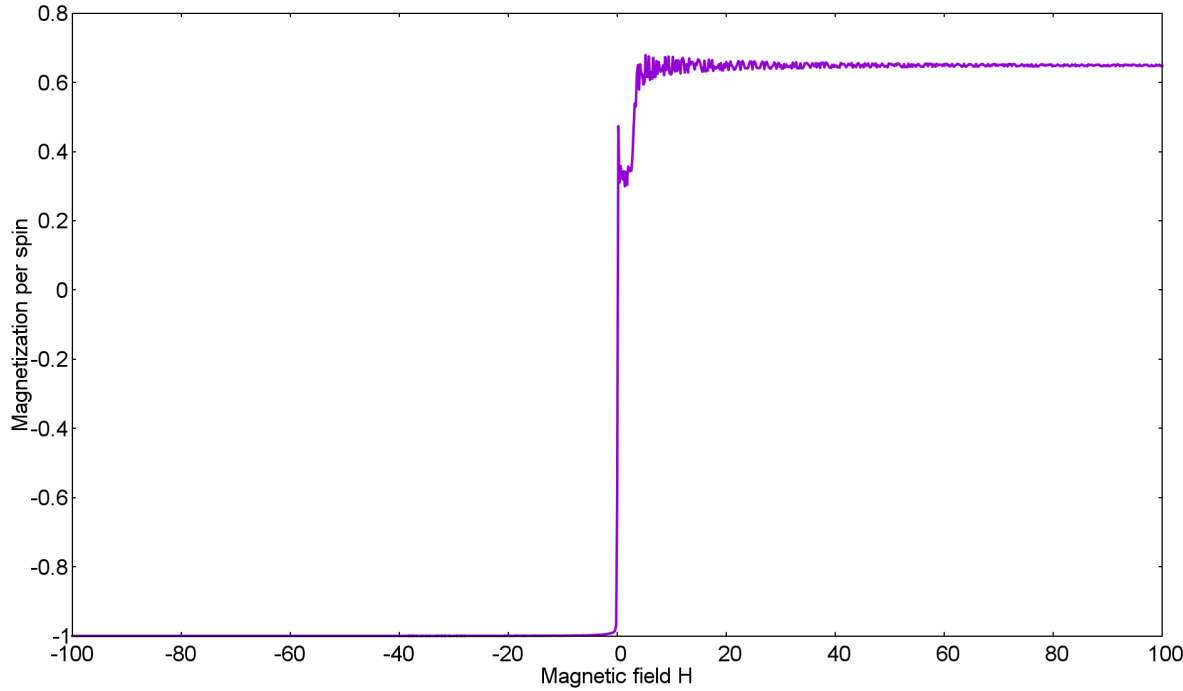


Figure 2.6: Instantaneous magnetization of the system state for  $\Gamma = 0.5$ ,  $H_0 = 100$  and  $c=0.01$ .

On increasing the total time for sweeping the field, i.e. decreasing the sweeping speed, the probability of staying in the ground state, by changing the state of magnetization should increase. This can be confirmed by comparing figures (2.5) and (2.6).

Finally, for verifying equation (2.6) the overlap of the resulting state with the ground state is computed for different times. Results obtained are shown in figure (2.7).

The value of minimum gap,  $\Delta E$  obtained was 0.162, which results in  $a = \frac{\pi \Delta E^2}{8\Delta H} = 5.182 \times 10^{-5}$ . The value of the fitting function obtained in figure (2.7) is  $5.239 \times 10^{-5}$ . Thus, Landau Zener formula is also found to hold for systems having more than two energy levels.

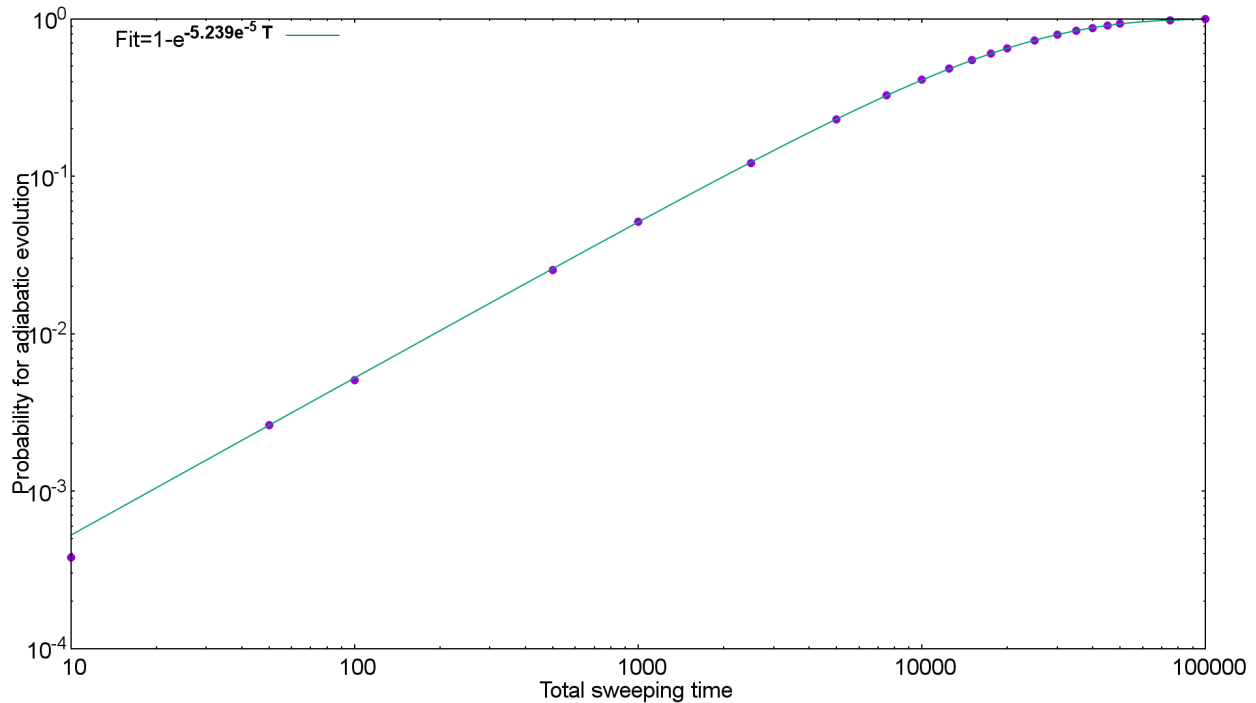


Figure 2.7: Probability for adiabatic evolution as a function of different sweep times for  $\Gamma = 0.5$  and  $J = 3$ .

Equation (2.6) will be used again as a check for adiabatic evolution in the subsequent chapters.



# Chapter 3

## Results with Original Hamiltonian

### 3.1 Second order

Since Suzuki-Trotter product formula is only an approximation to solve the time dependent Schrödinger equation, the error involved depends on the time interval  $t$  - the time step at which the evolution is computed (equation 1.19).

Thus, for checking if the evolution using the Suzuki-Trotter product formula is indeed second order, the dependence of the error should be verified to be quadratic in  $t$ , in accordance with equation (1.20).

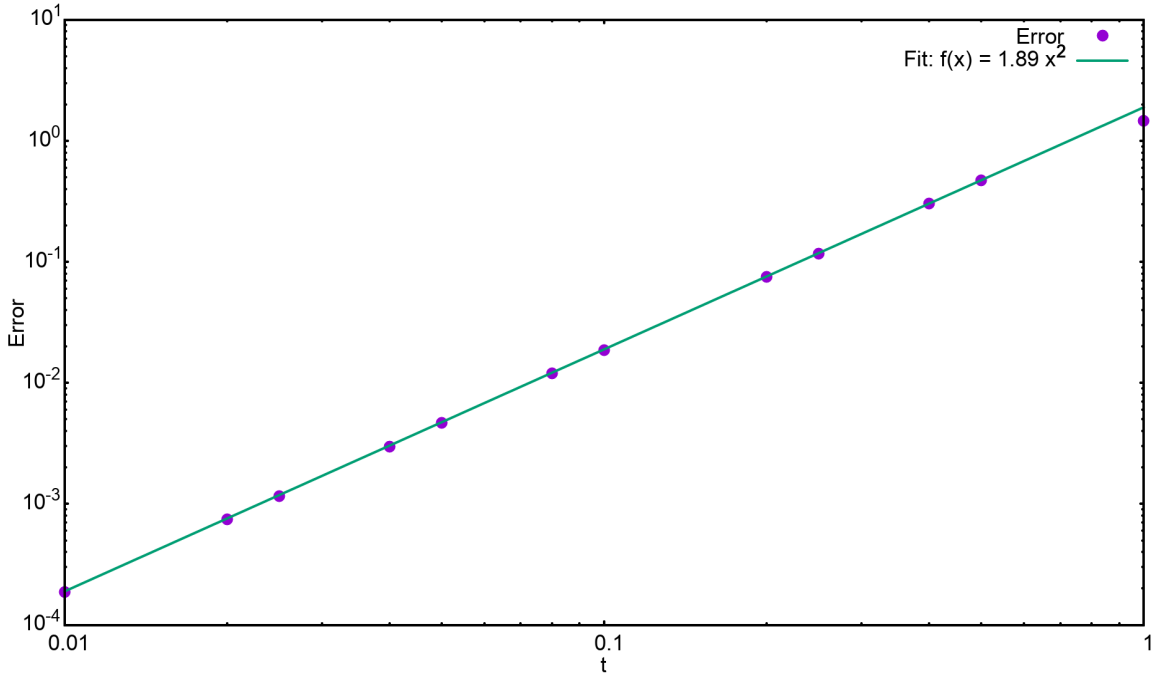


Figure 3.1: The error in Suzuki-Trotter formula relative to the full diagonalization method. The involved error grows quadratically in  $t$ .

Since the dependence of error on  $t$  can be approximated well by a straight line in the log scale, as shown in figure (3.1), the simulation implementing TDSE can be trusted to be following second order Suzuki-Trotter product formula.

For the course of this thesis, we worked with 8 spin and 12 spin 2-SAT problems. The first set had 91 unique problems, while the second set had 1000 such problems. All the problems had a predetermined unique ground state, and only one avoided crossing between the ground and the first excited state. The success probability was then obtained by calculating the overlap between the known ground state and the final state resulting from the code performing product evolution. Furthermore, for determining the energy spectra for specific problems, the exact diagonalization method was employed.

This chapter focusses on the results obtained for original annealing Hamiltonian, that is in the absence of any triggers.

For every problem belonging to both the sets, three annealing times were chosen to calculate the success probability. These correspond to  $T_A \in \{10, 100, 1000\}$ . For a given  $T_A$ , the resulting success probability is a function of the minimum energy gap,  $\Delta_{min}$ , between the ground and the first excited state. The smaller the value of the minimum energy gap, the smaller is the success probability expected to be, for an adiabatic sweep through the Hamiltonian in a fixed time  $T_A$ . Thus, the hardness of a problem can be estimated by its minimum energy gap.

As the first example, considered here is a 12-spin problem with high success probability,  $p = 0.9944$  for  $T_A = 100$ . Figure (3.2), shows the energy spectrum for this problem. The minimum energy gap,  $\Delta_{min}$  was found to be 0.4407 in this case. Also plotted in the figure are the instantaneous energy values obtained from annealing with the above-mentioned annealing times.

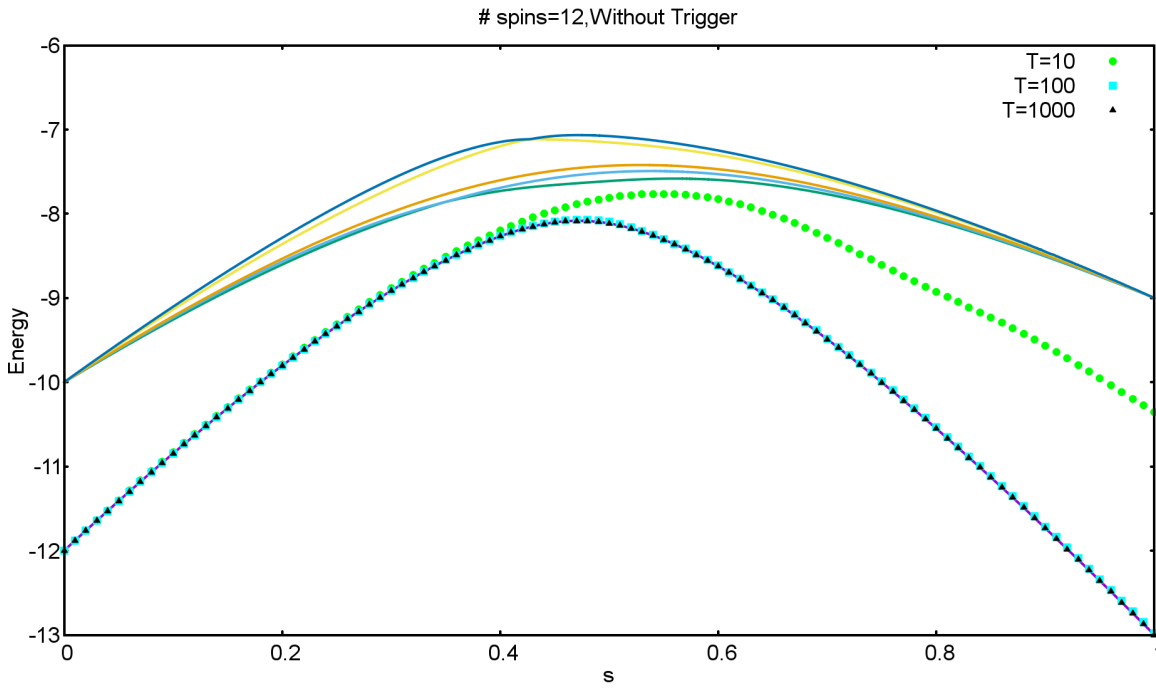


Figure 3.2: The energy spectrum for the selected problem, with instantaneous energy values corresponding to three annealing times. For  $T_A=100$ ,  $p$  was found to be 0.9944, while  $\Delta - min = 0.4407$ .

As expected, the overlap of the final state with the ground state of the problem Hamiltonian increases on increasing the total annealing time in figure (3.2).

Secondly, a 12-spin problem with small success probability,  $p = 0.0146$  at  $T_A = 100$ , was chosen. Figure (3.3) shows the energy spectrum and the instantaneous energy values corresponding to three annealing times, for this problem. It should be noted, that the minimum gap in figure (3.3) has decreased, to  $\Delta_{min} = 0.0312$ , in comparison to that in figure (3.2). This explains the decrease in success probability for same annealing time.

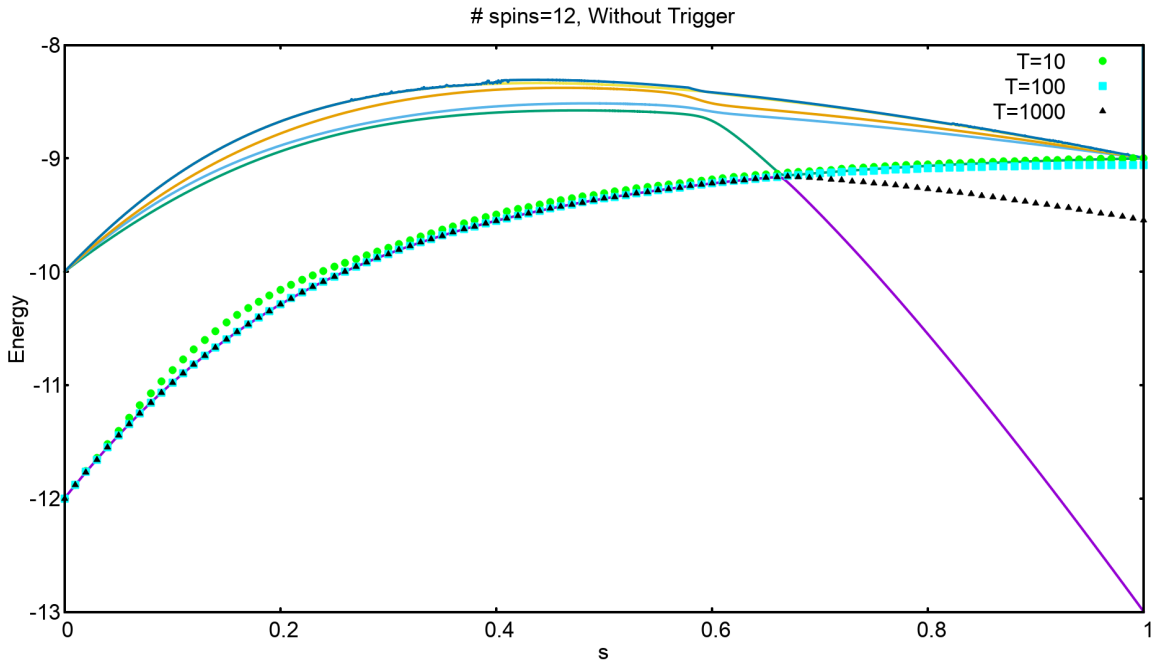


Figure 3.3: The energy spectrum for the selected problem, with instantaneous energy values corresponding to three annealing times. For  $T_A=100$ ,  $p$  was found to be 0.0146, while  $\Delta_{min} = 0.0312$ .

As the third case, another 12-spin problem with an intermediate success probability of  $p = 0.5199$  at  $T_A = 100$  has been considered. For this case too, the energy spectrum and the instantaneous energy values for the three annealing times was determined, as is shown in figure (3.4). As expected, the value of minimum gap is  $\Delta = 0.1573$  for this problem, which lies in between the above two cases.

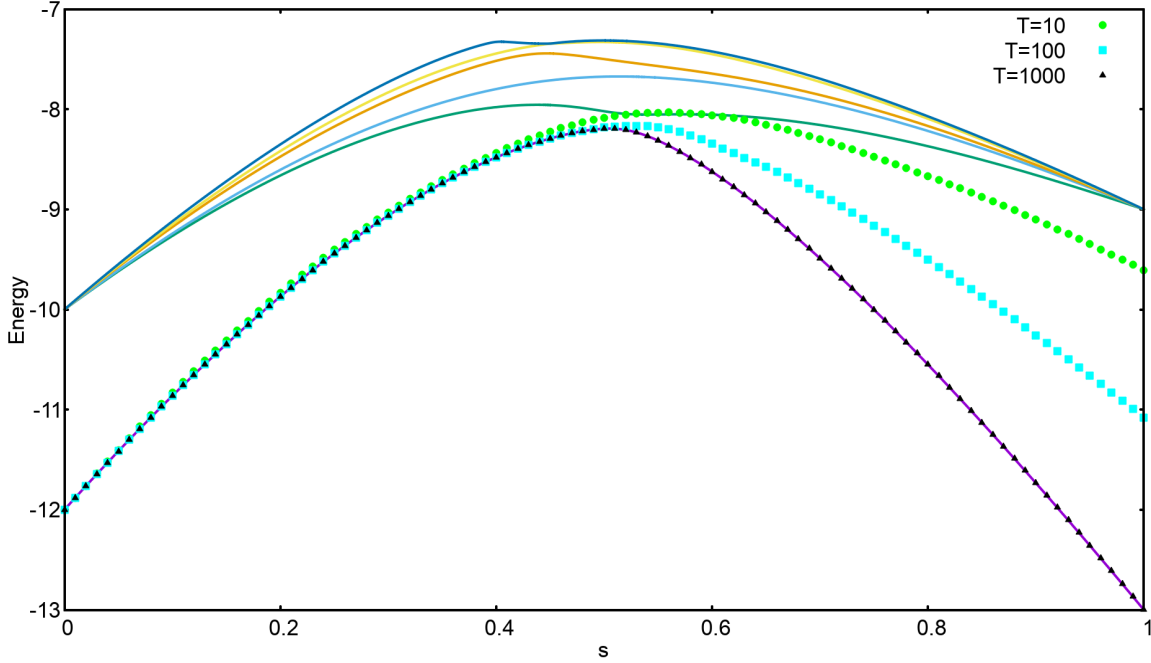


Figure 3.4: The energy spectrum for the selected problem, with instantaneous energy values corresponding to three annealing times. For  $T_A=100$ ,  $p$  was found to be 0.5199, while  $\Delta = 0.1573$ .

A similar trend was also obtained for 8-spin problems, where the cases with high success probability also were the ones with comparatively larger minimum energy gaps than cases with low success probability. As examples, three cases, with relatively large, small and intermediate success probabilities were chosen. The respective plots for their energy spectrum and the instantaneous energy values for the different annealing times are shown in the following figures (3.5, 3.6, 3.7).

The main feature of difference between the 12-spin and 8-spin problems is that the minimum energy gaps of the 8-spin problems were found to be larger than those of 12-spin problems. This can be understood with the help of equation (1.10), where the minimum gap is expected to close exponentially with increasing  $N$ . Even the gap corresponding to the case with smallest success probability in 8-spin problems (the smallest energy gap amongst 91 8-spin problems,  $\Delta_{min} = 0.4725$ ) is still larger than the the gap corresponding to the case with largest success probability in 12-spin problems (the largest energy gap amongst 1000 12-spin problems,  $\Delta_{min} = 0.4407$ ). Therefore, even an annealing time of  $T_A = 100$  yields a large success probability for almost all 8-spin cases.

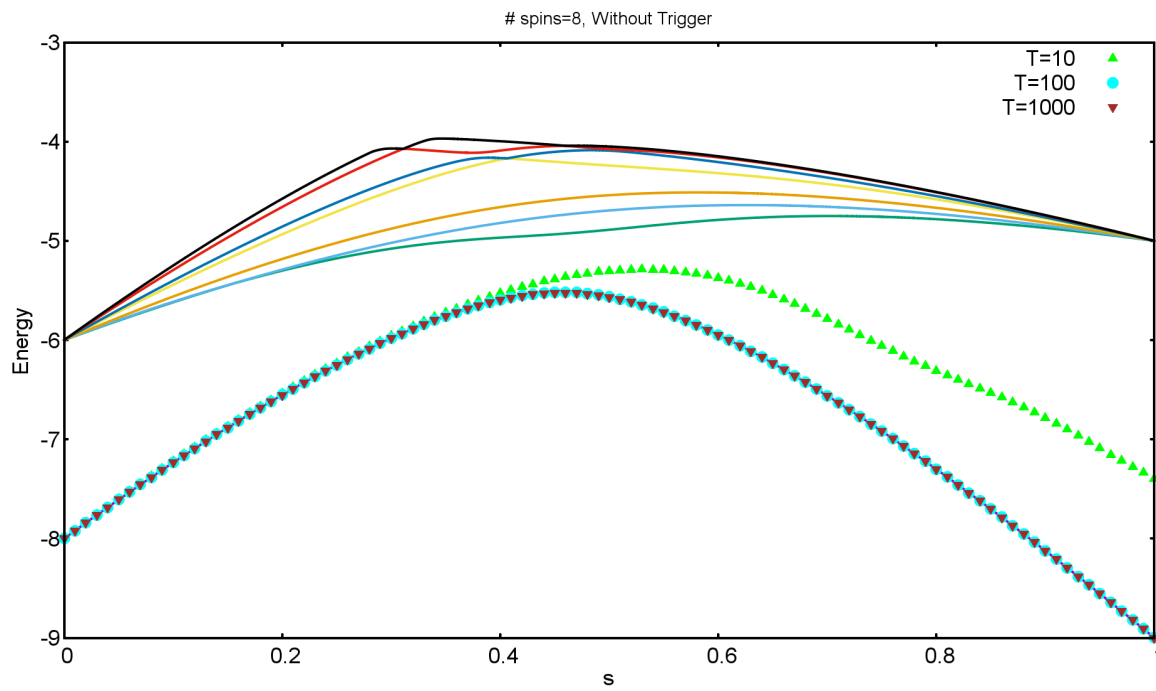


Figure 3.5: The energy spectrum for the selected problem, with instantaneous energy values corresponding to three annealing times. For  $T_A=100$ ,  $p$  was found to be 0.9999, while  $\Delta_{min} = 0.5875$ .

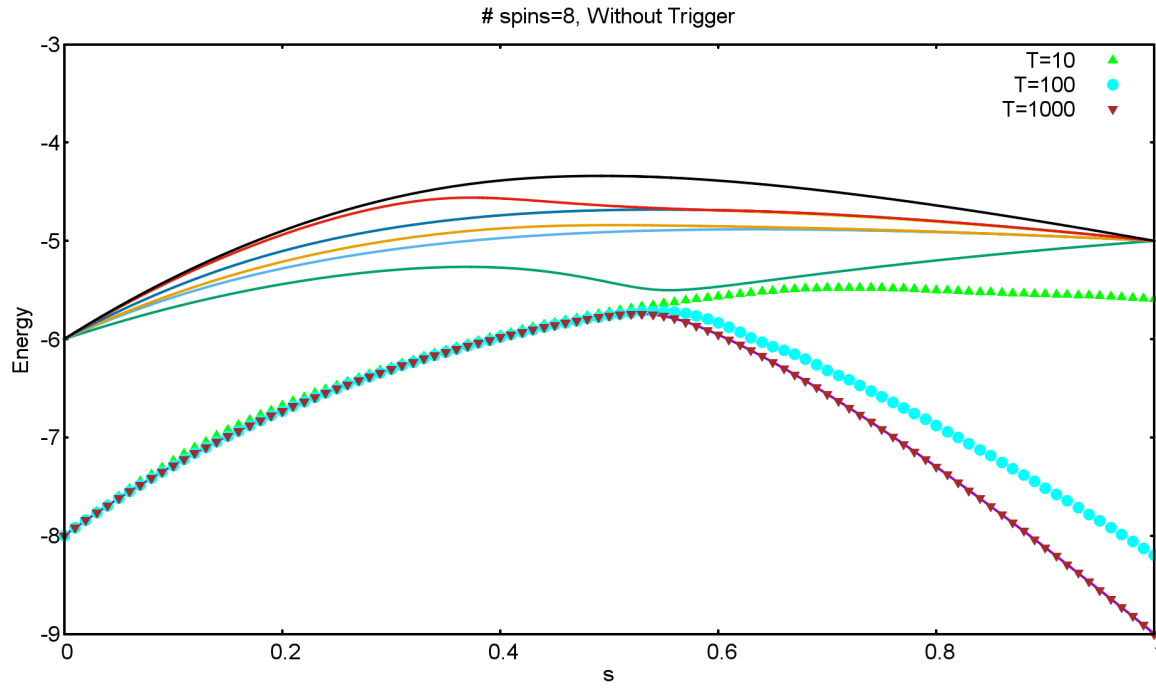


Figure 3.6: The energy spectrum for the selected problem, with instantaneous energy values corresponding to three annealing times. For  $T_A=100$ ,  $p$  was found to be 0.7994, while  $\Delta_{min} = 0.3225$ .

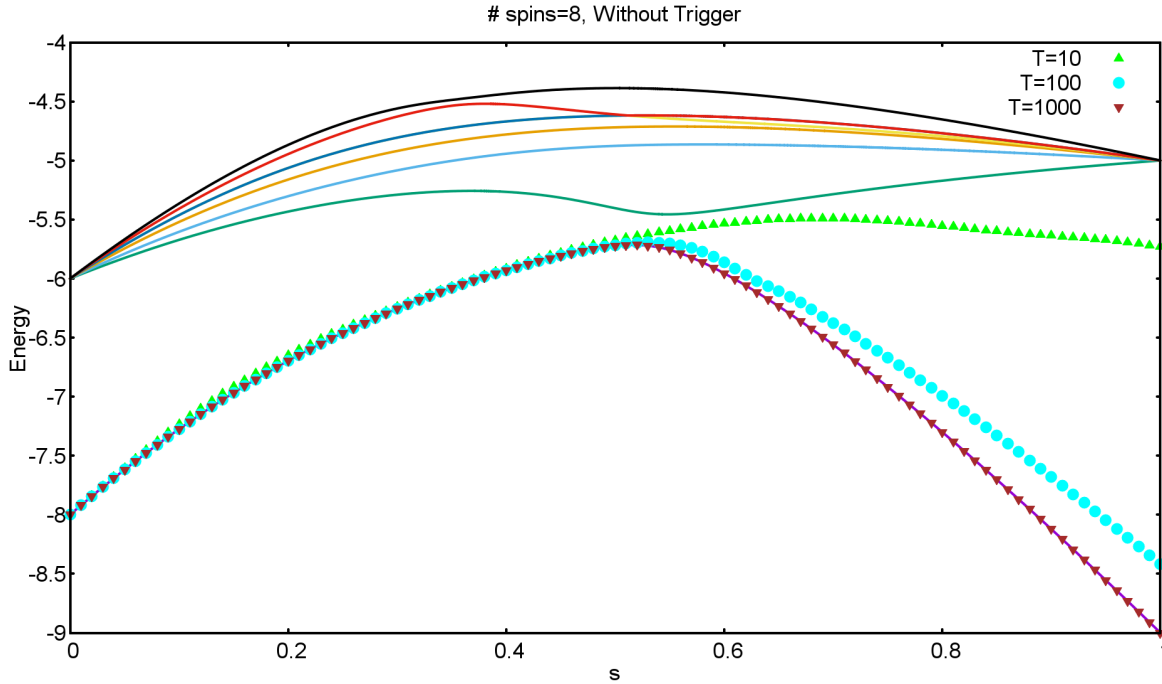


Figure 3.7: The energy spectrum for the selected problem, with instantaneous energy values corresponding to three annealing times. For  $T_A=100$ ,  $p$  was found to be 0.8549, while  $\Delta_{min} = 0.4725$ .

To obtain a rough estimate of the spread of the difficulty of the problems in the set being considered here, figure (3.8) shows a plot of the histogram of the probabilities of ending in the ground state of the problem Hamiltonian for an annealing time  $T_A = 100$ .

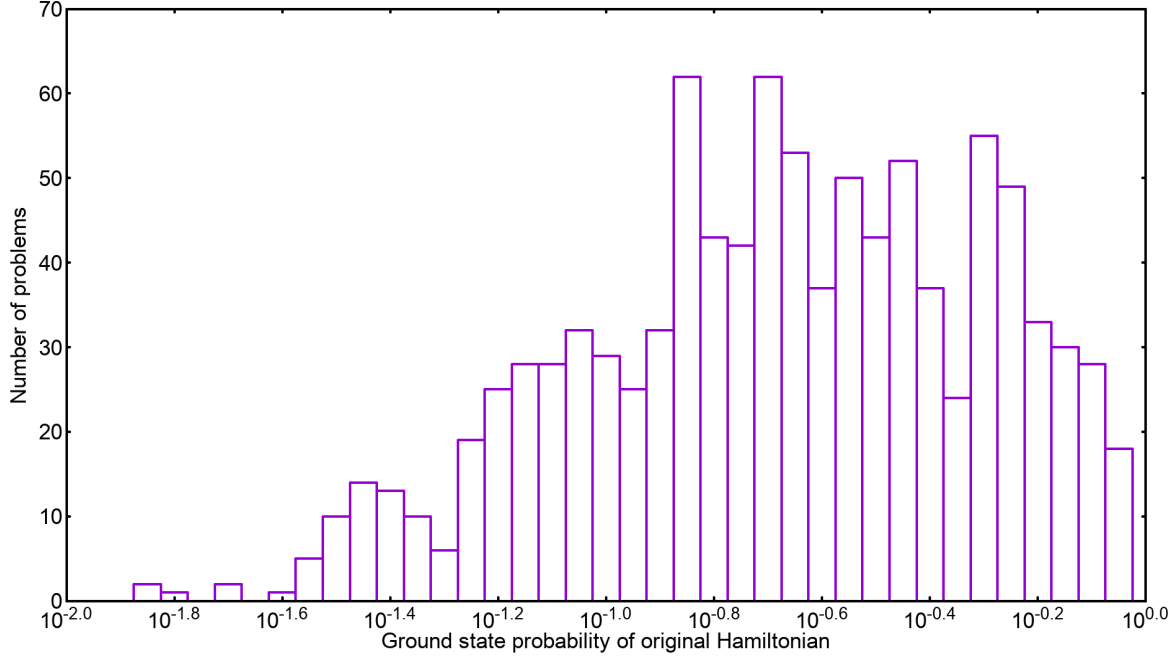


Figure 3.8: Histogram for success probability of the Hamiltonians without any triggers for 1000 12-spin problems and  $T_A=100$ .

The similar histogram for 8-spin problems is shown in figure (3.9) for an annealing time of  $T_A=10$ .

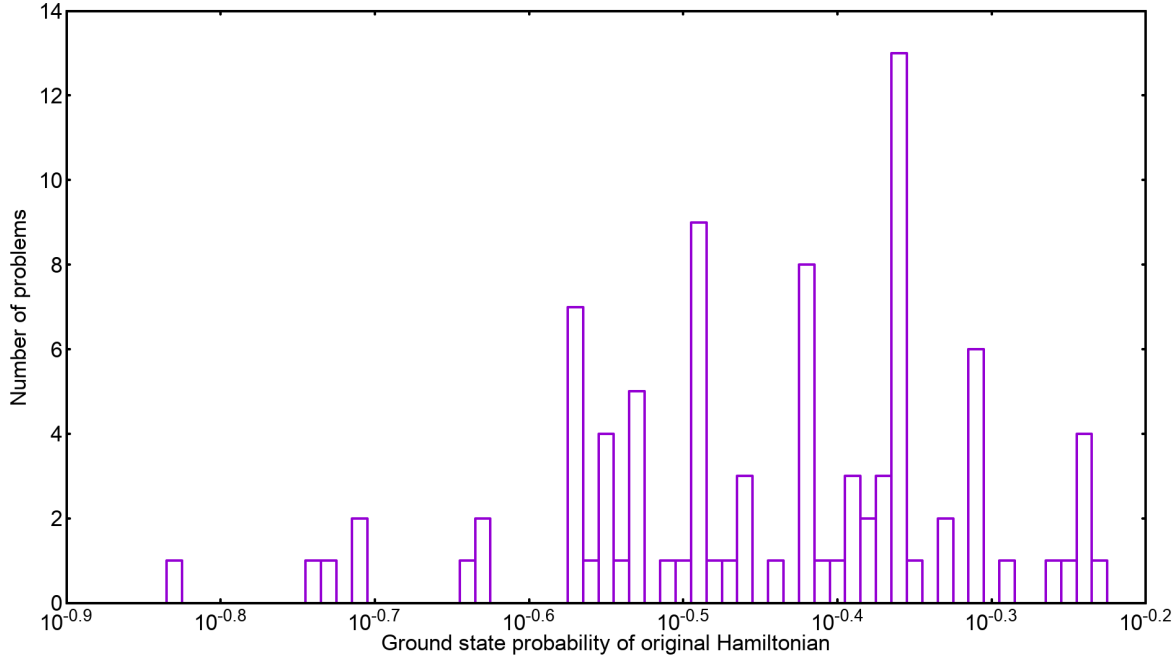


Figure 3.9: Histogram for success probability of the Hamiltonians without any triggers for 91 8-spin problems and  $T_A=10$ .

Finally, to check if the sweeping from the initial Hamiltonian to the final Hamiltonian is adiabatic, the success

probability of all the 12-spin problems have been plotted in figure (3.10).

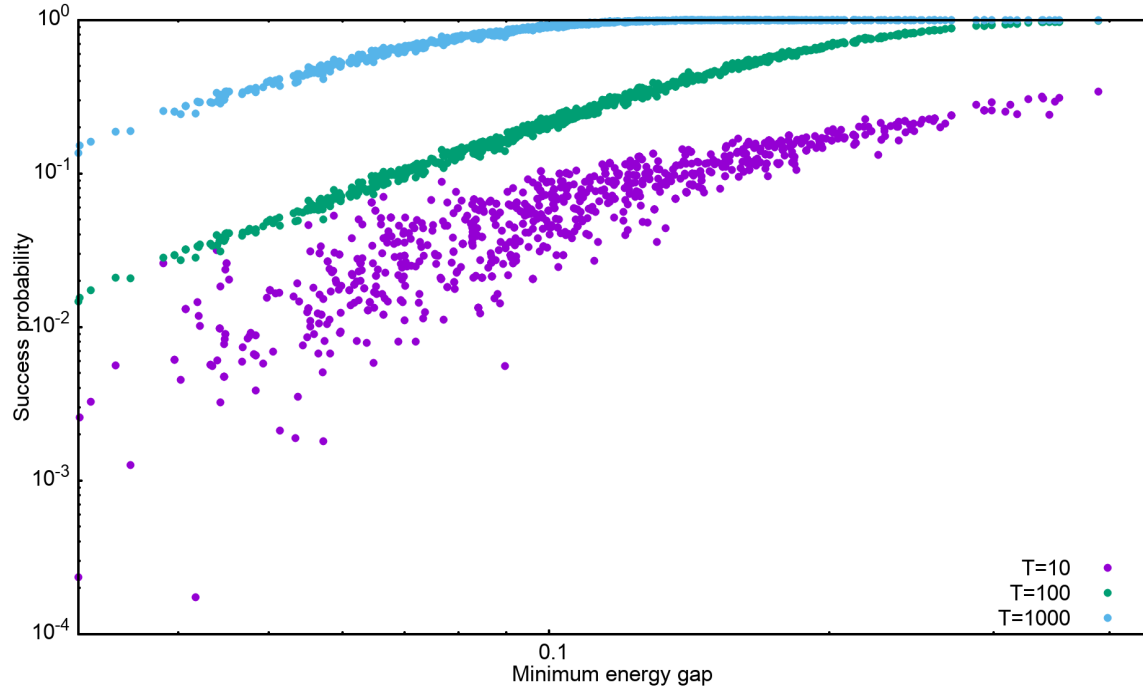


Figure 3.10: Success probability Versus minimum energy gaps for all the 12-spin problems for annealing times of 10, 100 and 1000.

From equation (2.4), the probability of ending in a state close to the ground state of the problem Hamiltonian increases exponentially with increasing the minimum energy gap between the ground and first excited state of the Hamiltonian, for fixed annealing time. Since different problems, corresponding to different minimum energy gaps are found to have an exponential relation in the success probability and the minimum energy gaps, the annealing is indeed adiabatic. However, for small annealing times, the scattering in the plot increases.

A similar plot for 8-spin problems is shown in figure (3.11).

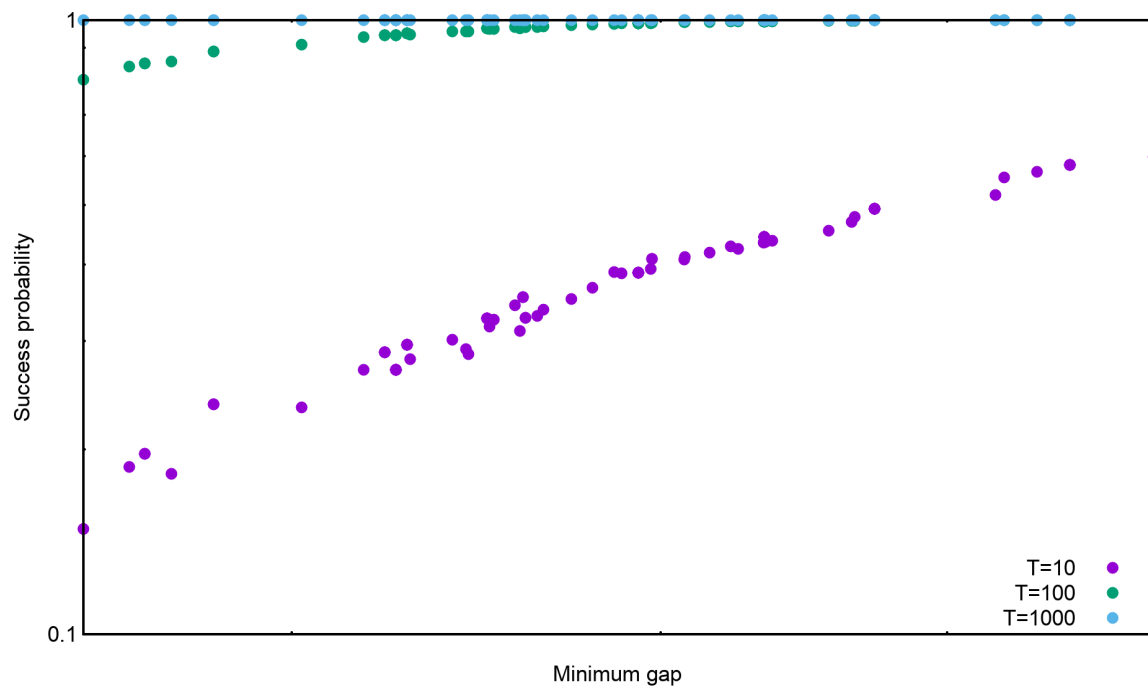


Figure 3.11: Success probability Versus minimum energy gaps for all the 8-spin problems for annealing times of 10,100 and 1000.

## Chapter 4

# Results with Ferromagnetic Trigger

As mentioned previously, there are two trigger Hamiltonians that were studied in the course of this thesis. This chapter focuses on the performance of quantum annealing on adding the ferromagnetic trigger,  $H_T^F$  to the Hamiltonian.

For the same transverse-field initial Hamiltonian, and each problem from the set of problem Hamiltonians (1000 12-spin SAT problems, and 91 8-spin SAT problems), ferromagnetic trigger was added to the Hamiltonian, with three different strengths, i.e. the strength parameter,  $g$  in equation (??) was chosen to be 0.5, 1 and 2.

In the subsequent segments the effect of adding the ferromagnetic trigger with different strengths will be discussed. For studying the dynamics during the evolution, same cases have been chosen as in Chapter Original Results, so that the results can be directly compared.

The first Hamiltonian considered in the previous chapter had high success probability (in the absence of any triggers). Figures (4.1),(4.2) and (4.3) show the energy spectra for this case upon adding the ferromagnetic trigger with strengths 0.5, 1 and 2 respectively. The corresponding instantaneous energy values have also been included in these plots.

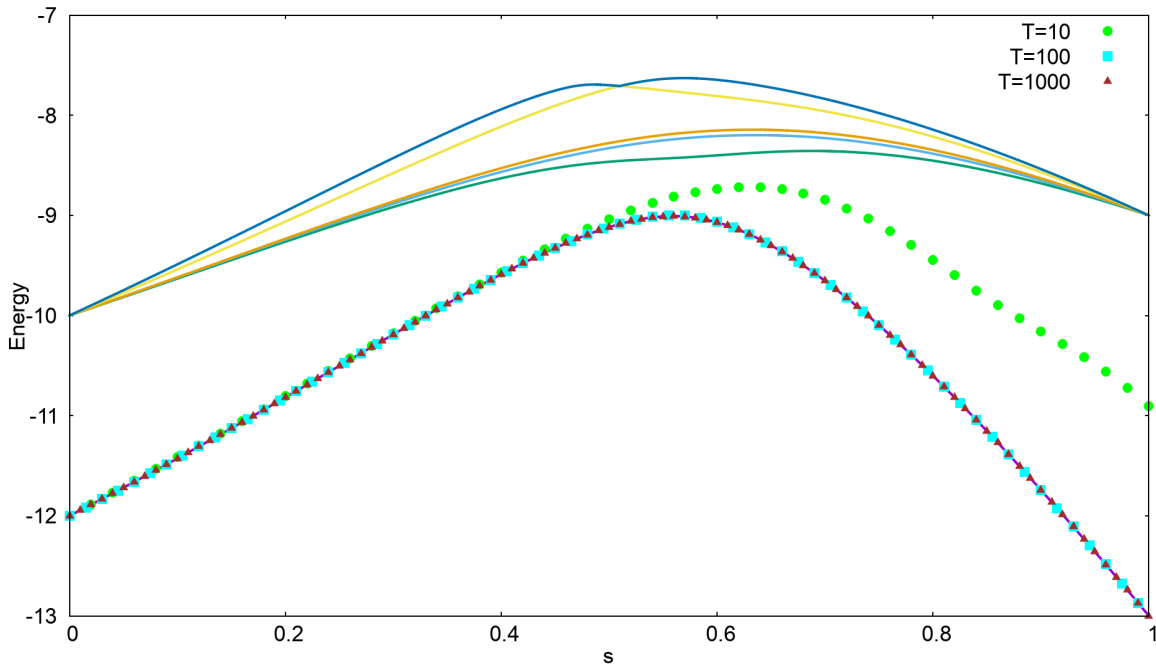


Figure 4.1: The energy spectrum for the first problem, with instantaneous energy values corresponding to three annealing times, with Ferromagnetic trigger, and  $g=0.5$ .  $\Delta_{min}$  was found to be 0.5779, while  $p=0.9996$  for  $T_A=100$ .

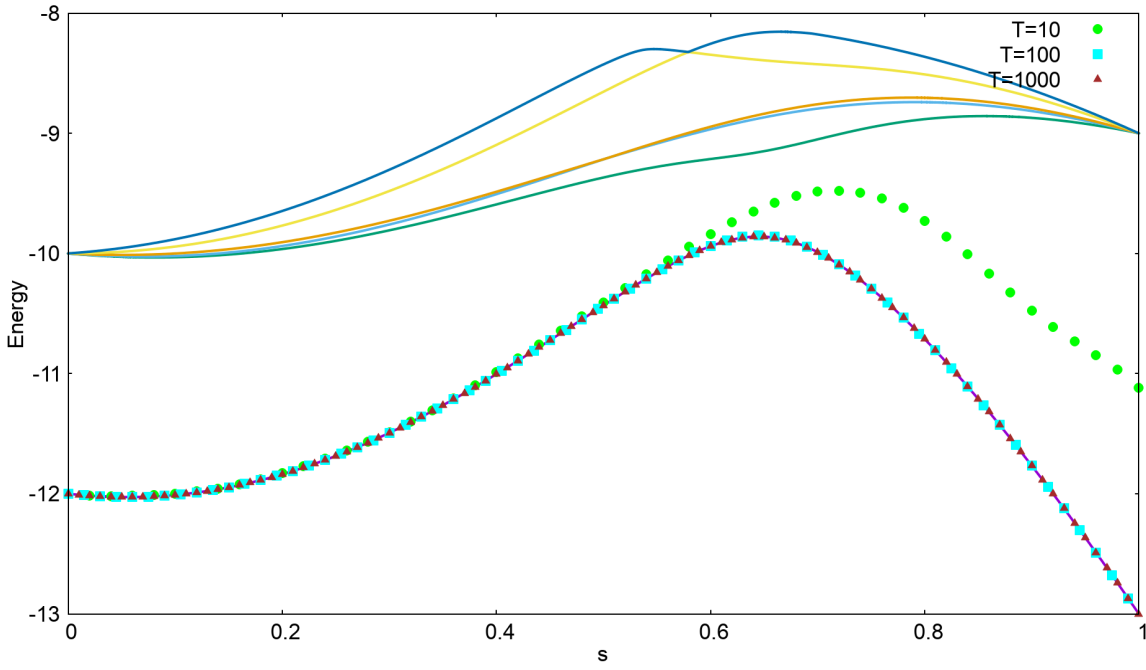


Figure 4.2: The energy spectrum for the first problem, with instantaneous energy values corresponding to three annealing times, with Ferromagnetic trigger, and  $g=1$ .  $\Delta_{min}$  was found to be 0.6908, while  $p=0.9998$  for  $T_A=100$ .

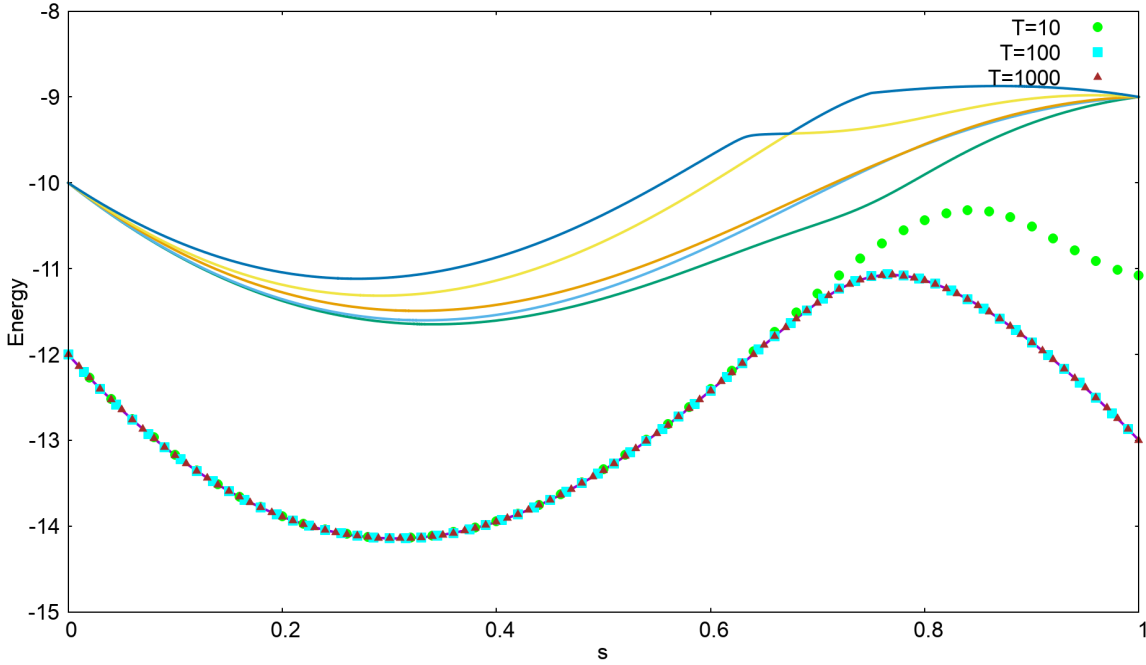


Figure 4.3: The energy spectrum for the first problem, with instantaneous energy values corresponding to three annealing times, with Ferromagnetic trigger, and  $g=2$ .  $\Delta_{min}$  was found to be 0.8333, while  $p=0.9997$  for  $T_A=100$ .

From these figures, it can be noted that compared to the original Hamiltonian, the minimum gap,  $\Delta_{min}$  has increased for all the three case. Furthermore, the  $\Delta_{min}$  becomes larger as the strength of the trigger Hamiltonian is increased from 0.5 to 2.

Secondly, the position of  $\Delta_{min}$  is shifted more towards the right upon increasing the strength. Additionally, the concavity of the ground state also increases with it. Finally, all the success probabilities upon adding the trigger are larger than the success probability of the original case, owing to the increase in the the minimum gaps. Therefore,

Case 1	Original Hamiltonian	Trigger=F, g=0.5	Trigger=F, g=1	Trigger=F, g=2
$\Delta_{min}$	0.4407	0.5779	0.6908	0.8333
p	0.9944	0.9996	0.9998	0.9997
s value at $\Delta_{min}$	0.459	0.552	0.629	0.733

Table 4.1: A comparison of the minimum gaps and the success probabilities at  $T_A=100$  for the first chosen case, between the original Hamiltonian and and the Hamiltonian with ferromagnetic trigger (F) of different strengths. The minimum gaps become larger as the strength of the ferromagnetic trigger is increased. The success probabilities are increased as a result. The value of s corresponding to the position of the minimum gap also becomes larger.

in general, the success probability also increases with increasing the strength of the trigger, though the final overlap also depends on the characteristics of the higher energy levels. Table (4.1) shows a comparison of the minimum gaps and success probabilities between the first problem with triggers of different strengths and the original problem. **Note that the success probability upon adding ferromagnetic trigger with g=2 is marginally small than that with g=1. This can be explained on the basis of**

Focussing now on the second case, which had small success probability with the original Hamiltonian, figures (4.4), (4.5), (4.6) show the energy spectra and the instantaneous energy values of the problem upon adding the ferromagnetic trigger with g=0.5, 1 and 2 respectively.

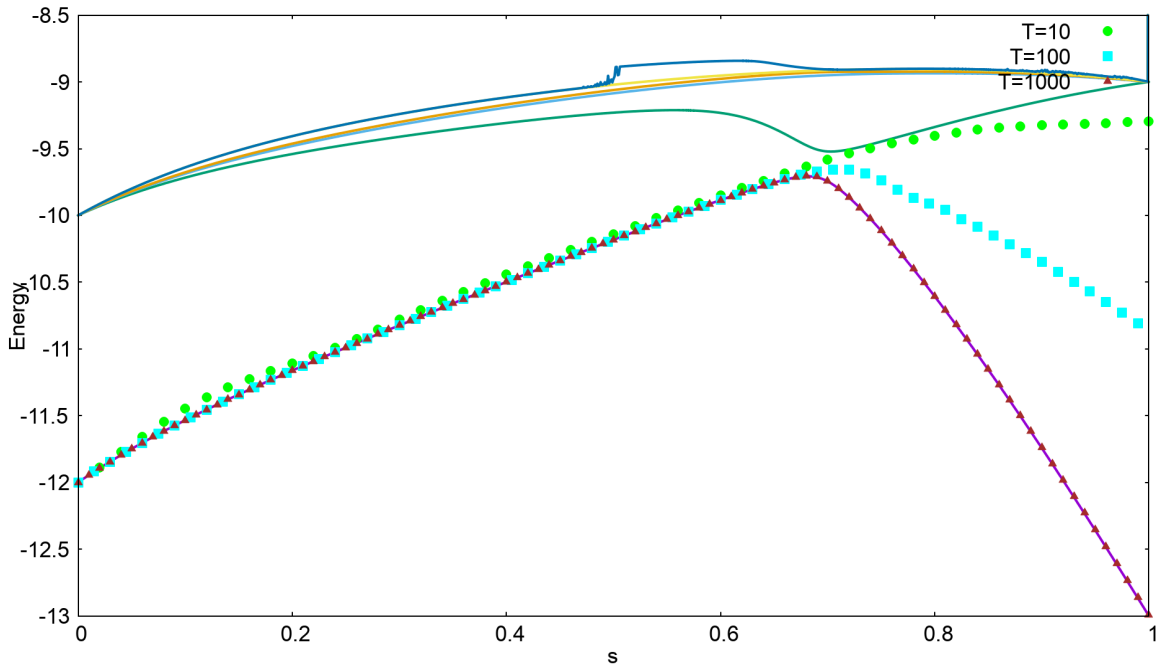


Figure 4.4: The energy spectrum for the second problem, with instantaneous energy values corresponding to three annealing times, with Ferromagnetic trigger, and  $g=0.5$ .  $\Delta_{min}$  was found to be 0.2074, while  $p=0.4650$  for  $T_A=100$ .

For this case too, the minimum energy gaps were found to have increased, leading to an improvement in the success probabilities. The improvements can be seen to become larger with increasing strengths of the trigger. The position of the minimum gap was again found to shift more rightwards in terms of the annealing parameter s upon increasing the strength, while the concavity of the ground state increased.

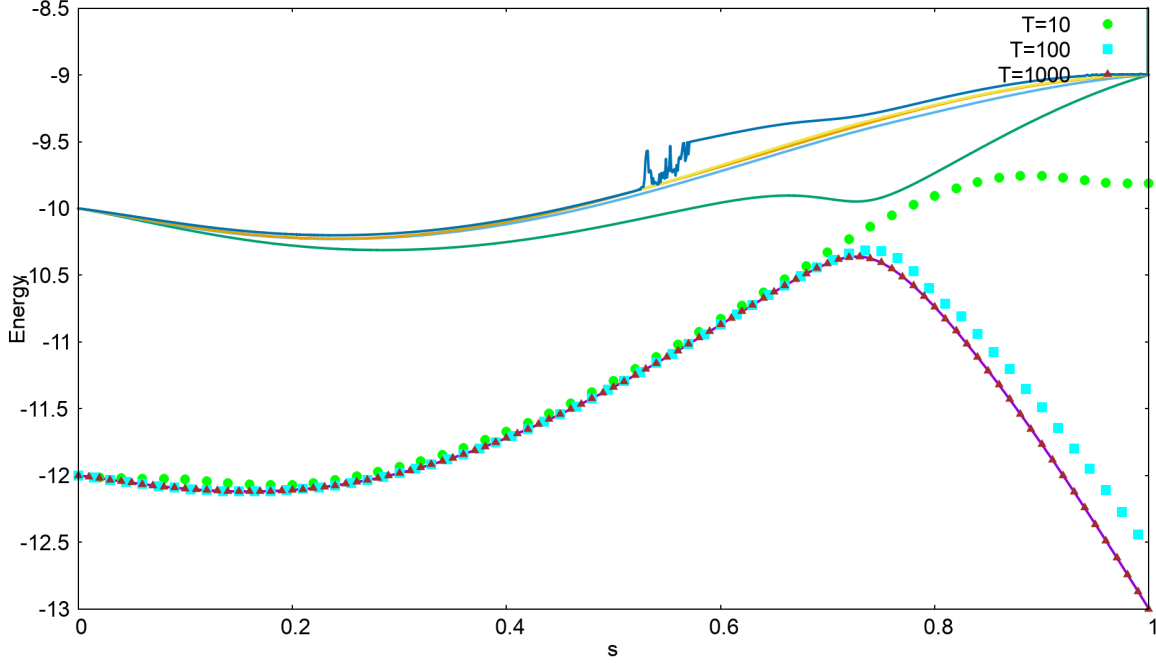


Figure 4.5: The energy spectrum for the second problem, with instantaneous energy values corresponding to three annealing times, with Ferromagnetic trigger, and  $g=1$ .  $\Delta_{min}$  was found to be 0.4129, while  $p=0.8889$  for  $T_A=100$ .

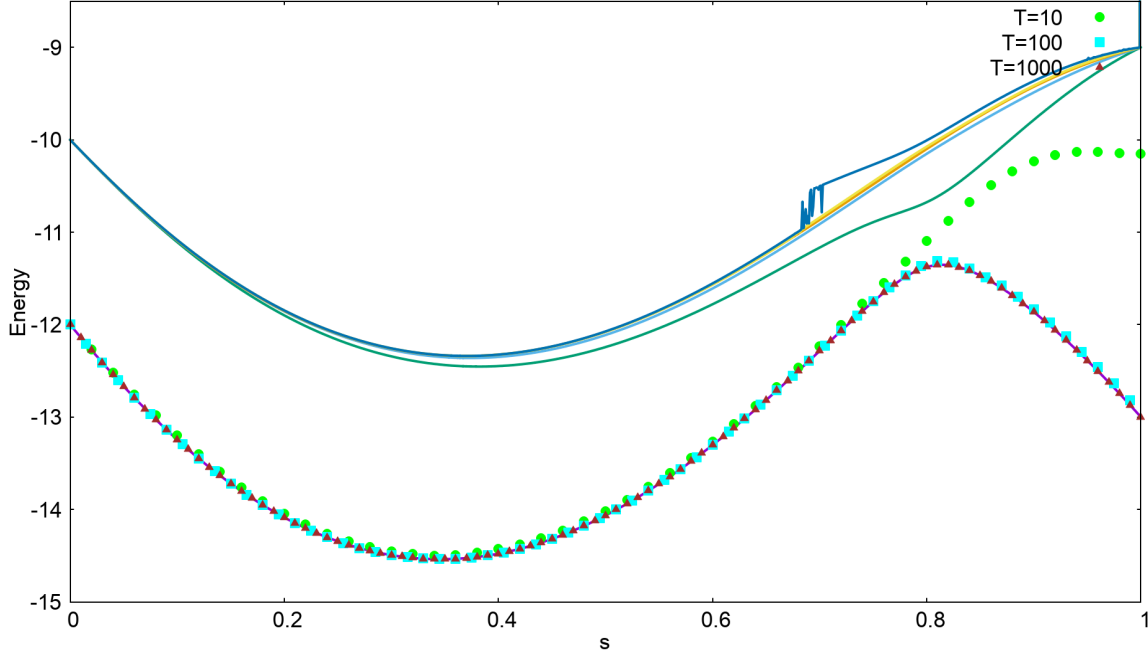


Figure 4.6: The energy spectrum for the second problem, with instantaneous energy values corresponding to three annealing times, with Ferromagnetic trigger, and  $g=2$ .  $\Delta_{min}$  was found to be 0.6943, while  $p=0.9870$  for  $T_A=100$ .

One feature of difference, however, compared to the first case was the factor by which the success probability is improved upon adding the ferromagnetic trigger to the original Hamiltonian. For the second case,  $T_A=100$ , and  $g=2$ , the ratio of the success probabilities upon adding the ferromagnetic trigger ( $p^F$ ) to the original success probability ( $p^O$ ), is  $\frac{p^F}{p^O}=67.6$ . In terms of the ratio of the corresponding minimum gaps this improvement was

Case 2	Original Hamiltonian	Trigger=F, g=0.5	Trigger=F, g=1	Trigger=F, g=2
$\Delta_{min}$	0.0312	0.2074	0.4129	0.6943
p	0.0146	0.4650	0.8889	0.9870
s value at $\Delta_{min}$	0.665	0.691	0.727	0.793

Table 4.2: A comparison of the minimum gaps and the success probabilities at  $T_A=100$  for the second chosen case, between the original Hamiltonian and and the Hamiltonian with ferromagnetic trigger of different strengths. The minimum gaps become larger as the strength of the ferromagnetic trigger (F) is increased. The success probabilities are increased as a result. The value of s corresponding to the position of the minimum gap also becomes larger.

$\frac{\Delta_{min}^F}{\Delta_{min}^O}=22.2$ . On the other hand, for the first chosen case,  $\frac{p^F}{p^O}=1.005$ , whereas  $\frac{\Delta_{min}^F}{\Delta_{min}^O}=1.89$  for  $g=2$ . Since for the first case, the instantaneous state lies close to the ground state even for the original Hamiltonian (figure 3.2), adding the trigger cannot do much improvement. On the contrary, since for the second case the minimum gap is comparatively very small, the instantaneous state comes close to the first excited state upon approaching the minimum energy anti-crossing. Adding the ferromagnetic trigger can then open this gap so that the system state always stays close to the ground state. This can explain the difference in the improvement ratios for the two cases.

Table (4.2) gives the comparison of the minimum gaps and the success probabilities for  $T_A=100$  for this case, between the original Hamiltonian and the Hamiltonian upon adding ferromagnetic triggers with different strengths.

Next, we consider the third case of intermediate success probability with original Hamiltonian. Figures (4.7), (4.8) and (4.9) show the energy spectra and the instantaneous energy values after adding the ferromagnetic trigger with strengths 0.5, 1 and 2 respectively.

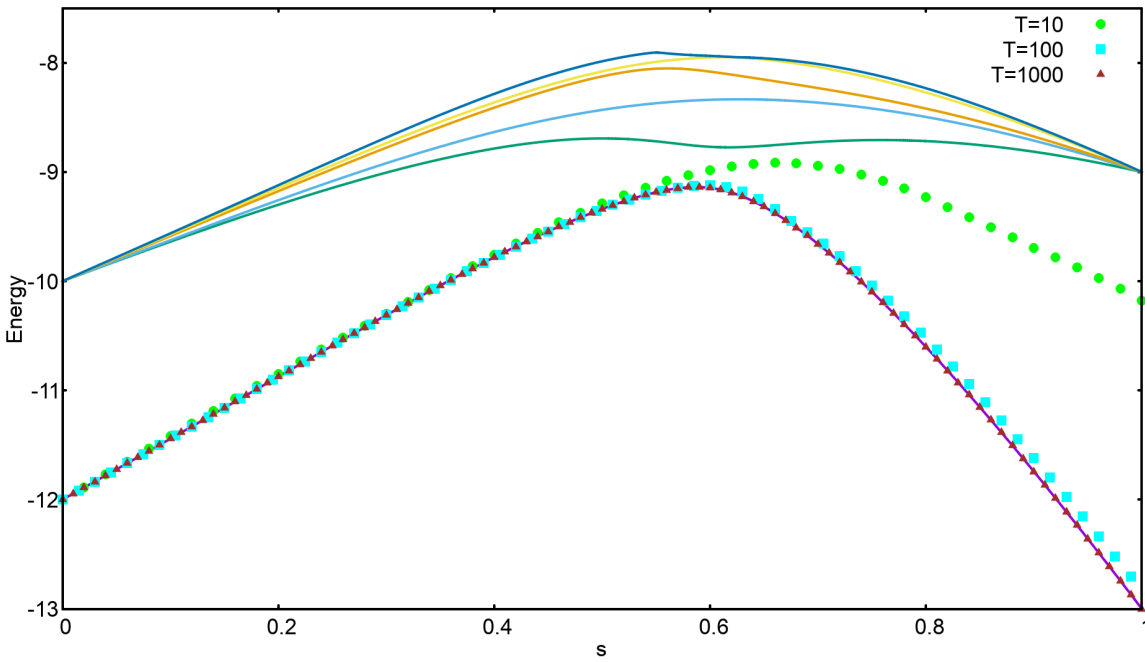


Figure 4.7: The energy spectrum for the third problem, with instantaneous energy values corresponding to three annealing times, with Ferromagnetic trigger, and  $g=0.5$ .  $\Delta_{min}$  was found to be 0.3748, while  $p=0.9577$  for  $T_A=100$ .

For this case too, the minimum energy gaps were found to have increased, leading to an improvement in the success probabilities. The improvements can be seen to become larger with increasing strengths of the trigger. The position of the minimum gap was again found to shift more rightwards in terms of the annealing parameter s upon increasing the strength, while the concavity of the ground state increased.

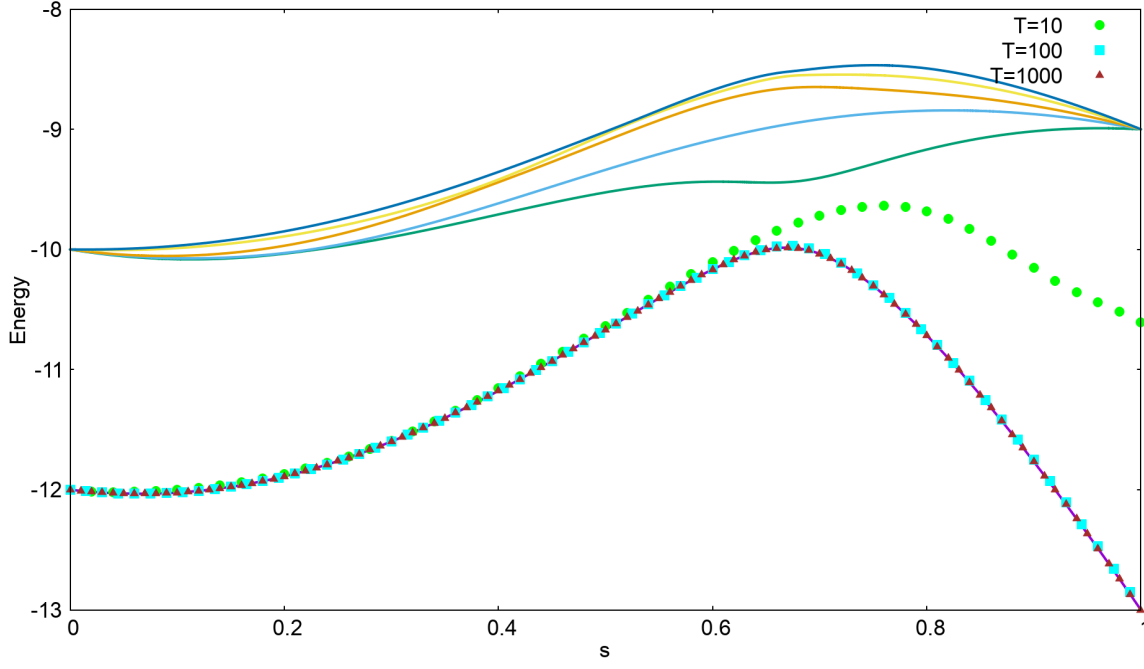


Figure 4.8: The energy spectrum for the third problem, with instantaneous energy values corresponding to three annealing times, with Ferromagnetic trigger, and  $g=1$ .  $\Delta_{min}$  was found to be 0.5439, while  $p=0.9945$  for  $T_A=100$ .

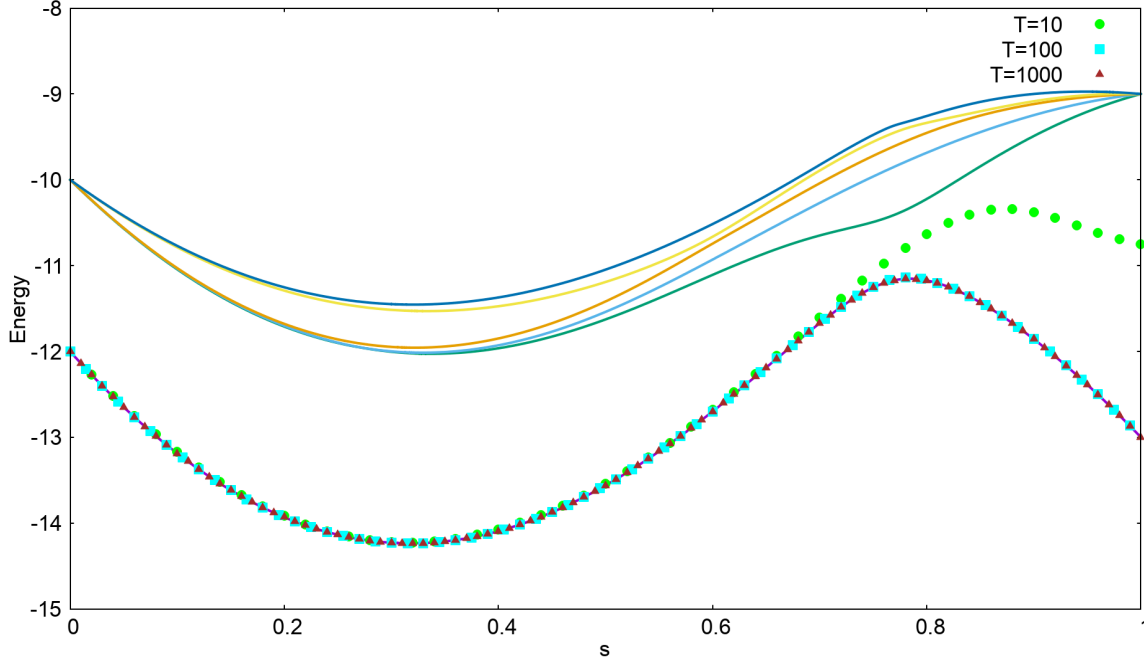


Figure 4.9: The energy spectrum for the third problem, with instantaneous energy values corresponding to three annealing times, with Ferromagnetic trigger, and  $g=2$ .  $\Delta_{min}$  was found to be 0.7512, while  $p=0.9981$  for  $T_A=100$ .

The improvement ratio for this case,  $\frac{p^F}{p^O}=1.91$ , while  $\frac{\Delta_{min}^F}{\Delta_{min}^O}=4.77$  at  $g=2$ . These values are also intermediate to those for the first and the second case. Table (4.3) shows a comparison of the success probabilities and the minimum gaps, between the original Hamiltonian and the Hamiltonian after adding the ferromagnetic trigger with

Case 3	Original Hamiltonian	Trigger=F, g=0.5	Trigger=F, g=1	Trigger=F, g=2
$\Delta_{min}$	0.1573	0.3748	0.5439	0.7512
p	0.5199	0.9577	0.9945	0.9981
s value at $\Delta_{min}$	0.514	0.595	0.665	0.760

Table 4.3: A comparison of the minimum gaps and the success probabilities at  $T_A=100$  for the third chosen case, between the original Hamiltonian and and the Hamiltonian with ferromagnetic trigger (F) of different strengths. The minimum gaps become larger as the strength of the ferromagnetic trigger is increased. The success probabilities are increased as a result. The value of s corresponding to the position of the minimum gap also becomes larger.

different strengths.

Next, the minimum gaps and the success probabilities were computed for all the problems belonging to 12-SAT problems, before and after adding the ferromagnetic trigger, with  $g \in \{0.5,1,2\}$ , for  $T_A \in 10,100,1000$ .

Figure (4.10) shows the scatter plot of the original minimum energy gaps with the corresponding minimum energy gaps upon adding the ferromagnetic trigger with different strengths, for all the problems of the set.

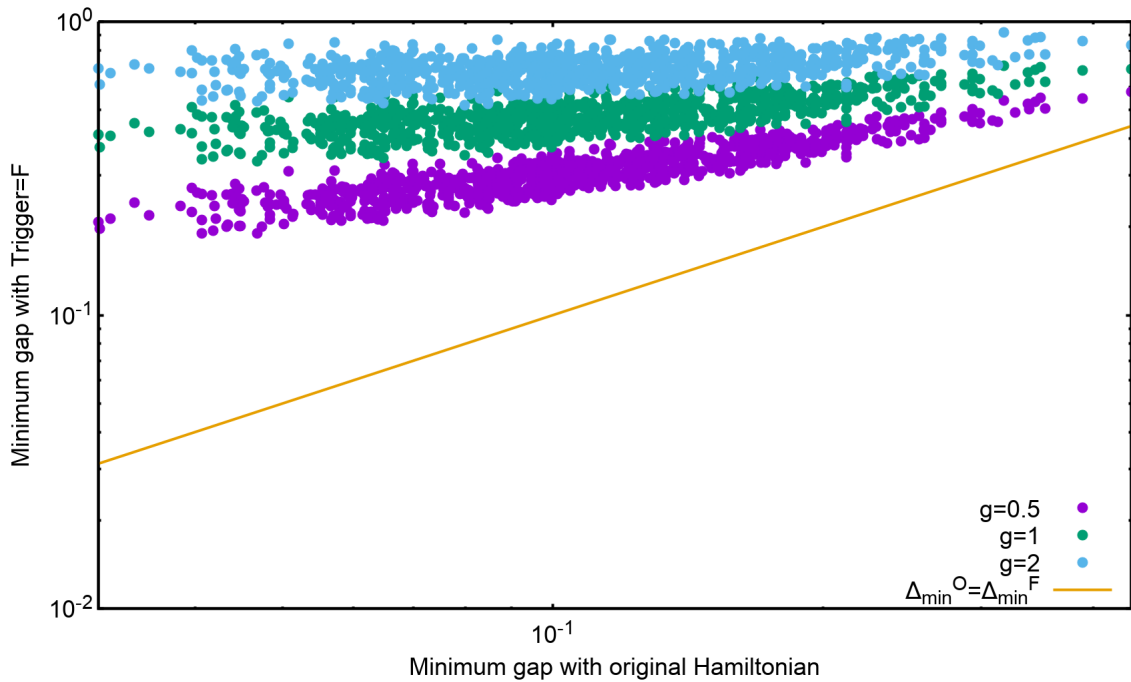


Figure 4.10: Scatter plot of the minimum gaps of the original Hamiltonians with those upon adding the ferromagnetic trigger with  $g \in \{0.5,1,2\}$ . The solid line represents the region where the minimum gap remains unchanged.

With ferromagnetic trigger, all the minimum gaps were found to have increased, for the three strengths of the trigger. Furthermore, for all the problems, the gaps became larger, as the ferromagnetic trigger became stronger, and the distribution of points can be observed to be systematic. As explained previously in terms of the improvement ratios of the first and the second chosen cases, the improvement for harder cases (small minimum gaps) is much larger than the improvement for easier cases (large minimum gaps).

For gauging the performance of the Hamiltonian after adding the ferromagnetic triggers, scatter plots of the original success probability with that obtained upon adding the trigger have been shown in figure (4.11), (4.12) and (4.13) corresponding to  $g= 0.5, 1$  and  $2$  respectively.

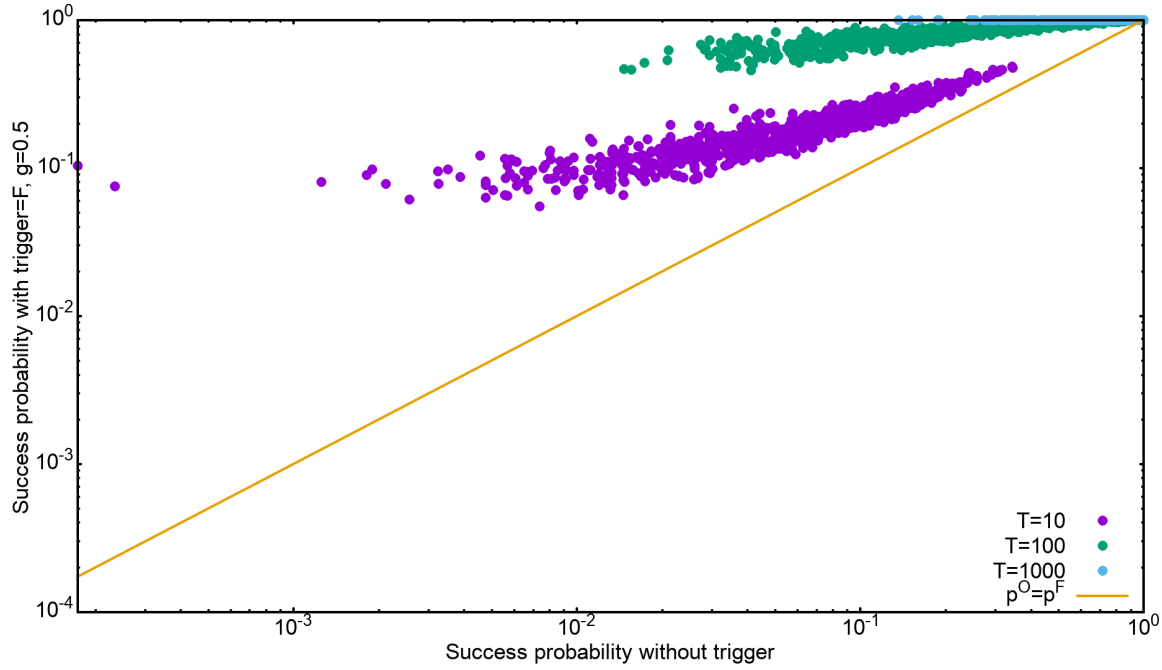


Figure 4.11: Scatter plot for the success probability after adding ferromagnetic trigger with the success probability of the original Hamiltonian, for annealing time  $T_A \in \{10, 100, 1000\}$ . The solid line represents the region where the success probability remains unchanged.

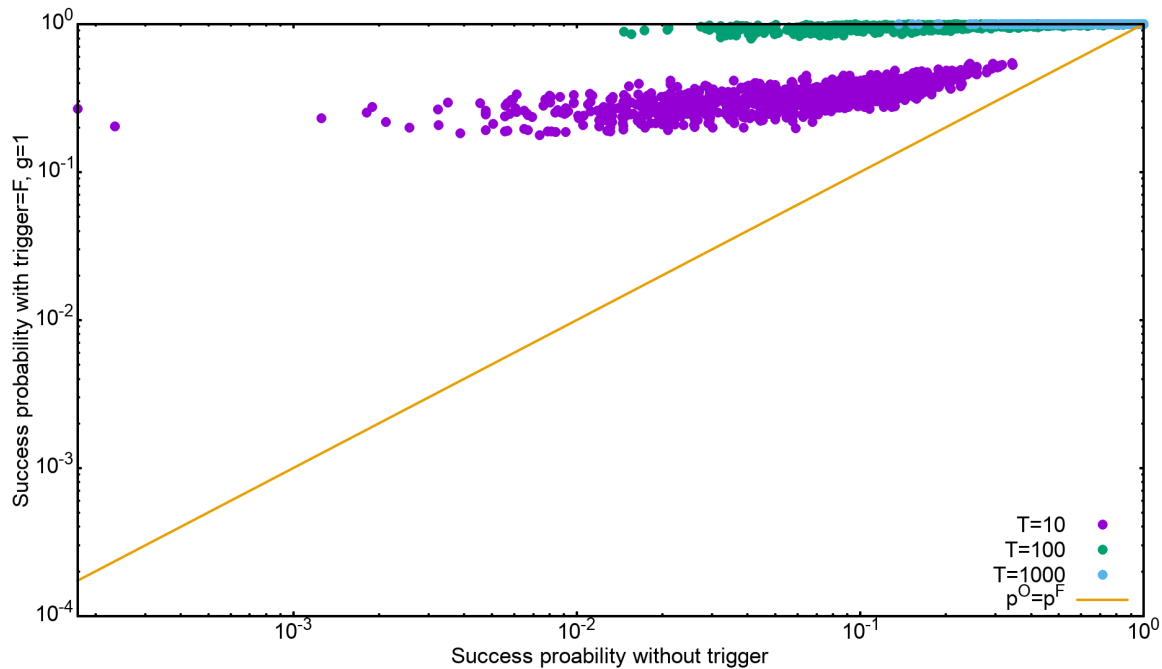


Figure 4.12: Scatter plot for the success probability after adding ferromagnetic trigger with the success probability of the original Hamiltonian, for annealing time  $T_A \in \{10, 100, 1000\}$ . The solid line represents the region where the success probability remains unchanged.

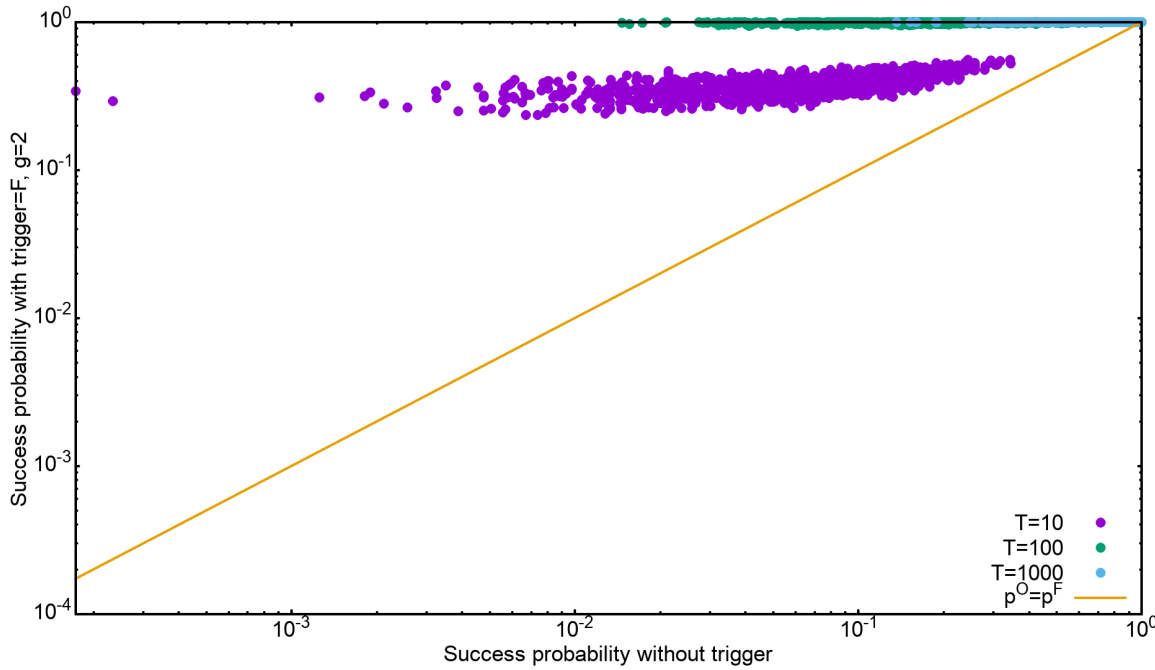


Figure 4.13: Scatter plot for the success probability after adding ferromagnetic trigger with the success probability of the original Hamiltonian, for annealing time  $T_A \in \{10, 100, 1000\}$ . The solid line represents the region where the success probability remains unchanged.

For all the three cases, and all the problems in the set, the success probability after adding the trigger was found to be greater than the success probability of the original Hamiltonian. Since in the adiabatic regime, the overlap of the final state with the ground state increases with increasing the annealing times, the success probability of the original Hamiltonians with long annealing times ( $T_A=1000$ ) is already large ( $\approx 1$ ). Adding the ferromagnetic trigger can therefore not improve the success probability too much. This explains the confinement of  $T_A=1000$  points close to the solid line ( $p^O = p^F$ ) on the upper right corner for all the three values of the strength parameter. Owing to the same reason, the points corresponding to  $T_A=10$  have a much larger spread. For the easy cases (larger  $p^O$ ), the success probability upon adding the trigger ( $p^F$ ) has a similar value. Such points lie close to the line. On the other hand, for the more difficult cases (smaller  $p^O$ ) the improvement can be larger, and such points lie away from the line.

Furthermore, since for a given problem, increasing the strength of the ferromagnetic trigger makes the minimum gaps larger, the success probability for that case also becomes larger. This explains the distribution of the points getting successively more flat with increasing strength of the trigger, for all annealing times (compare figures 4.11, 4.12 and 4.13).

Finally, we look at the dynamics of the evolution. According to equation (2.4), for an adiabatic evolution of the state of the system, the success probability,  $p$ , i.e. the measure of the overlap of the final state with the ground state of the Hamiltonian, is related to the minimum energy gap,  $\Delta_{min}$  as follows:

$$p = 1 - \exp(-C\Delta_{min}^2), \quad (4.1)$$

for some constant  $C$ . Since different problems in the problem set correspond to different minimum energy gaps, a plot of the success probability with these gaps should follow equation (2.4) if the evolution of the state for a problem is adiabatic. Moreover, adding the trigger changes the energy spectra, and thereby the minimum energy gaps of these problems. Figure (4.14) shows the success probability versus the minimum energy gap plot for all the problems upon adding the ferromagnetic trigger with three different strengths (0.5, 1 and 2), and for three annealing times (10, 100 and 1000).

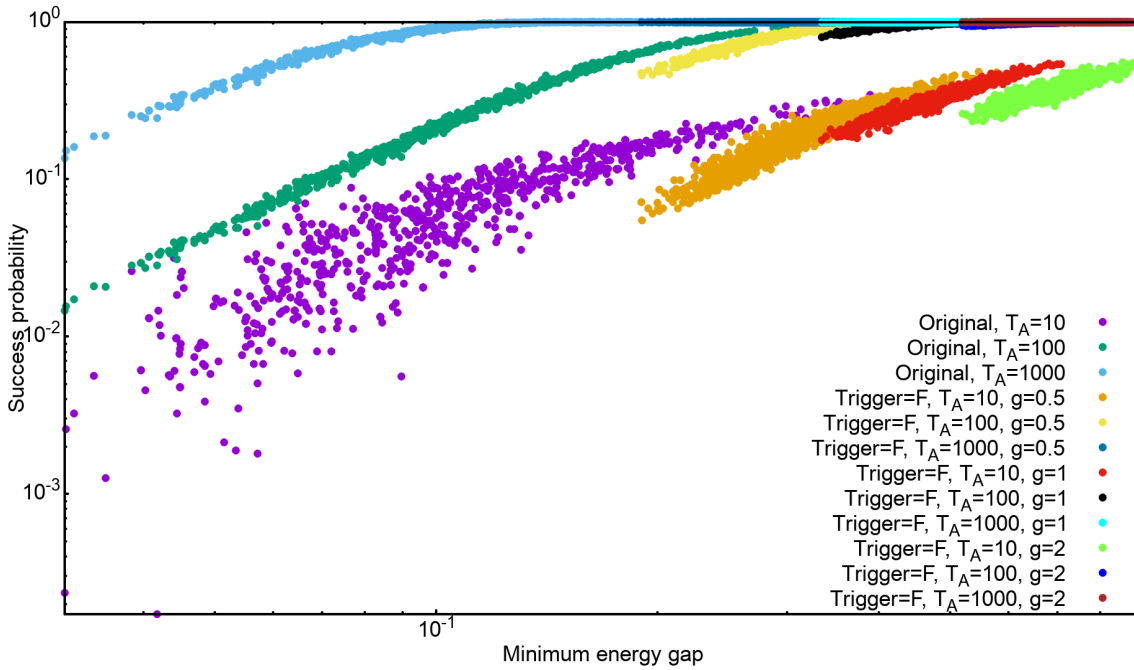


Figure 4.14: Plot of success probability versus the minimum energy gaps for all the problems belonging to the set. The plot shows the effect of adding ferromagnetic trigger to the original Hamiltonian with strengths 0.5, 1 and 2, while the annealing time is chosen to 10, 100 and 1000.

From the figure (4.14) it can be noted that all the curves roughly follow the exponential relation of equation (2.4). However, for the original Hamiltonian, and  $T_A=10$ , the scattering is quite larger compared to the other curves. The scattering of the curves decreases on increasing the annealing times, suggesting that longer annealing times ascertain the evolution of the state to be adiabatic. Since adding the ferromagnetic trigger enlarges the minimum energy gaps, the curves are shifted to the right upon adding the trigger and increasing their strength.

# Chapter 5

## Results with Anti-ferromagnetic Trigger

This chapter will focus on the effects on the performance of quantum annealing algorithm upon adding the second trigger, namely the anti-ferromagnetic trigger, to the original Hamiltonian. Unlike in the case of the ferromagnetic trigger, for anti-ferromagnetic trigger the strength parameter,  $g$  in equation (1.12) plays a more decisive role than merely controlling the extent by which the minimum gap is enlarged. The anti-ferromagnetic trigger alters the energy spectra, the minimum energy gaps, and the number of anti-crossings between the ground and first excited energy state of the Hamiltonian, depending on the strength with which the trigger is added, as well as on the problem itself. We shall begin by observing the effects of adding the anti-ferromagnetic trigger to the original Hamiltonian, for the three chosen problems. The following sections will then showcase the role that the strength parameter -  $g$  plays.

### The chosen problems

Let us begin by considering the first chosen case, with largest success probability.

Figures (5.1), (5.2) and (5.3) show the energy spectra and the instantaneous energy values after adding the anti-ferromagnetic trigger to the first chosen case, with strengths 0.5, 1 and 2 respectively.

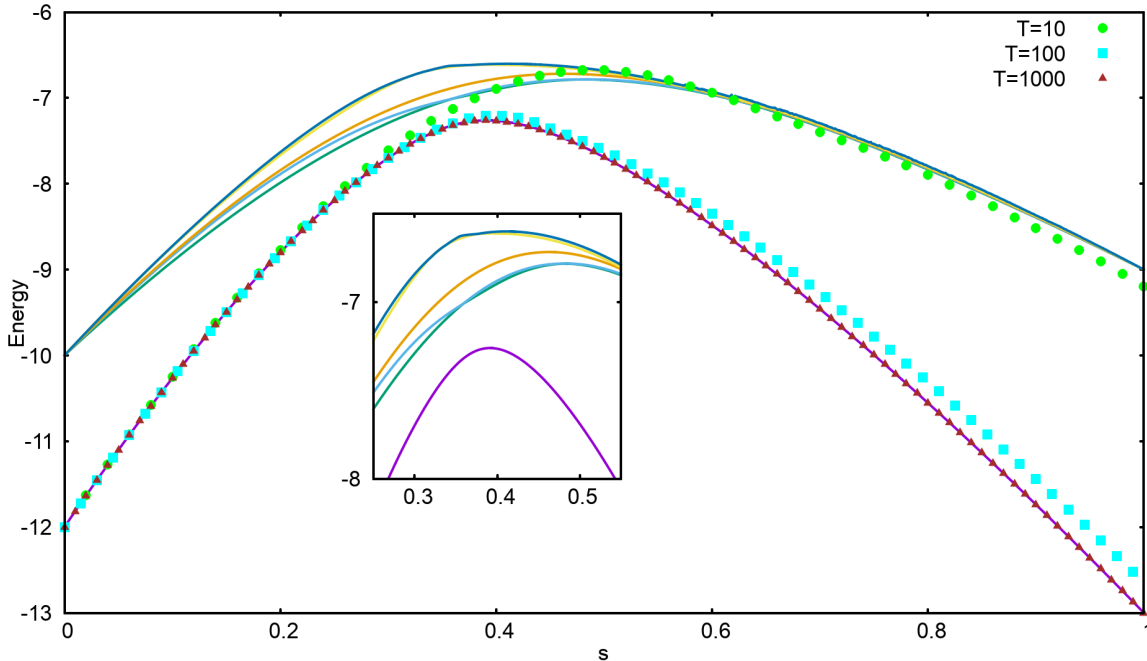


Figure 5.1: The energy spectrum for the first problem, with instantaneous energy values corresponding to three annealing times, with Anti-ferromagnetic trigger, and  $g=0.5$ .  $\Delta_{min}$  was found to be 0.3070, while  $p=0.9117$  for  $T_A=100$ .

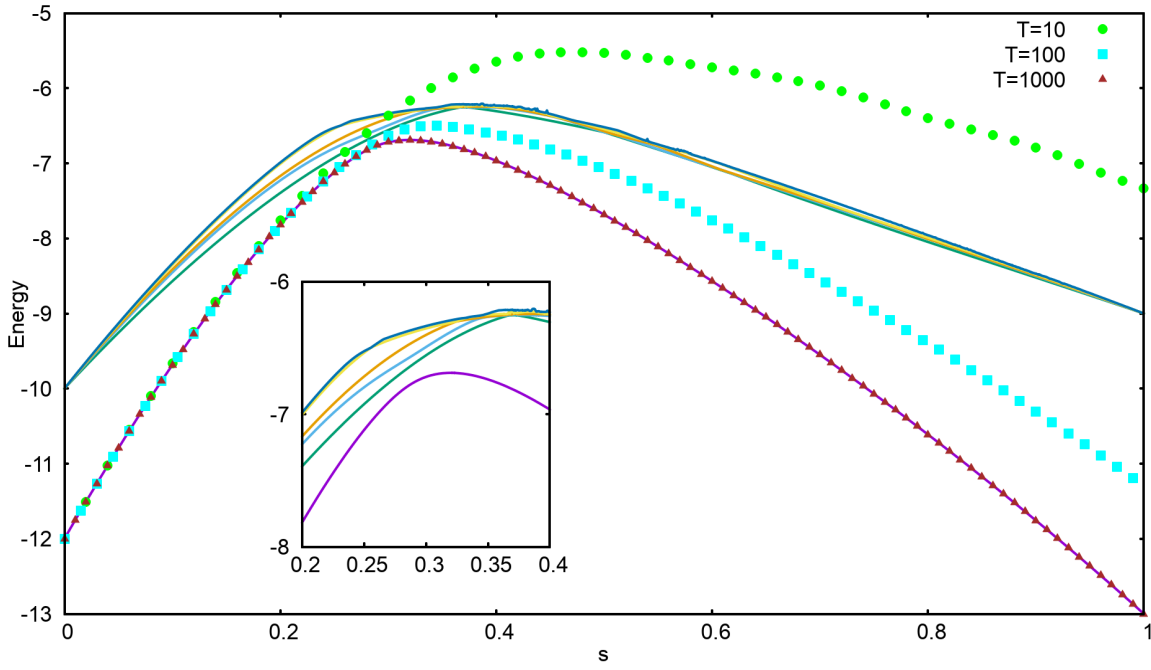


Figure 5.2: The energy spectrum for the first problem, with instantaneous energy values corresponding to three annealing times, with Anti-ferromagnetic trigger, and  $g=1$ .  $\Delta_{min}$  was found to be 0.1349, while  $p=0.5747$  for  $T_A=100$ .

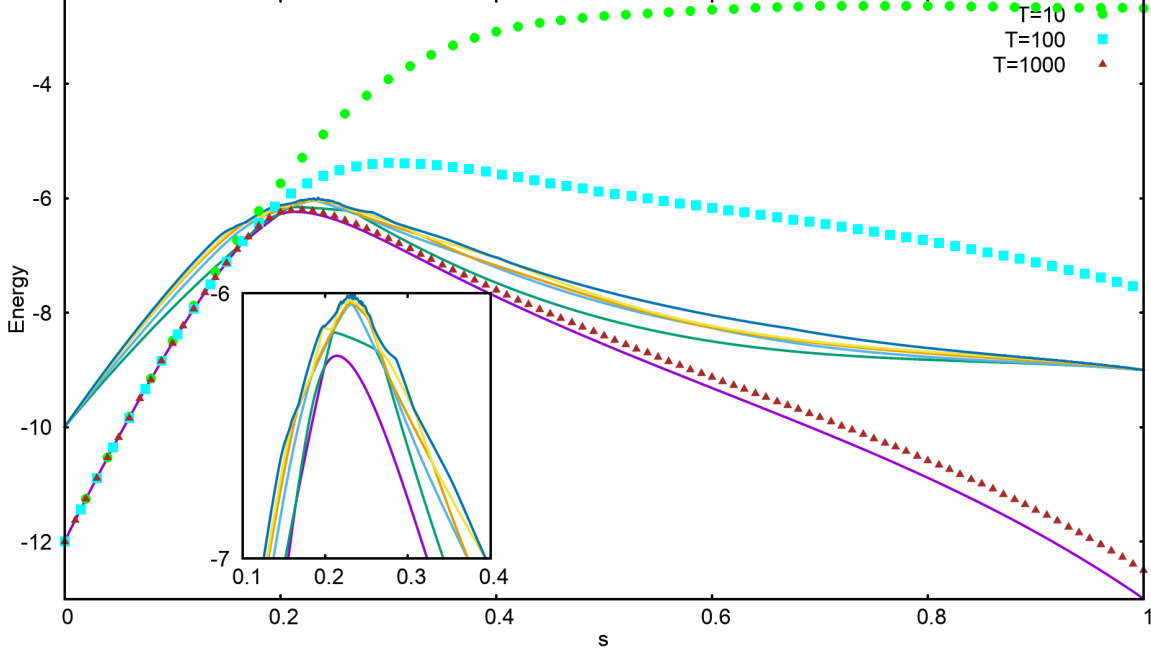


Figure 5.3: The energy spectrum for the first problem, with instantaneous energy values corresponding to three annealing times, with Anti-ferromagnetic trigger, and  $g=2$ .  $\Delta_{min}$  was found to be 0.0020, while  $p=0.0273$  for  $T_A=100$ .

Table (5.1) shows a comparison of the success probabilities -  $p$ , and minimum energy gaps -  $\Delta_{min}$  between the original Hamiltonian and the Hamiltonian after adding the anti-ferromagnetic triggers with different strengths.

CASE 1	Original Hamiltonian	Trigger=A, g=0.5	Trigger=A, g=1	Trigger=A, g=2
$\Delta_{min}$	0.4407	0.3070	0.1349	0.0020
$p(T_A=10)$	0.3444	0.1446	0.0279	$1.271 \times 10^{-4}$
$p(T_A=100)$	0.0044	0.9117	0.5747	0.0273
$p(T_A=1000)$	0.9999	0.9999	0.9999	0.8761
s value at $\Delta_{min}$	0.459	0.367	0.282	0.254
Number of anti-crossings	1	2	1	4

Table 5.1: A comparison of the minimum gaps and the success probabilities for the first chosen case, between the original Hamiltonian and and the Hamiltonian with anti-ferromagnetic trigger (A) of different strengths. The minimum gaps become successively smaller as the strength of the anti-ferromagnetic trigger is increased. The success probabilities are decreased as a result. The value of s corresponding to the position of the minimum gap also becomes smaller.

As can be noted from the table above, the minimum energy gap decreases upon adding the ferromagnetic trigger, and this decrease becomes larger as the strength of the trigger is increased. Consequently, the success probabilities (after adding the trigger) are found to be decreasing as well. The value of annealing parameter - s also become smaller with increasing strength of the trigger. A new feature observed after adding the anti-ferromagnetic trigger is the change in the number of anti-crossings between the ground and the first energy state. For strengths g=0.5 and g=2, the number of energy anti-crossings increase to 2 and 4 respectively, while for g=1 it remains unchanged. Moreover, when the anti-ferromagnetic trigger is added with strength 2, the energy spectrum changes quite drastically in comparison to the original spectrum (3.2), as can be more clearly seen in the inset of figure (5.3).

Next, let us consider the second chosen problem that had small success probability in absence of any triggers. Figures (5.4), (5.5), and (5.6) show the energy spectrum and the instantaneous energy values corresponding to three annealing times.

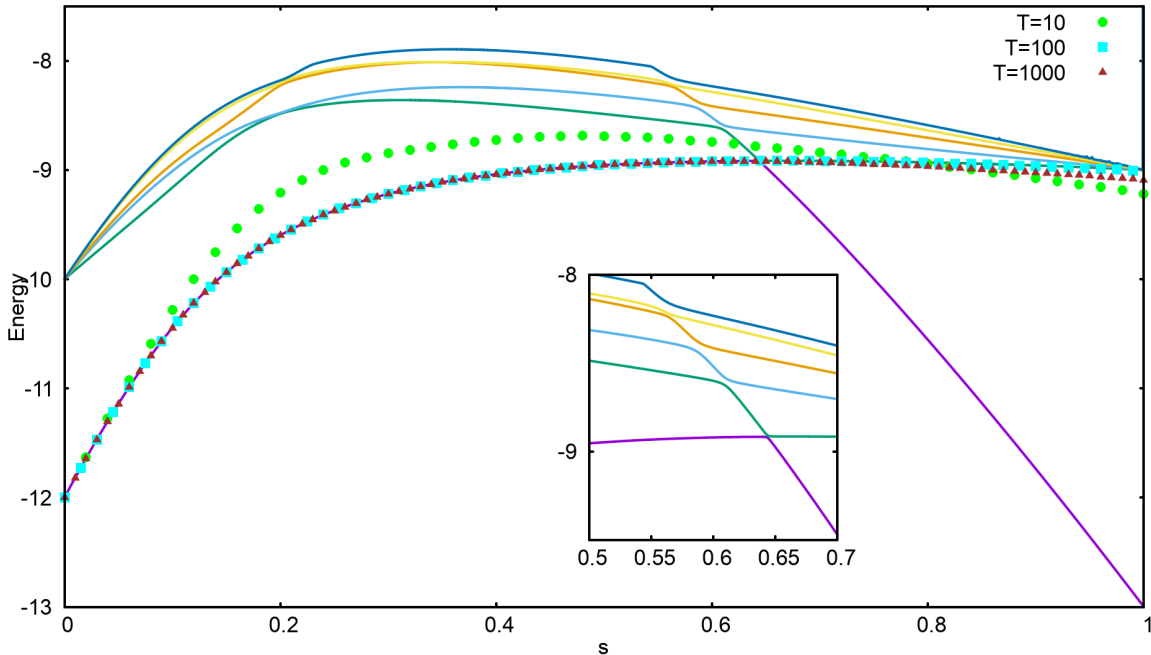


Figure 5.4: The energy spectrum for the second problem, with instantaneous energy values corresponding to three annealing times, with Anti-ferromagnetic trigger, and g=0.5.  $\Delta_{min}$  was found to be 0.0130, while  $p=0.0022$  for  $T_A=100$ .

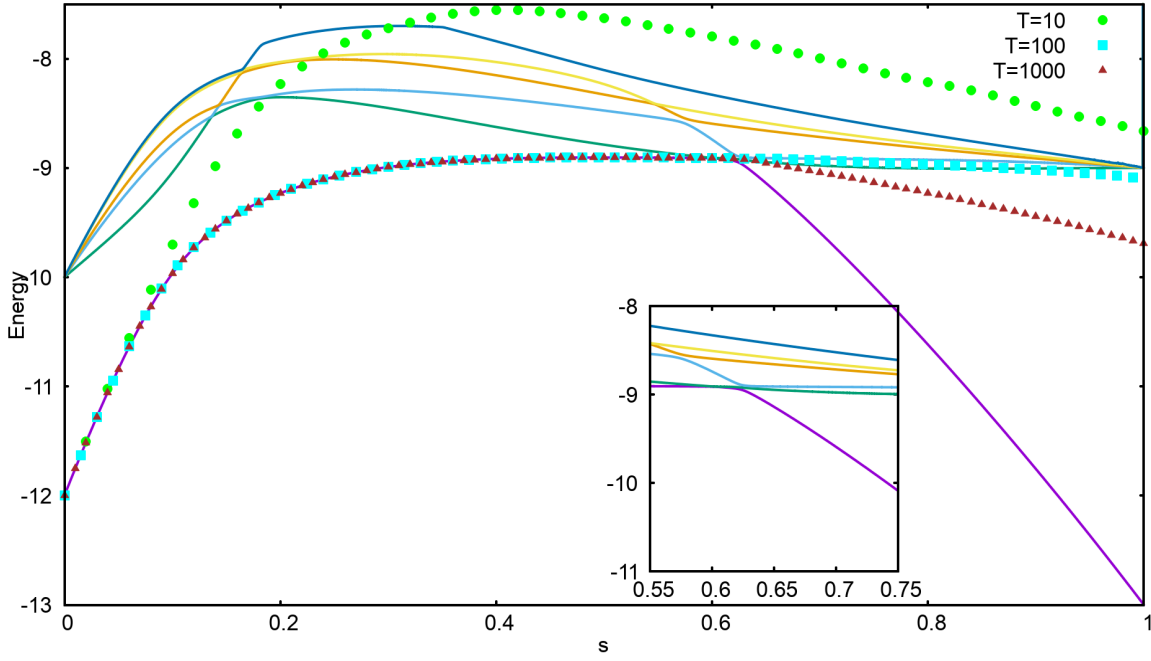


Figure 5.5: The energy spectrum for the second problem, with instantaneous energy values corresponding to three annealing times, with Anti-ferromagnetic trigger, and  $g=1$ .  $\Delta_{min}$  was found to be 0.0019, while  $p=0.0239$  for  $T_A=100$ .

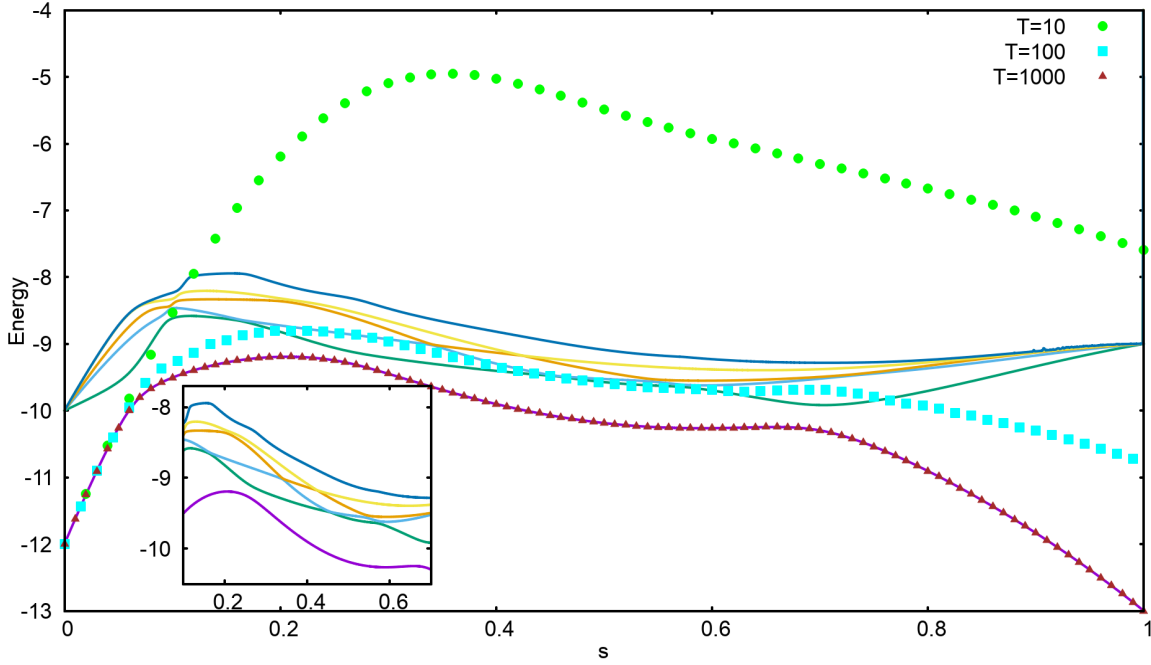


Figure 5.6: The energy spectrum for the second problem, with instantaneous energy values corresponding to three annealing times, with Anti-ferromagnetic trigger, and  $g=2$ .  $\Delta_{min}$  was found to be 0.1784, while  $p=0.4468$  for  $T_A=100$ .

For this case, table (5.2) shows a comparison of the minimum energy gaps, and success probabilities (corresponding to different annealing times) between the original Hamiltonian and the Hamiltonian upon adding the anti-ferromagnetic trigger with different strengths.

CASE 2	Original Hamiltonian	Trigger=A, g=0.5	Trigger=A, g=1	Trigger=A, g=2
$\Delta_{min}$	0.0312	0.0130	0.0019	0.1784
$p(T_A=10)$	$2.343 \times 10^{-4}$	0.0567	0.0017	0.0071
$p(T_A=100)$	0.0146	0.0022	0.0239	0.4468
$p(T_A=1000)$	0.1362	0.0228	0.1729	0.9999
s value at $\Delta_{min}$	0.665	0.644	0.601	0.263
Number of anti-crossings	1	1	2	3

Table 5.2: A comparison of the minimum gaps and the success probabilities for the second chosen case, between the original Hamiltonian and and the Hamiltonian with anti-ferromagnetic trigger (A) of different strengths. The minimum gap becomes small for  $g=0.5$ , and even smaller for  $g=1$ , while it becomes even larger than the original minimum energy gap for  $g=2$ . The value of s corresponding to the position of the minimum gap becomes smaller with increasing strength of the trigger.

The minimum energy gaps decrease with respect to the original energy gaps upon adding the trigger with strengths 0.5, and 1. However, the success probability at  $T_A=10$  for anti-ferromagnetic trigger with  $g=0.5$  and  $g=1$  is larger compared to that of the original Hamiltonian, owing to different reasons.

Since upon adding the anti-ferromagnetic trigger with strength 0.5, the minimum energy gap becomes smaller, the annealing time of  $T_A=10$  is so short that the state of the system transits to the first excited state even before the minimum gap anti-crossing. Upon approaching the minimum gap anti-crossing the system state shifts some of the amplitude back to the ground state, increasing the success probability in this case (figure 5.4). However, for the original Hamiltonian the gap is large enough for an annealing time of 10 for the state to not shift to the first excited state before the minimum energy gap (figure 3.3). The state therefore stays close to the first excited state after passing the anti-crossing. Furthermore, for annealing times  $T_A=100$  and  $T_A=1000$ , the system state transitions only at the minimum gap anti-crossing and closely follows the second and first excited states respectively. The overlap with the ground state decreases, and therefore the success probability in both these cases also reduces.

For the other case - with anti-ferromagnetic trigger with strength 1, the number of energy anti-crossings increases to 2. The first energy anti-crossing is small enough for just  $T_A=10$  to shift the system state to the first excited state. Quickly after transitioning to the first excited state, the system state shifts to higher energy levels (figure 5.5). Since the state of the system is a superposition of many energy eigenstates, the present state of system has small, yet finite overlap with the ground state. In the original Hamiltonian, however, the system state shifts to the first excited state at the only energy anti-crossing, and therefore the overlap with the ground state becomes negligible (figure 3.3).

By choosing the strength to be 2, the minimum energy gap of this problem becomes larger than the original minimum energy gap, while the number of anti-crossings between the ground and the first excited state increases to 3. The success probability in this case is always larger than the original success probability for all annealing times. For  $T_A=10$ , the state of the system shifts to the first excited state at first energy anti-crossing, and then quickly shifts to a superposition state with the higher energy states. This results in a larger overlap with the ground state compared to the case of the state closely following the first excited state after reaching the only energy anti-crossing in case of the original problem (3.3).

For  $T_A=100$ , the state starts transitioning to the first excited state only as it approaches the second energy anti-crossing. The state does further shift to higher energy levels, but comes back to the first excited state before the third energy anti-crossing. After passing by the third anti-crossing some of the amplitude of the wave function shifts to the ground state again, and therefore the success becomes larger than the original problem.

Finally, for  $T_A=1000$ , the annealing time and the minimum energy gap is large enough for the system to always stay close to the ground state, hence the larger success probability.

Lastly, figures (5.7), (5.8) and (5.9) show the energy spectra and instantaneous energy values for the third problem, after adding the anti-ferromagnetic trigger with strengths 0.5, 1 and 2 respectively.

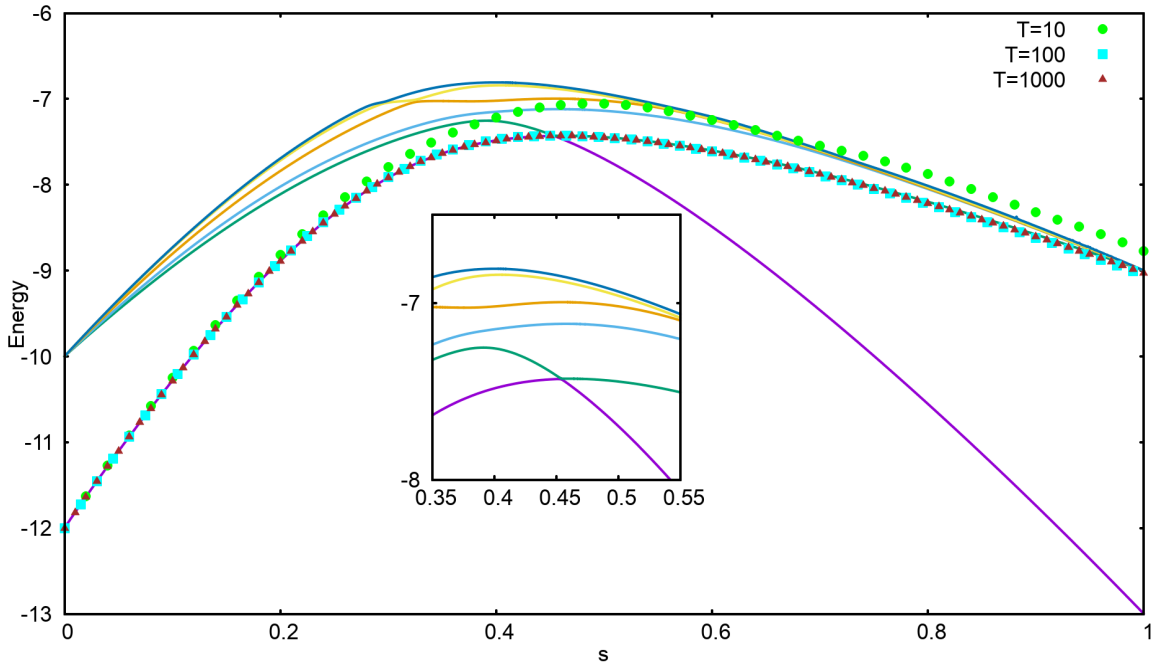


Figure 5.7: The energy spectrum for the third problem, with instantaneous energy values corresponding to three annealing times, with Anti-ferromagnetic trigger, and  $g=0.5$ .  $\Delta_{min}$  was found to be 0.0049, while  $p=0.0120$  for  $T_A=100$ .

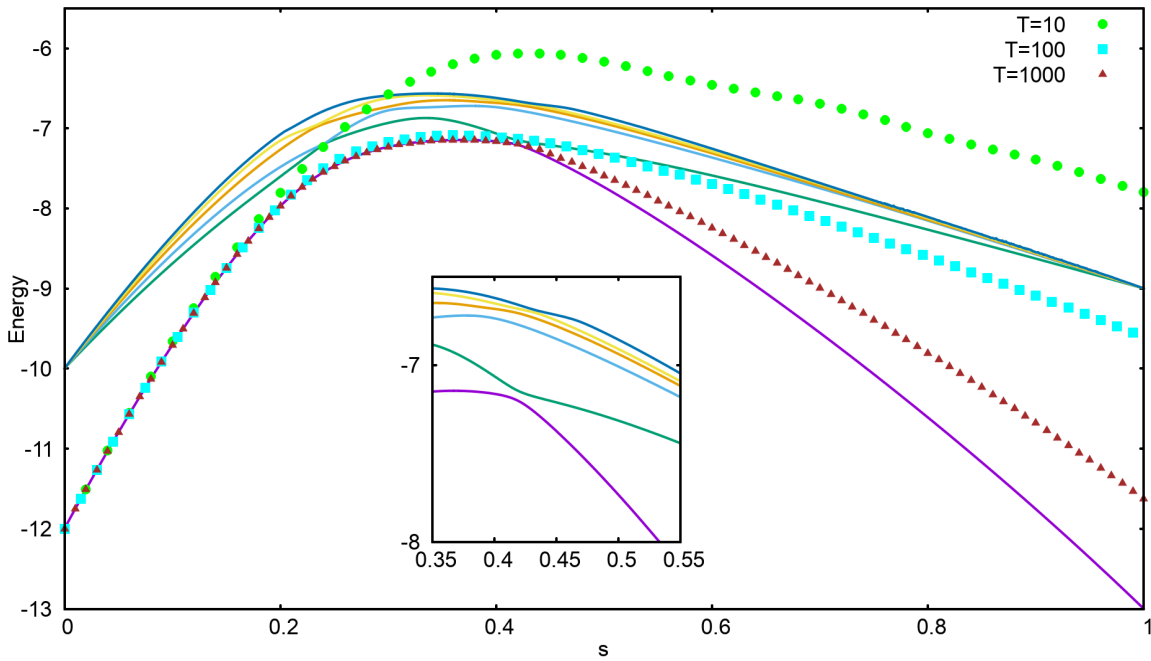


Figure 5.8: The energy spectrum for the third problem, with instantaneous energy values corresponding to three annealing times, with Anti-ferromagnetic trigger, and  $g=1$ .  $\Delta_{min}$  was found to be 0.0562, while  $p=0.1517$  for  $T_A=100$ .

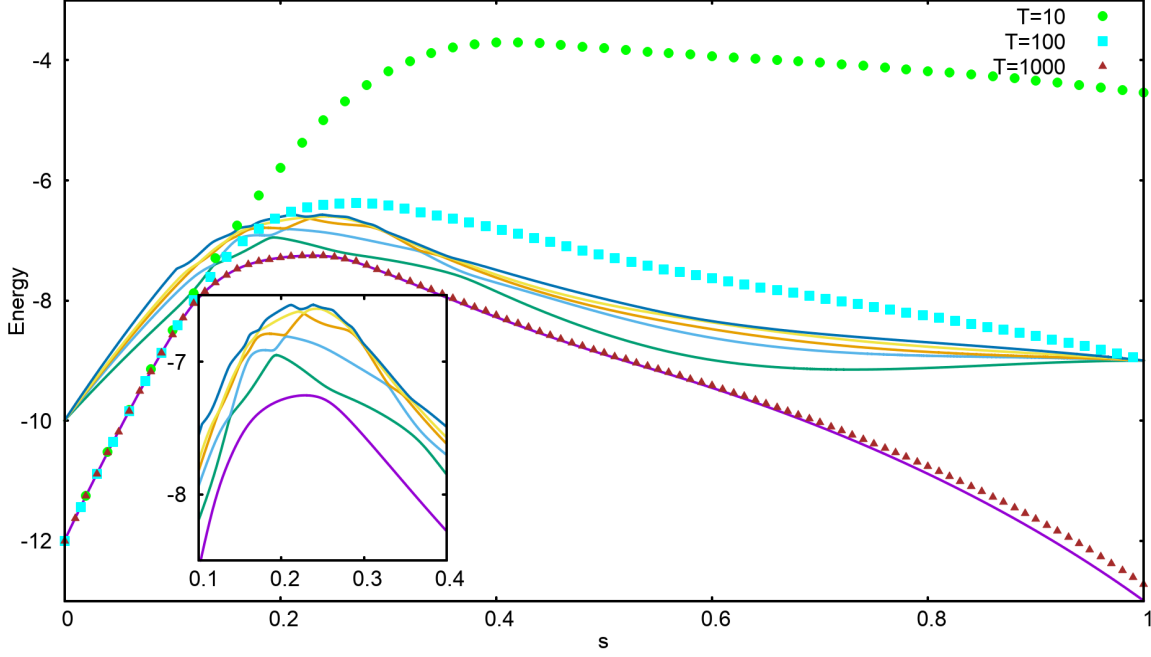


Figure 5.9: The energy spectrum for the third problem, with instantaneous energy values corresponding to three annealing times, with Anti-ferromagnetic trigger, and  $g=2$ .  $\Delta_{min}$  was found to be 0.1008, while  $p=0.0480$  for  $T_A=100$ .

Table (5.3) shows a comparison of the minimum energy gaps, and success probabilities (corresponding to different annealing times) between the original Hamiltonian and the Hamiltonian upon adding the anti-ferromagnetic trigger with different strengths.

CASE 3	Original Hamiltonian	Trigger=A, g=0.5	Trigger=A, g=1	Trigger=A, g=2
$\Delta_{min}$	0.1573	0.0049	0.0562	0.1008
$p(T_A=10)$	0.1577	0.0573	0.0368	$4.21 \times 10^{-5}$
$p(T_A=100)$	0.5199	0.0120	0.1517	0.0480
$p(T_A=1000)$	0.9992	0.0071	0.6565	0.9313
s value at $\Delta_{min}$	0.514	0.454	0.418	0.256
Number of anti-crossings	1	1	3	4

Table 5.3: A comparison of the minimum gaps and the success probabilities for the third chosen case, between the original Hamiltonian and the Hamiltonian with anti-ferromagnetic trigger (A) of different strengths. The minimum energy gaps after adding the trigger are smaller than the original minimum gap, for all the values of  $g$ . They however become large upon increasing the strength of the anti-ferromagnetic trigger. The value of  $s$  corresponding to the position of the minimum gap becomes smaller with increasing strength of the trigger.

For this problem, it was observed that adding the anti-ferromagnetic trigger made the minimum energy gaps smaller than the original gap, for all the three values of the strength chosen. The gaps however increased with increasing the strength of the trigger. The original success probabilities, for all annealing times, are therefore larger than the resulting success probabilities upon adding the triggers with different  $g$ . Additionally, for all annealing times but  $T_A=10$ , the success probabilities become larger when the anti-ferromagnetic trigger is added with strength 1 compared to when added with strength 0.5, as the minimum energy gap for the former is larger. For  $T_A=10$ , and both  $g=0.5$  and  $g=1$  cases, the system state transitions to the first excited state prior to the first energy anti-crossing. This is followed by the state shifting to higher energy levels soon after. Since the energy spectrum becomes more complex (in terms of the number of anti-crossings between the higher energy states and their proximity,) as

the strength of the trigger is increased, the system state shifts farther away from the ground state. Consequently, the success probability decreases in the case with  $g=0.5$ .

Although the gap becomes even larger with  $g=2$ , the success probability is smaller compared the case with  $g=1$ . This can be explained by observing that adding the anti-ferromagnetic trigger with  $g=2$  changes the energy spectrum of the Hamiltonian even more drastically. Not only do the number of anti-crossings between the ground and the first excited state increase to 4, the higher lying energy levels also become more involved and have larger number of anti-crossings. Hence, as annealing times  $T_A=10$  and  $T_A=100$  are not large enough for the state to stay close to the ground state upon reaching the first energy anti-crossing, the system state settles even farther away from the ground state as compared to the  $g=1$  case. Hence, the success probability for  $T_A=10$  and  $g=2$  case is negligible. As the annealing time is increased further to  $T_A=1000$ , the minimum energy gap becomes large enough to keep the state of the system close to the ground state, and the success probability becomes comparable to the original success probability.

## **g=0.5**

This section will focus on the performance of the quantum annealing algorithm upon adding the anti-ferromagnetic trigger to each of the original Hamiltonian from 12-spin SAT problems, with strength 0.5. For each problem, annealing time was chosen to be 10, 100 and 1000.

As a measure of quantifying the performance with respect to the original Hamiltonian, a metrics Relative success probability was defined as the ratio of the success probability upon adding the anti-ferromagnetic trigger ( $p^A$ ) to the original success probability ( $p^O$ ). Figures (5.10), (5.11) and (5.12) show the distribution of the relative success probability for annealing times of 10, 100 and 1000 respectively, with the strength of the trigger Hamiltonian chosen to be 0.5.

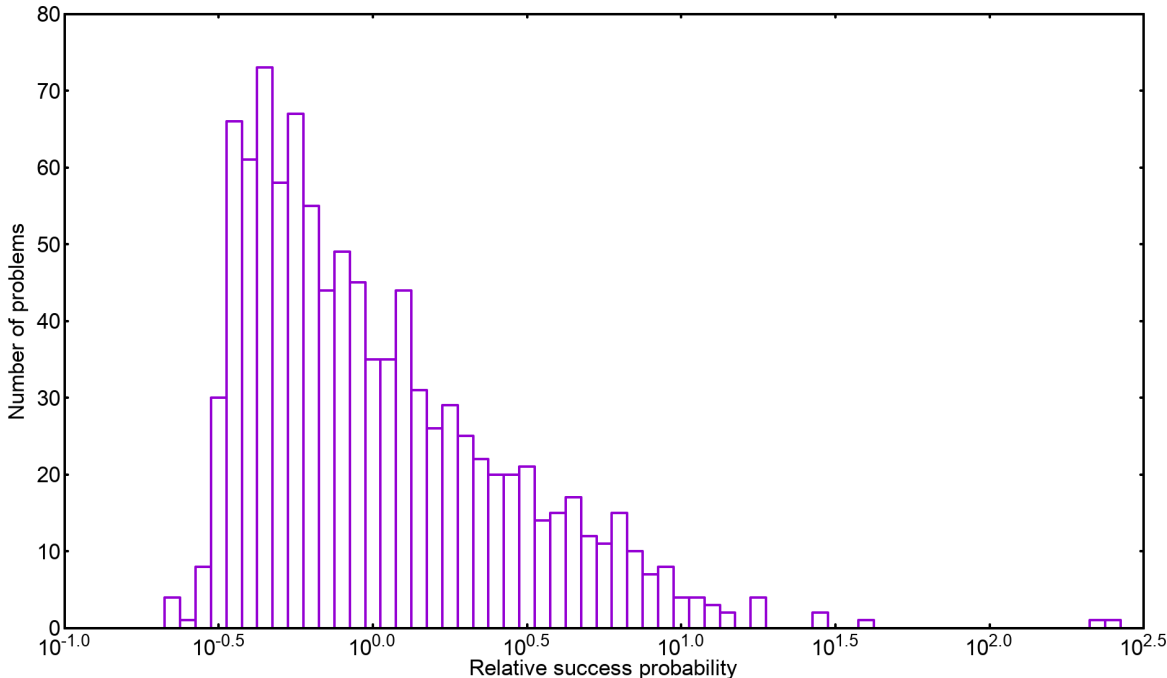


Figure 5.10: The distribution of relative success probability  $\frac{p^A}{p^O}$  for  $g=0.5$  and  $T_A=10$ . 43.9% of the cases were found to have a higher success probability after adding the trigger.

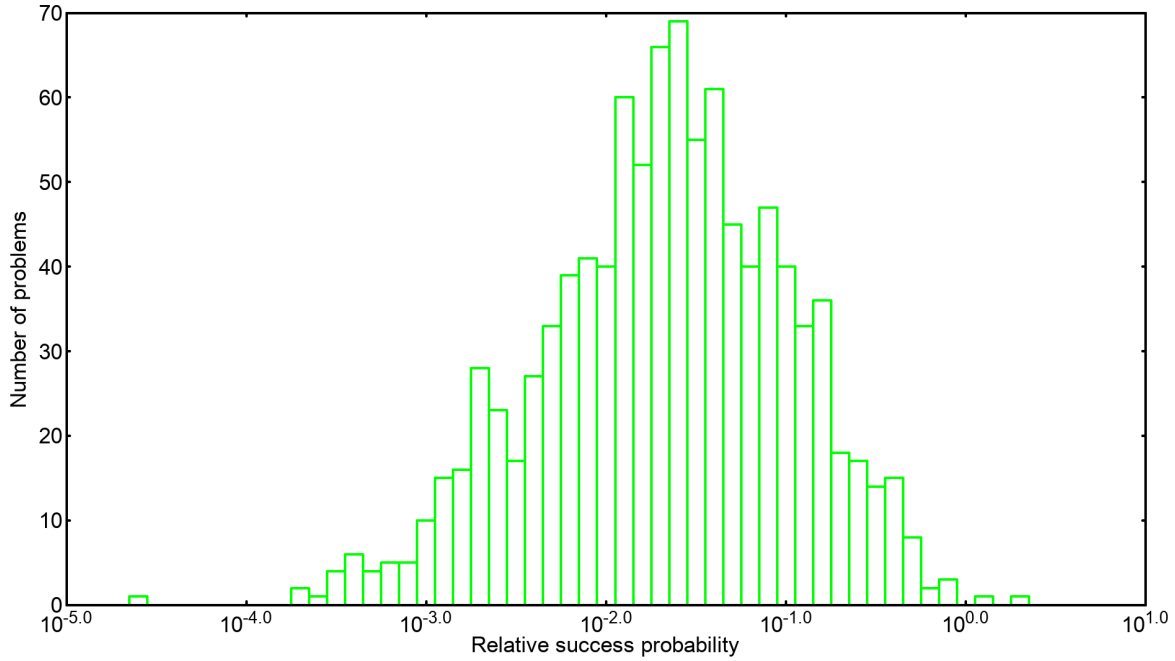


Figure 5.11: The distribution of relative success probability  $\frac{p^A}{p^O}$  for  $T_A=100$ . 0.2% of the cases were found to have a higher success probability after adding the trigger.

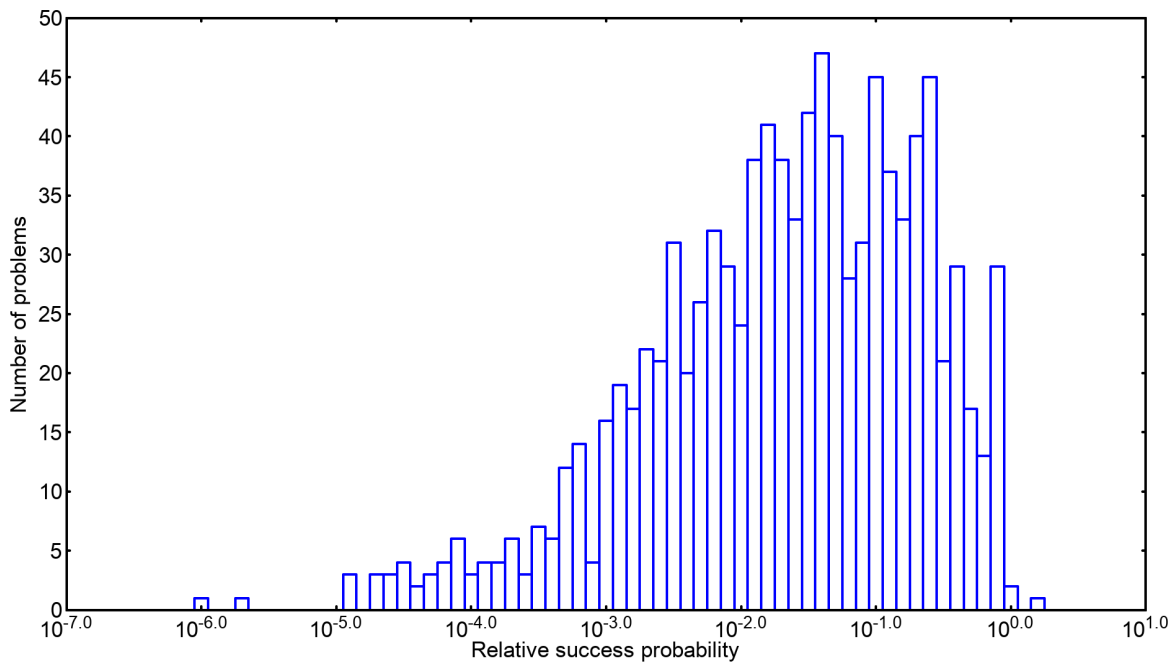


Figure 5.12: The distribution of relative success probability  $\frac{p^A}{p^O}$  for  $T_A=1000$ . 0.2% of the cases were found to have a higher success probability after adding the trigger.

For an annealing time  $T_A=10$ , it was found that 43.9% of the problems of the set were improved after the anti-ferromagnetic trigger with  $g=0.5$ . On increasing the annealing time to 100 and 1000, the percentage of cases with improved success probability dropped to 0.2% for both the cases. Furthermore, the largest value of the relative success ratio is a little more than 250 for  $T_A=10$ , while it reduces to 1.995 for  $T_A=100$ , and to 1.585 for  $T_A=1000$ . In

order to understand the reasons for this decrease in the performance on increasing the annealing time, the minimum energy gaps of all the problems were calculated after adding the trigger. Figure (5.13) shows a plot of the minimum energy gaps after adding the anti-ferromagnetic trigger ( $\Delta_{min}^A$ ) with the original minimum energy gaps ( $\Delta_{min}^O$ ).

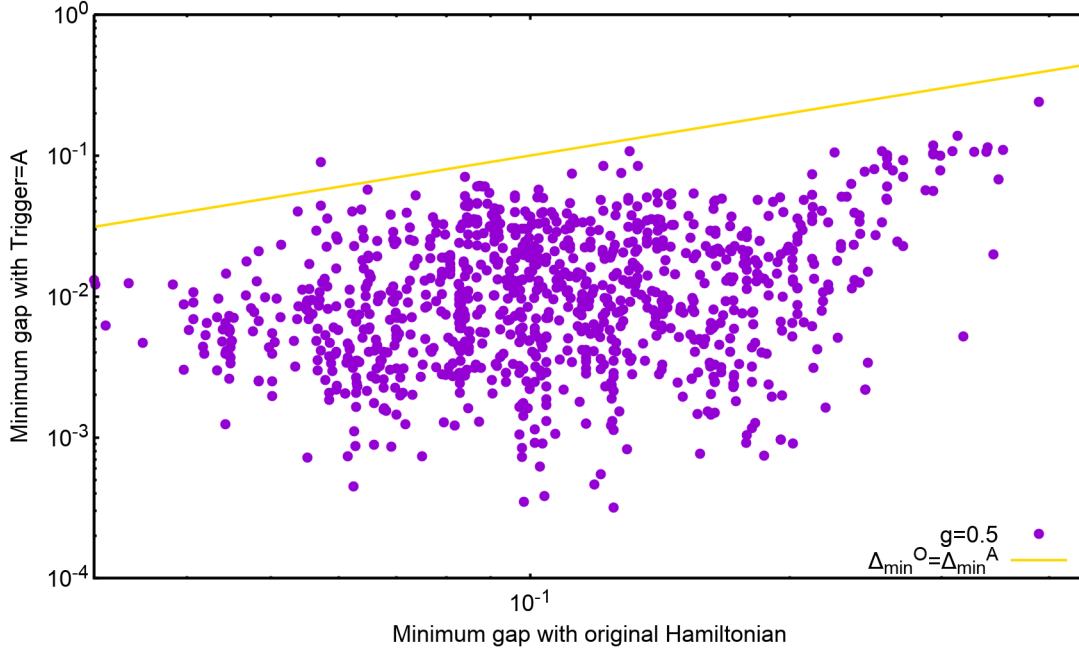


Figure 5.13: A plot of the minimum energy gaps after adding the anti-ferromagnetic trigger with  $g=0.5$  ( $\Delta_{min}^A$ ), with the original minimum energy gaps ( $\Delta_{min}^O$ ). For 99.9% of the minimum energy gap was found to have decreased after adding the trigger.

As is clear from figure (5.13), for 99.9% of the cases, the minimum energy gaps reduce after adding the anti-ferromagnetic trigger with strength 0.5. Additionally, it was found that 92.3% of all the cases still had a single anti-crossing between the ground and the first excited state, while for the other 7.7% of the cases, it increased to 2.

For shorter annealing times, like  $T_A=10$ , the success probability can benefit because of two reasons. As seen in the second chosen problem in the previous section, for small minimum energy gaps, and smaller annealing times, the state of the system can shift to the first excited state prior to the minimum gap anti-crossing. The overlap with the ground state can then increase because of the following non-adiabatic processes:

- If there are no higher energy states close to the state of the system, the wave function of the state can transfer some amplitude back to the ground state, at one of the anti-crossings.
- If the higher energy states come close to the system state, before it approaches the energy anti-crossing, the system state can further transit to a superposition state of the higher energy levels. This might increase the overlap of the state with the ground state compared to the case where the state closely follows the first excited state after crossing the energy anti-crossing.

Thus, when the annealing time is increased to 100 or 1000, the state of the system stays close to the ground state till it reaches the energy anti-crossing, and transitions to the first excited state afterwards. This explains the drop in the percentage of improved cases upon increasing the annealing time and adding the anti-ferromagnetic trigger.

To get an estimate of the difficulty of the affected problems, figure (5.14) shows the scatter plot of the success probabilities after adding the trigger with the original success probabilities, for the three annealing times. It should be noted that the 43.9% of the problems improved upon by adding anti-ferromagnetic trigger for  $T_A=10$ , are the ones that had relatively smaller original success probabilities (harder problems with smaller minimum energy gaps). Adding the anti-ferromagnetic trigger reduces the minimum energy gap, thereby increasing the success probability by either of the two mechanisms listed above.

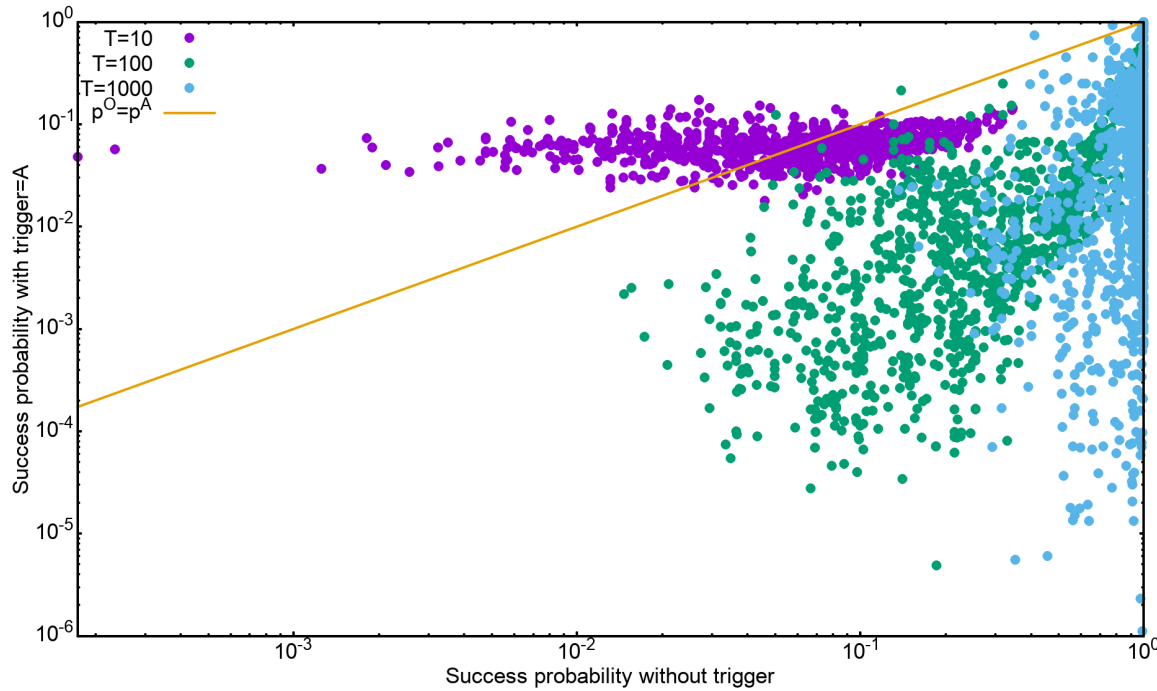


Figure 5.14: A plot of the success probabilities after adding the anti-ferromagnetic trigger with  $g=0.5$  ( $p^A$ ), with the original success probabilities( $p^O$ ) for annealing time 10, 100 and 1000.

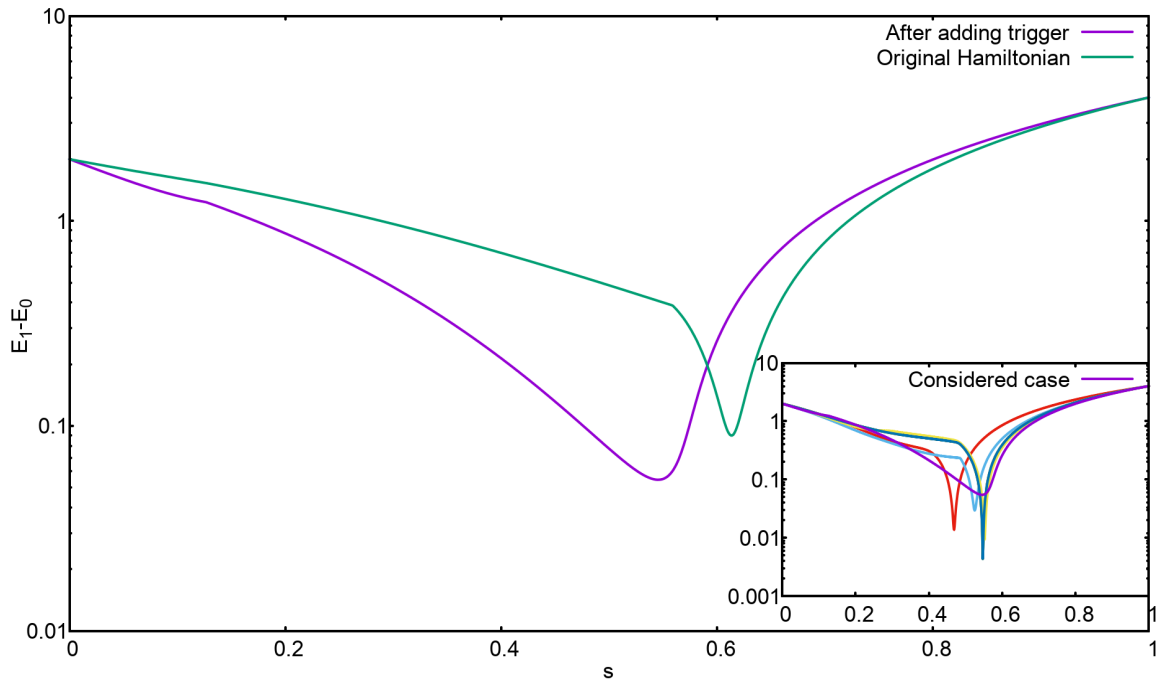


Figure 5.15: Considered here is the case with increased success probability in spite of a decrease in the minimum energy gap. The energy gap between the two lowest energy levels is compared for this case with that in the original case. The inset shows a comparison with some other problems after adding the trigger. The key difference for the considered case is that the slope of the curve is not symmetric about the point of minimum gap, unlike all other cases.

It should also be noted that for  $T_A=100$  and  $T_A=1000$ , the original success probabilities are already quite high,

giving way to another reason for the decrease in the relative success probability with increasing annealing time.

For both  $T_A=100$  and  $T_A=1000$  the two problems that had a higher success probability after adding the anti-ferromagnetic trigger, were indeed the same. One of these problem happened to be the only problem that had a larger minimum energy gap upon adding the anti-ferromagnetic trigger, and hence the increase in the success probability.

For the other problem, figure (5.15) shows the energy gap between the ground energy level and the first excited state of the Hamiltonian (as a function of the annealing parameter), before and after adding the anti-ferromagnetic trigger. The inset of the figure also shows the energy gaps for some other problems after adding the trigger. As can be observed in the figure, the shape of the curve for the case with larger success probability (in spite of the decrease in the minimum energy gap) is different from both the original Hamiltonian and the other problems. The slope in this case, unlike the other cases, is not symmetric about the minimum gap value. While comparing the

success probabilities across different problems (and assuming  $p = 1 - e^{-\frac{-T\Delta^2}{c}}$ ), the slope ( $c$ ) for each problem was supposed to have a similar structure and only changes in the minimum gaps were accounted for. Since this assumption breaks down for this case, the success probability deviates from the expected value.

Finally, for checking if the dynamics during the evolution of the state under the action of the anti-ferromagnetic trigger is adiabatic, equation (2.4) should be verified, as was done in the last chapter. We plotted the success probability against the minimum energy gaps for all the problems of the set, before and after adding the ferromagnetic trigger, for all the three annealing times. The resulting plot is shown in figure (5.16).

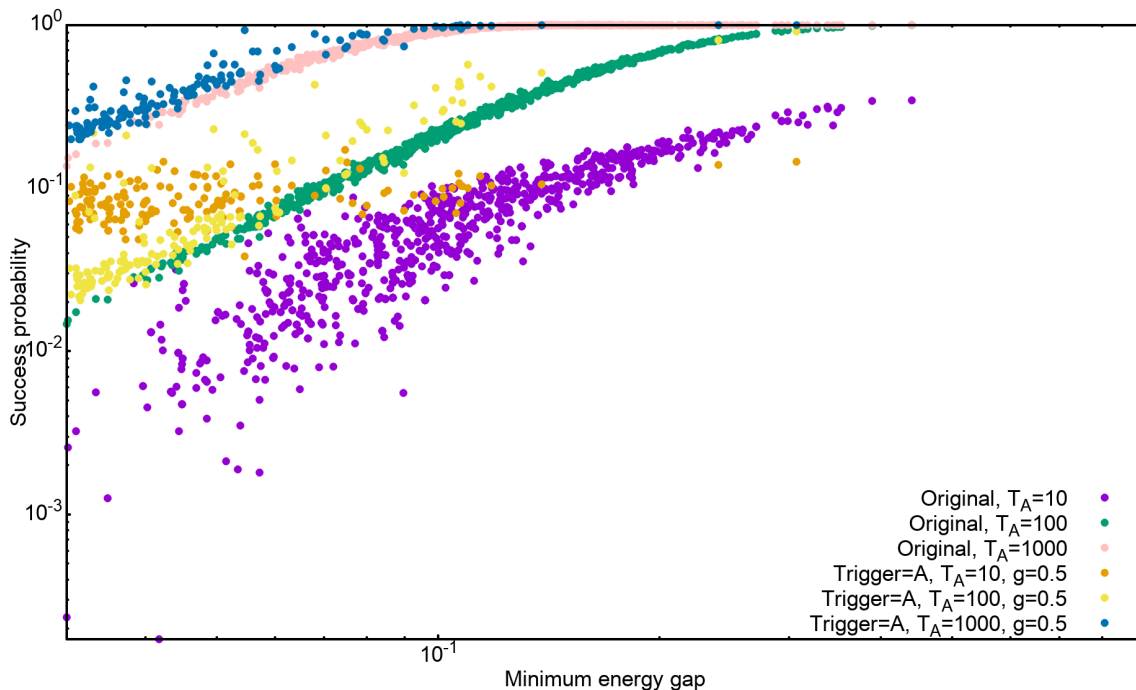


Figure 5.16: Success probability versus minimum energy plot for all the problems belonging to the set of 12-spin SAT problems, for annealing times 10, 100 and 1000, in the absence and presence of ferromagnetic trigger.

It can be noted from figure (5.16) that the original success probabilities mostly follow the exponential dependence on minimum energy gaps, although the scattering for  $T_A=10$  is comparatively large. As the annealing time is increased, the curve becomes more defined. However, upon adding the trigger, the scattering becomes even larger, so that the points corresponding to  $T_A=10$  appear rather flat. Also, for smaller gaps, these points have a higher success probability than the points corresponding to  $T_A=100$ , due to non-adiabatic evolution. Although in this case too the curves become successively more defined by increasing the annealing time, the general effect of adding the trigger with strength  $g=0.5$  is to shift the data points leftwards by reducing the minimum energy gaps, and thus limiting the performance.

**g=1**

In this section, the same analysis will be shown as in the last section but with the value of the strength parameter set to 1. We begin by showing the distribution of the relative success probability after adding the anti-ferromagnetic trigger with g=1, for annealing times 10, 100 and 1000, in figures (5.17), (5.18) and (5.19) respectively.

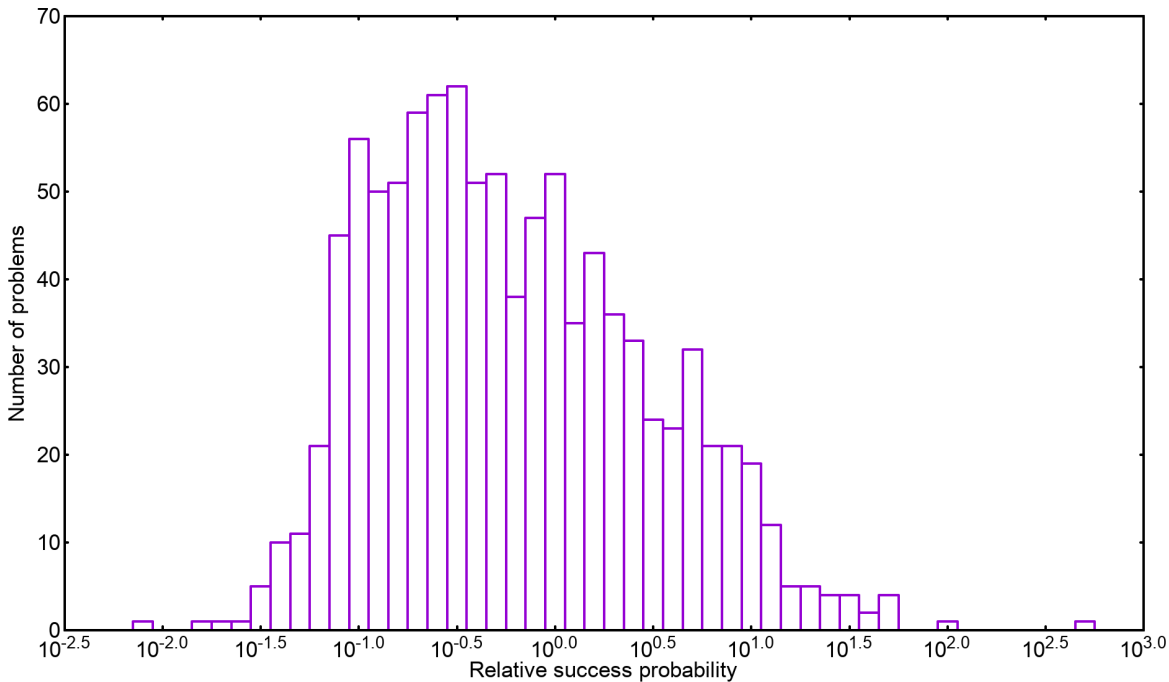


Figure 5.17: The distribution of relative success probability  $\frac{p^A}{p^O}$  for  $T_A=10$ . 37.7% of the cases were found to have a higher success probability after adding the trigger.

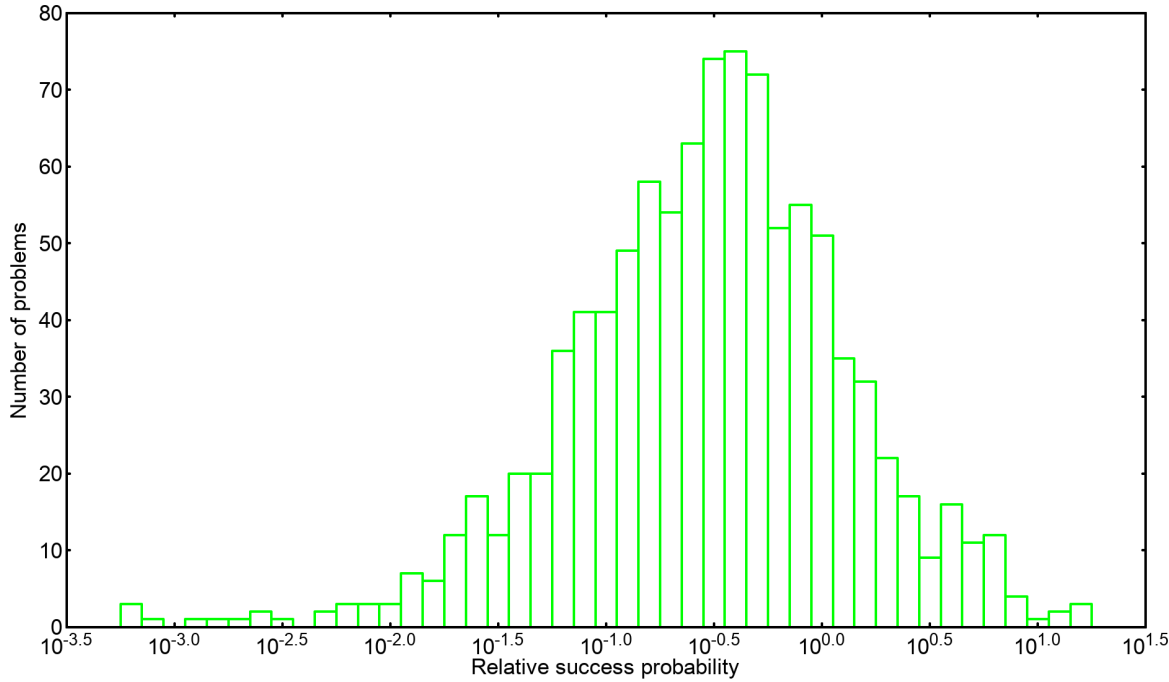


Figure 5.18: The distribution of relative success probability  $\frac{p^A}{p^O}$  for  $T_A=100$ . 21.5% of the cases were found to have a higher success probability after adding the trigger.

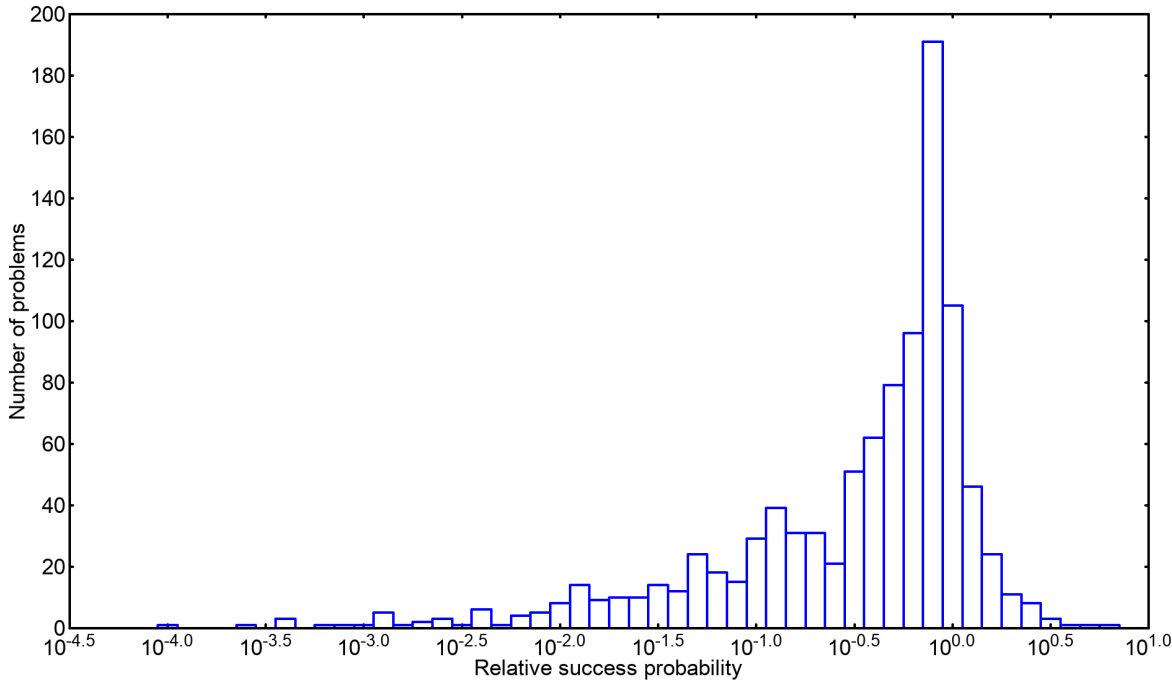


Figure 5.19: The distribution of relative success probability  $\frac{p^A}{p^O}$  for  $T_A=1000$ . 20% of the cases were found to have a higher success probability after adding the trigger.

37.7% of the cases had an improved success probability after adding the anti-ferromagnetic trigger for  $T_A=10$ . This percentage reduced to 21.5% and 20% respectively upon increasing the annealing time to 100 and 1000 respectively. Moreover, as the annealing time was increased, the largest value of the relative success probability

dropped from 501 at  $T_A=10$ , to 15.85 at  $T_A=100$ , to 6.31 at  $T_A=1000$ . Again, for obtaining more insights about the effects of adding the anti-ferromagnetic trigger with  $g=1$ , the minimum energy gaps were computed for all the problems of the set after adding the trigger. Figure (5.20) shows the resulting scatter plot between the original minimum energy gaps and the gaps after adding the trigger.

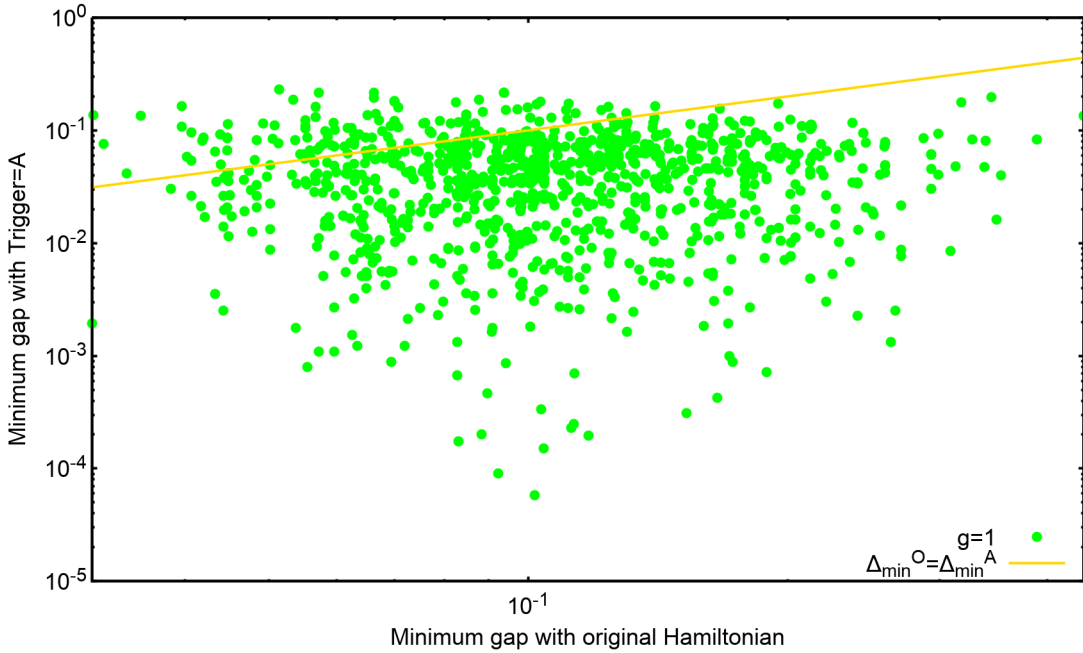


Figure 5.20: A plot of the minimum energy gaps after adding the anti-ferromagnetic trigger with  $g=1$  ( $\Delta_{\min}^A$ ), with the original minimum energy gaps ( $\Delta_{\min}^O$ ). For 87.9% of the minimum energy gap was found to have decreased after adding the trigger.

In this case 87.9% of the cases were found to have smaller minimum energy gaps upon the addition of the trigger. Thus, a decrease in the success probability for most of the cases compared to the original seems to be plausible.

Furthermore, for most of the cases the number of energy anti-crossings between the ground state and the first excited state increased to 2, while in one case it was noted to be 4. Table (5.4) shows the percentage of cases for different number of anti-crossings.

Number of anti-crossings	Number of cases (%)
1	20.2
2	70.5
3	9.2
4	0.1

Table 5.4: Number of cases with different number of anti-crossings after adding the anti-ferromagnetic trigger.

For obtaining an estimate for the difficulty of the problems which have a relative success ratio greater than one, a scatter plot of the original success probability and that after adding the anti-ferromagnetic trigger has been shown in figure (5.21).

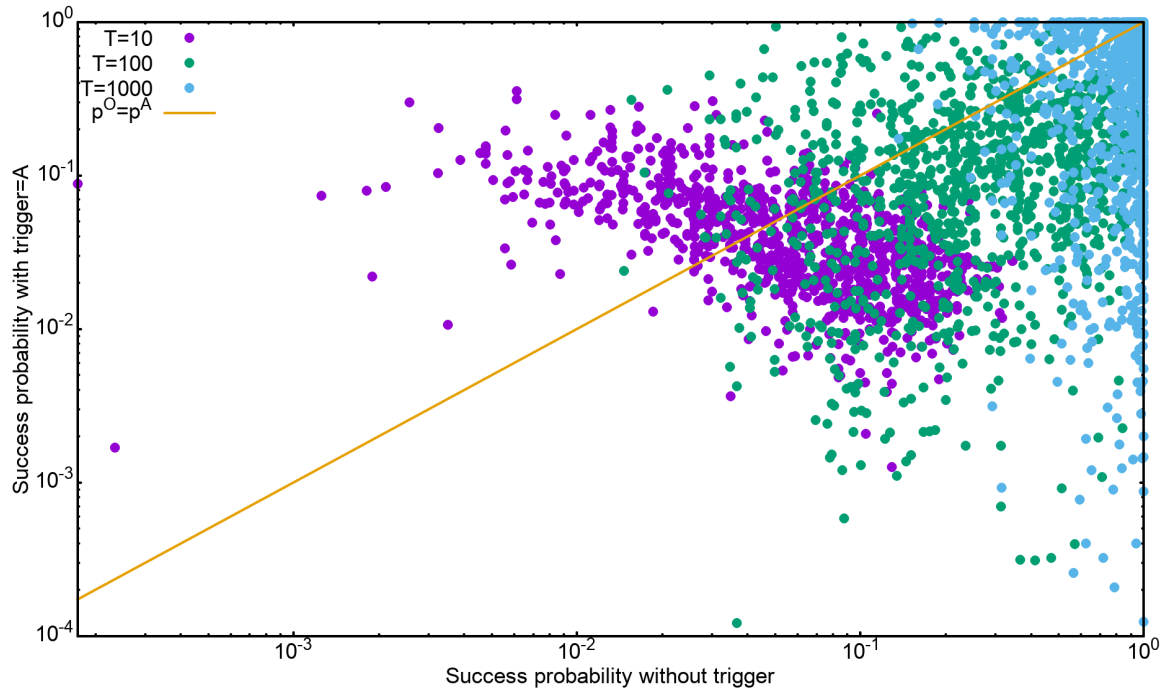


Figure 5.21: A plot of the success probabilities after adding the anti-ferromagnetic trigger with  $g=1$  ( $p^A$ ), with the original success probabilities( $p^O$ ) for annealing time 10, 100 and 1000.

Again, it can be noted that for  $T_A=10$ , the 37.7% of the problems that have a higher success probability after adding the anti-ferromagnetic trigger are limited to the cases with smaller original success probability (smaller gaps). Since adding the trigger reduces the minimum energy gap in most of the cases, the cases with smaller  $p^O$  benefit from a non-adiabatic evolution (shorter annealing time).

For understanding the role that the annealing time plays in improving the success probability, scatter plots of original and modified minimum gaps (upon adding the trigger) were plotted for the cases with relative success probability higher than 1, for the three annealing times. These plots have been shown in figure . (5.22), (5.25) and (5.26).

In the 37.7% of the cases with higher success probability after adding the trigger for  $T_A=10$ , 27.9% of the cases were found to have smaller minimum gaps as a result of adding the trigger. These cases can therefore be expected to have a non-adiabatic evolution at  $T_A=10$ , explaining the observed trend. On the other hand, for the rest 9.8% of the cases the minimum gaps were increased. It was noted that except for 2 cases with larger minimum gaps that were improved for  $T_A=10$ , were also improved for  $T_A=100$  and  $T_A=1000$ . This suggests that for these cases adding the anti-ferromagnetic trigger increased the minimum energy gap, making the evolution more adiabatic even for  $T_A=10$ .

Additionally, for the two cases with enlarged minimum gap and higher success probability for  $T_A=10$  but not for  $T_A=100$ , the energy spectra and instantaneous energies were studied. Same mechanics were found to be governing the trend, therefore the energy spectra for one of the problems is shown here. Figures (5.23) and (5.24) show the energy spectrum and the instantaneous energies before and after adding the trigger.

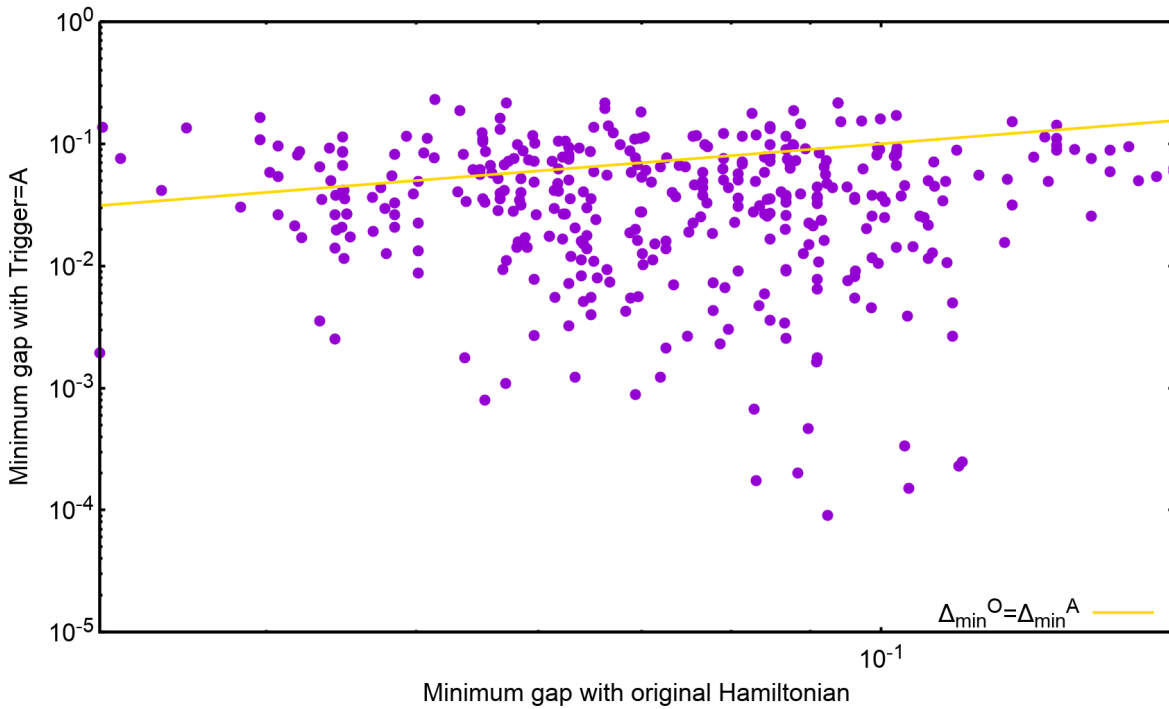


Figure 5.22: For the cases with higher success probability for  $T_A=10$  after adding the anti-ferromagnetic trigger with  $g=1$ , the scatter plot of energy gaps  $\Delta^A$  with  $\Delta^O$ . 279 out of 377 of such cases were found to have smaller minimum energy gaps after adding the trigger.

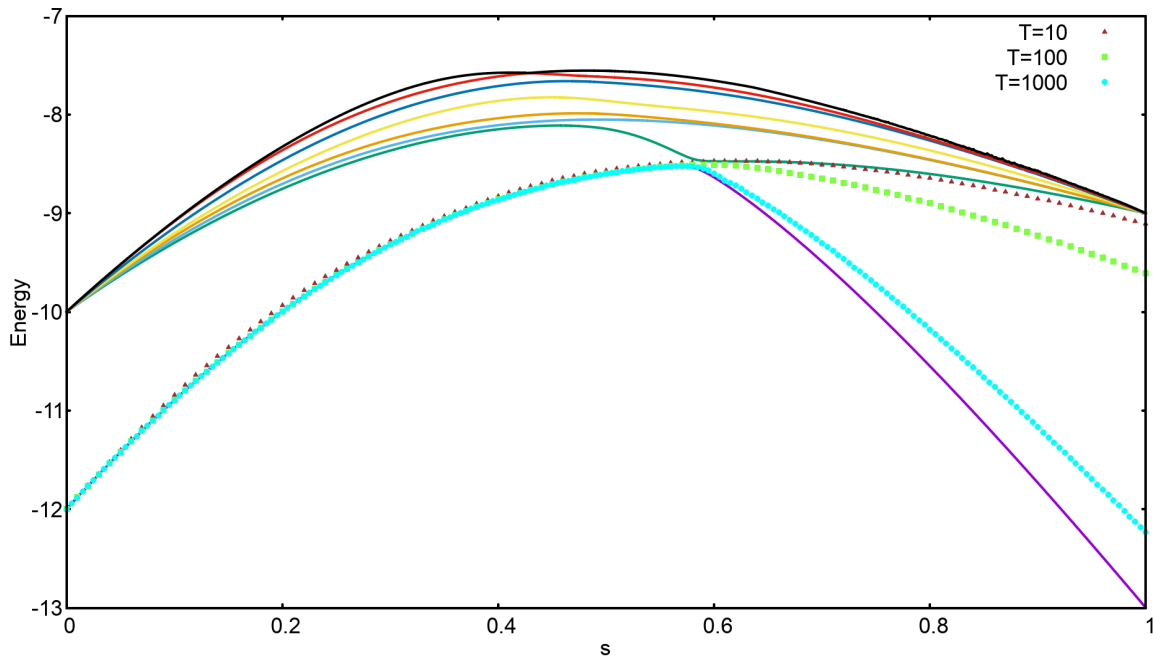


Figure 5.23: Energy spectrum and instantaneous energy values for the original Hamiltonian of the problem with enlarged minimum energy gap, improved success probability for  $T_A=10$ , but decreased success probability for  $T_A=100$ , as a consequence of adding the anti-ferromagnetic trigger.

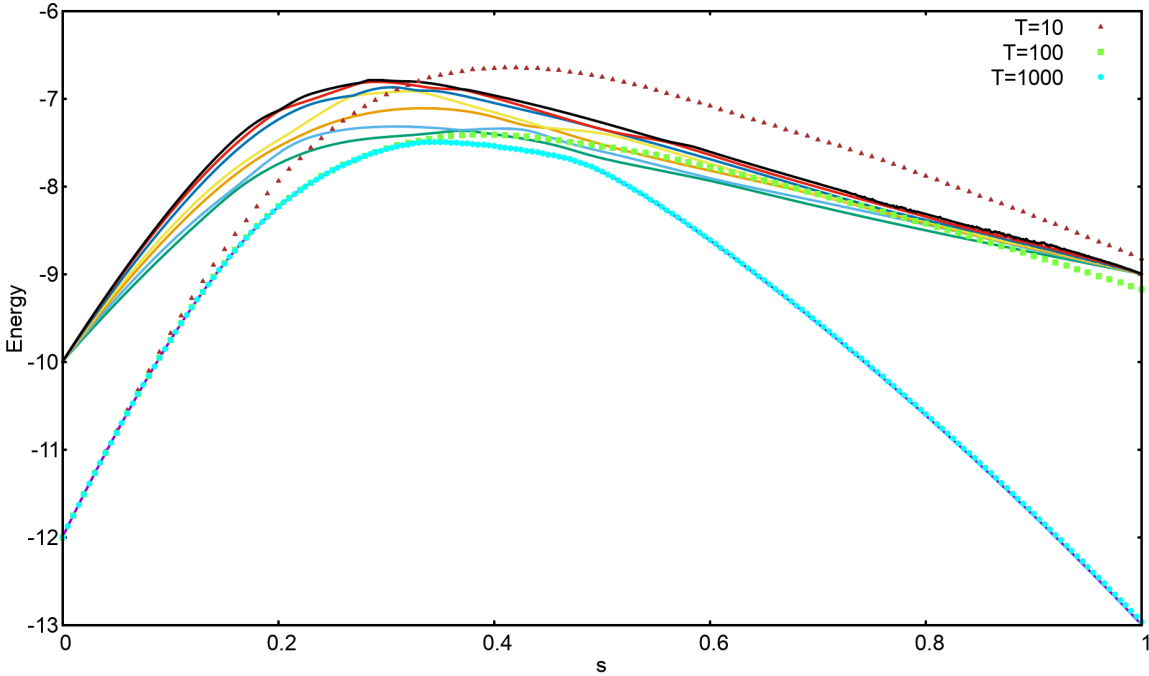


Figure 5.24: Energy spectrum and instantaneous energy values for the Hamiltonian with anti-ferromagnetic trigger, of the problem with enlarged minimum energy gap, improved success probability for  $T_A=10$ , but decreased success probability for  $T_A=100$ , as a consequence of adding the anti-ferromagnetic trigger.

Although adding the trigger enlarges the minimum gap in these cases, the spectrum of the problem is changed in a way that the state has more chances of going to higher energy levels. For  $T_A=10$  the system transitions to higher energy levels even before the first energy anti-crossing, and coincidentally ends in a state with larger overlap with the ground state than in the original case where it closely follows the first excited state after the anti-crossing. For  $T_A=100$ , and in the presence of the trigger, the state shifts to the higher excited state at the second energy anti-crossing, but this time the overlap of the final state with the ground state is smaller than that in the case of the original Hamiltonian. Finally, an annealing time of  $T_A=1000$  becomes long enough for the evolution to become adiabatic, and since the minimum energy gap is increased after adding the trigger, the success probability in the presence of the trigger becomes larger.

Next, from figures (5.25) and (5.26) it can be noted that the majority of the problems improved by adding anti-ferromagnetic trigger, and choosing the annealing time to be  $T_A=10$  or  $T_A=1000$  correspond to the cases where the minimum energy gaps became larger upon adding the trigger. 11.7% of the 21.5% of the cases improved after adding the trigger for  $T_A=100$ , and 12.1% of the 20% of those for  $T_A=1000$  had larger minimum gaps after including the trigger.

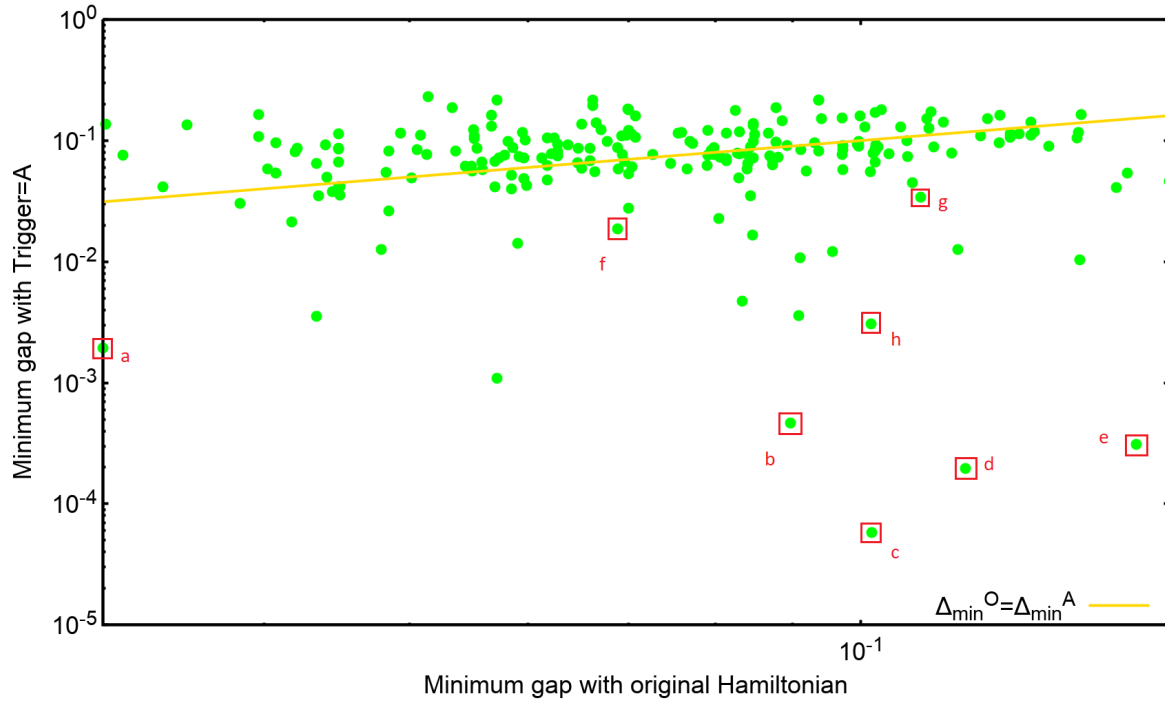


Figure 5.25: For the cases with higher success probability for  $T_A=100$  after adding the anti-ferromagnetic trigger with  $g=1$ , the scatter plot of energy gaps  $\Delta^A$  with  $\Delta^O$ . 117 out of 215 of such cases were found to have larger minimum energy gaps after adding the trigger. Some of the rest 98 cases were studied separately, and have been marked in the figure (a-h).

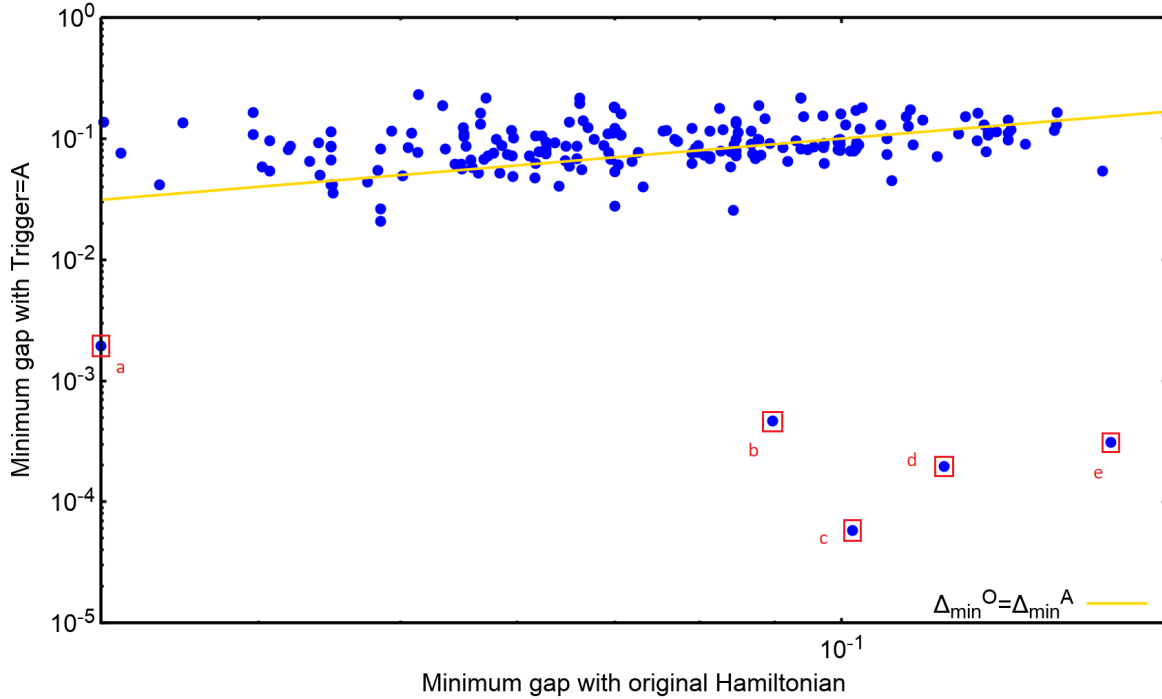


Figure 5.26: For the cases with higher success probability for  $T_A=1000$  after adding the anti-ferromagnetic trigger with  $g=1$ , the scatter plot of energy gaps  $\Delta^A$  with  $\Delta^O$ . 121 out of 200 of such cases were found to have larger minimum energy gaps after adding the trigger. Some of the rest 79 cases were studied separately, and have been marked in the figure (a-e).

Some of the outliers from the above two plots were selected and their dynamics was studied. Firstly, it should be noted that the cases a-e are the ones that appear in both the figures. Out of them, for cases b, c and d there are exactly two anti-crossings where the energy gap is relatively small and comparable to each other. Figures (5.27) and (5.28) show the energy spectrum and the instantaneous energies for case c, in the absence and presence of the trigger, respectively.

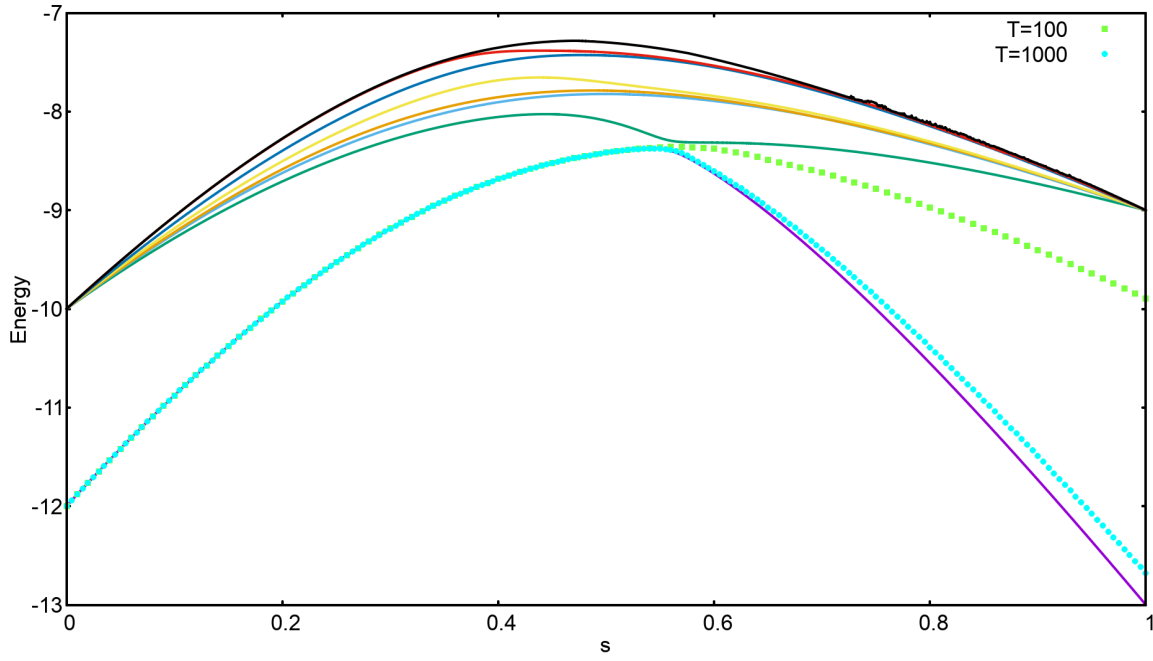


Figure 5.27: A plot of the success probabilities after adding the anti-ferromagnetic trigger with  $g=1$  ( $p^A$ ), with the original success probabilities( $p^O$ ) for annealing time 10, 100 and 1000.

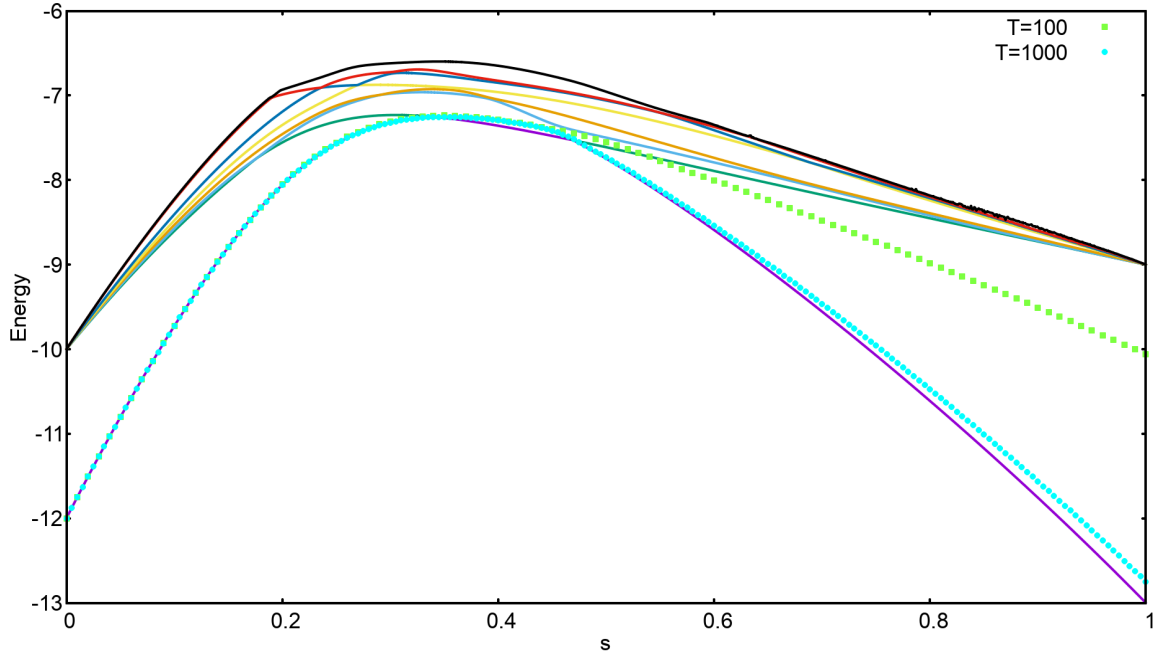


Figure 5.28: A plot of the success probabilities after adding the anti-ferromagnetic trigger with  $g=1$  ( $p^A$ ), with the original success probabilities( $p^O$ ) for annealing time 10, 100 and 1000.

In this problem, the state of the system shifts to the first excited state at the first energy anti-crossing, but transits back to the ground state at the second one. Therefore, although the minimum energy gap has become smaller, the success probability after adding the trigger increases.

Moreover, for cases a and e similar kind of mechanism is at play for increasing the success probability after including the trigger, despite of a decrease in the minimum energy gap. Case a was found to be the same as the

second chosen problem in the first section of the chapter. It can be noted from figure (5.8) that adding the trigger changes the spectrum in such a way that the ground state and the first excited state stay close to each other for a longer amount of time. When the gap between these levels starts to increase again, the system state shifts most amplitude to the ground state again.

It was also noted that there were additional cases in the scatter plot for the minimum energy gap ( $\Delta_{min}^A$  vs  $\Delta_{min}^O$ ) for  $T_A=100$ . Cases f, g and h, marked in figure (5.27) were additionally studied and were found to have similar dynamics. For cases g and h the number of anti-crossing was found to have increased to 2, where both the gaps were small enough for the state to transit at  $T_A=100$ , hence working in favour of the success probability.

For case f , figures (5.31) and (5.30) show the plots for the energy spectrum and the instantaneous energy values before and after adding the trigger.

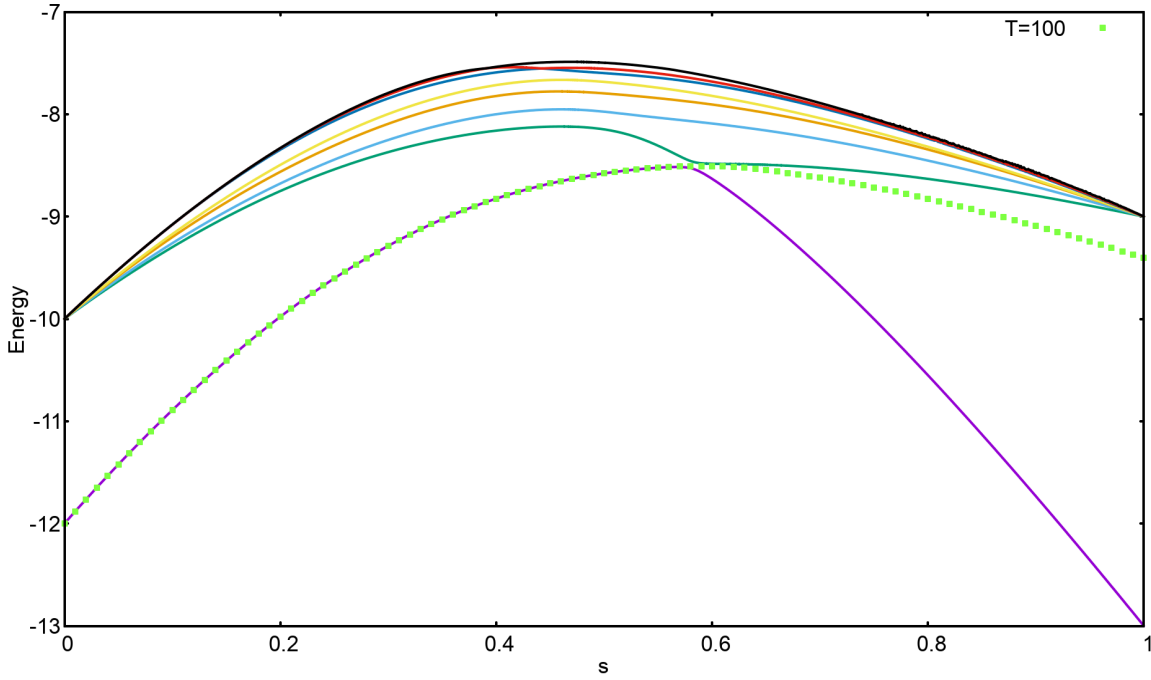


Figure 5.29: A plot of the success probabilities after adding the anti-ferromagnetic trigger with  $g=1$  ( $p^A$ ), with the original success probabilities( $p^O$ ) for annealing time 10, 100 and 1000.

In this case, adding the trigger increases the number of anti-crossings to 2, while also making the energy spectrum more involved. The energy levels come close enough for the state to shift to higher or lower levels at other points than just the anti-crossings. (**Explain better.**)

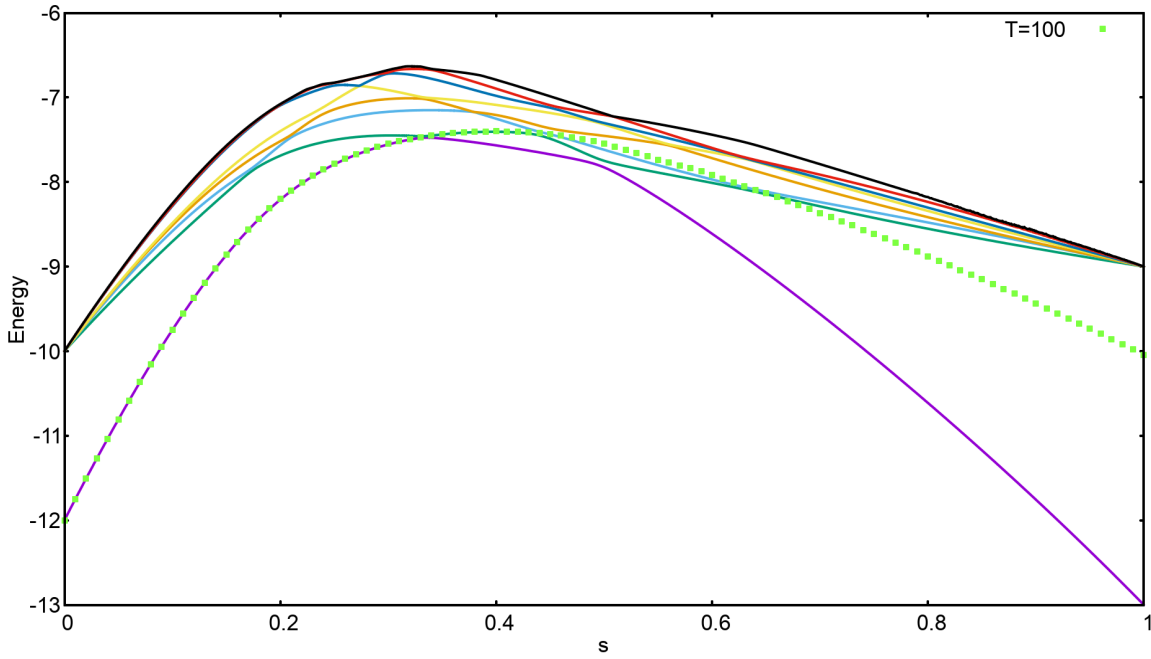


Figure 5.30: A plot of the success probabilities after adding the anti-ferromagnetic trigger with  $g=1$  ( $p^A$ ), with the original success probabilities( $p^O$ ) for annealing time 10, 100 and 1000.

Again, for checking if the dynamics after adding the anti-ferromagnetic trigger with  $g=1$  was adiabatic, the success probabilities for different problems were plotted against the corresponding minimum gaps. Figure (5.31) shows the resulting plot.

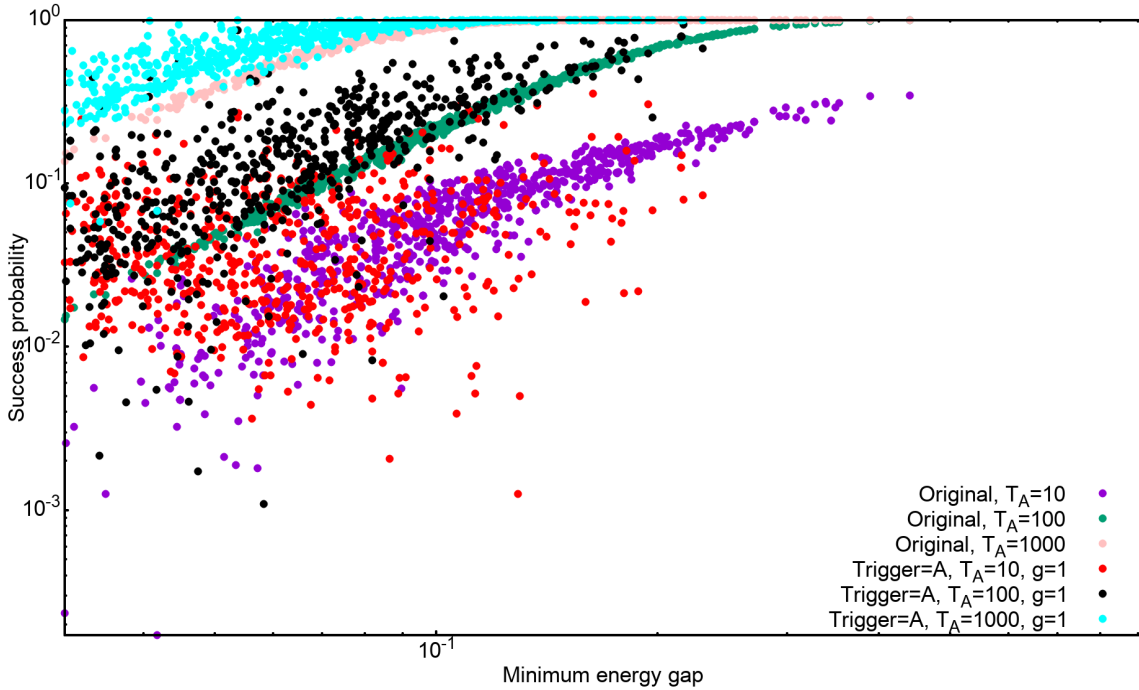


Figure 5.31: Success probability versus minimum energy plot for all the problems belonging to the set of 12-spin SAT problems, for annealing times 10, 100 an 1000, in the absence and presence of ferromagnetic trigger.

It can be noted that the scattering of the curves has increased substantially, although the form of the curves is defined better in this case compared to the last section (5.16). (MORE)

**g=2**

Finally, in this section the effects of adding the anti-ferromagnetic with strength 2 will be discussed.